D,L-Cyclic Peptides as Structural Materials

D,L-Cyclic Peptides as Structural Materials

A dissertation presented

by

Daniel James Rubin

to

The School of Engineering and Applied Sciences

in partial fulfillment of the requirements

for the degree of

Doctor of Philosophy

in the subject of

Engineering Sciences

Harvard University

Cambridge, Massachusetts

January 2015

Dissertation Advisor: Dr. Neel S. Joshi Daniel James Rubin

D, L-Cyclic Peptides as Structural Materials

ABSTRACT

The bioengineer has a choice of building with proteins, peptides, polymers, nucleic acids, lipids, metals and minerals, each class containing tremendous diversity within its category. While the platforms are diverse, they can be unified by a common goal: to engineer nano- and micro-scale order to improve functionality. In doing so, self-assembling systems aim to bring the lessons learned from the order in natural systems[83] into the therapeutics, materials, and electronics that society uses every day. The rigid geometry and tunable chemistry of D,L-cyclic peptides make them an intriguing building-block for the rational design of nano- and microscale hierarchically structured materials. Herein, we utilize a combination of electron microscopy, nanomechanical characterization including depth sensing-based bending experiments, and molecular modeling methods to obtain the structural and mechanical characteristics of cyclo-[(Gln-D-Leu)$_4$] (QL4) assemblies. QL4 monomers assemble to form large, rod-like structures with diameters up to 2 μm and lengths of 10s to 100s of μm. Image analysis suggests that large assemblies are hierarchically organized from individual tubes that undergo bundling to form larger structures. With an elastic modulus of 11.3 ± 3.3 GPa, hardness of 387 ± 136 MPa and strength (bending) of 98 ± 19 MPa the peptide crystals are among the

most robust known proteinaceous micro- and nano-fibers. The measured bending modulus of micron-scale fibers (10.5 ± 0.9 GPa) is in the same range as the Young's modulus measured by nanoindentation indicating that the robust nanoscale network from which the assembly derives its properties is preserved at larger length-scales. Materials selection charts are used to demonstrate the particularly robust properties of QL4 including its specific flexural modulus in which it outperforms a number of biological proteinaceous and non-proteinaceous materials including collagen and enamel.

We then demonstrate a composite approach to mechanical reinforcement of polymeric systems by incorporating synthetic D,L-cyclic peptide nanotube bundles as a structural filler in electrospun poly D-, L-lactic acid fibers. With 8 wt% peptide loading, the composite fibers are >5-fold stiffer than fibers composed of the polymer alone, according to AFM-based indentation experiments. The facile synthesis, high modulus, and low density, and reinforcing capabilities of QL4 fibers indicate that they may find utility as a filler material in a variety of high efficiency, biocompatible composite materials. This study represents the first experimental mechanical characterization of D,L-cyclic peptide assemblies or composites.

Table of Contents

List of Figures and Tables

FIGURES

TABLES

Acknowledgements

Each student's PhD experience is unique. The area of inquiry, project, lab, advisor, and peer group are cobbled together and observed from the student's unique point of view, colored by past experience and projections of what the future might hold. Differences aside, there are overarching characteristics that unify the otherwise disparate experiences. First, earning a PhD takes time. Second, over that time, the student is sure to grow and change. With that, I'd like to acknowledge and thank Professor Joshi for providing guidance while offering me the freedom to take control of my project, find collaborations, and participate in non-research activities. Thank you, Neel, for allowing me to grow, change, and find my own path.

The work described herein was made possible by the contributions of my fellow Joshi lab members and collaborators. I'd like to thank the old-guard of the Joshi Lab, Glenna, Peter and Zsofia for their help along the way, as well as our newer members, Rajiv, Richie, Anna, and Bom. I'd also like to thank my collaborators, Dr. Ortiz and Hadi, Dr. Gevelber and Thierry, Dr. Miserez and Shahrouz, and Dr. Su and Feng. Your direct and indirect contributions made this work possible.

As a child, I asked my mother why it was so important for me to attend school every day. She made it pretty simple. "The adults go to work and the kids go to school. School is your job." Apparently that was all the justification I needed to stay in school for nearly three decades. I'd like to thank my mother and father, Karen and David, and my siblings Josh and Julia, for their continued support throughout my PhD (and the rest of my life). You are great listeners and empathizers, and you always have guiding wisdom to share.

The first two years of my PhD were riddled with thoughts of opportunity cost. Committing to five or more years of academic research in a world that is changing so rapidly was difficult. The desire to hop a plane back to California and get a job in the bay area was finally quelled when a certain woman moved back to Boston. I'd like to thank my wife, Rebekah, for her unwavering and selfless support. I almost certainly would not be writing these acknowledgements if not for you. We are a team and this accomplishment belongs to the both of us.

Daniel James Rubin

January 2015

Chapter 1: Biologically Inspired Self-Assembling Materials: Inspiration, Structure and Properties

The purpose of this introductory chapter is to provide foundational information in areas pertinent to the research described in Chapters 2 and 3. An initial description of relevant chemical and structural components of natural materials, as well as a selected subset of biologically inspired self-assembling systems, will provide a broad context and background for the research reported in subsequent chapters. This review will then describe the state of knowledge within our particular material of interest, the D,L-cyclic peptide. Lastly, our research hypotheses and general methodology will be discussed.

1.1 NATURE'S STRUCTURAL MATERIALS

Introduction

Natural materials have evolved to utilize a diverse set of building blocks, often blended together to form a composite.[1] Whether composed of proteins[2, 3], polysaccharides[4, 5], minerals[6], metals[7], or combinations thereof, they are remarkably efficient in that they manifest impressive and effective structural properties with a minimal amount of material (Figure 1.1).[8] In fact, certain natural materials have evolved to outperform even the most robust known synthetic materials. For example, spider dragline silk exhibits extremely high toughness, surpassing nylon, rubber, Kevlar 49 and carbon fiber.[9] Furthermore, natural materials are degradable, synthesized under benign conditions[10], and often serve multiple roles within the organism such as providing structural support and molecular cues, as is displayed by the human extra-cellular

matrix.[11] Nature has provided the scientist with a rich array of inspiring systems to discover and analyze with the objective of mimicking their properties within new, environmentally friendly, functional materials.

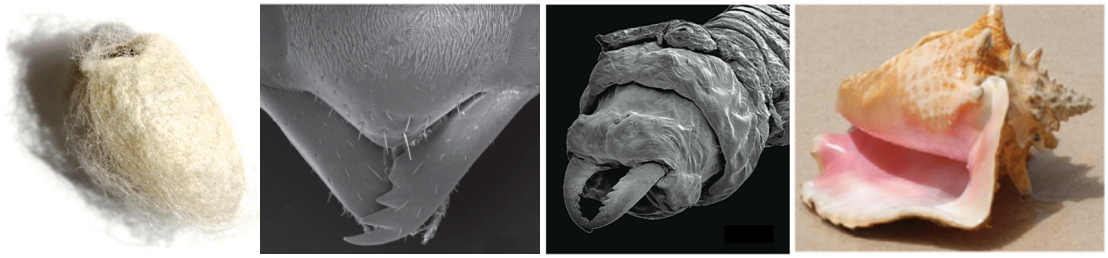

Figure 1.1. Natural biological materials. From left to right: Proteinaceous silk cocoon of the silk worm, chitosan-rich mandible of a wasp, metal-doped mandible of a marine polychaete, and mineral rich conch shell. Figures adapted from Broomell et al.[12] and Amini et al.[13]

This review will focus on materials that have major protein or amino acid components. Proteins are truly nature's workhorses.[14] Even in materials in which protein is a minority component, such as abalone nacre[15], the protein often serves to 'guide' the synthesis of the surrounding material. The remarkable properties of proteinaceous materials are a function of the material's chemistry, nano-structure, and microstructure.[16] These factors are often inextricably linked, such that in natural systems, a mutation that changes a molecule's chemistry will have downstream impacts on the structure, potentially leading to fatal consequences.[17] At times, harmful structural changes can occur without mutation, simply through protein misfolding events as is seen in an array of neurodegenerative diseases.[18] Indeed, controlling both chemistry and structure across length scales remains a significant challenge to scientists and engineers. Before delving into a discussion of biomimetic analogs, collagen and silk, two well-characterized, hierarchically structured protein materials will be discussed in some detail as examples of

the remarkable control over both chemistry and structure that is accomplished through biological processes and evidenced in naturally constructed materials.

Example 1: Collagen

By weight, collagen is the most abundant protein in the human body. It plays a critical role in the structure of bones, ligaments, tendons, vasculature, skin, and even the cornea of the eye.[8] Herein the focus will be on Type I fibrillar collagen as this type of collagen has a well-ordered structure across length scales. The ubiquity of collagen across multiple material types in the body is a testament to the importance of material processing in determining material properties. Collagen is characterized by a specific repeated amino acid motif, Glycine-X-Y in which the X or Y often represents a proline residue that may be post-translationally modified to hydroxyproline (Figure 1.2a).[2] The extended GXY repeat is flanked by cysteine containing 'telopeptide' domains. The flexibility of the glycine residue coupled with repeating proline residues results in a helical conformation that is stabilized when interacting with two fellow collagen molecules. The three chains interact through hydrogen bonds, stabilizing the supramolecular 'tropocollagen' structure.

Next, the tropocollagen molecules are packed densely in the form of a liquid crystal for preparation for cellular export. Dense packing forces strict alignment of tropocollagen, creating the anisotropy that is observed in collagen fibrils. During export, flanking domains are cleaved, and the cysteine residues oxidize to form stabilizing disulfide bonds, locking the molecules together into a microfibril with a characteristic banding pattern of 67 nm (Figure 1.2). After export, microfibrils bundle to form

subfibrils, fibrils, fascicles, and tendon via multiple layers of hierarchical organization (Figure 1.2).[19] Lastly, in their mature form collagen fibrils contain a wavy microstructure with a periodicity on the order of 10 μm – 200 μm to augment the response to mechanical deformation at low strains.[20]

The resultant tendon is able to efficiently transfer stress from muscle to bone while maintaining sufficient compliance when strains are low, preventing undue wear and tear.[21] A tendon's characteristic combination of compliance, strength, and durability is a direct result of the chemistry, beginning with the amino acid sequence, to the crosslinked microfibril, bundled fascicle, and crimp. The human body's control over the structure and chemistry of collagen from the molecular-to-macroscopic scale is beyond what is currently achievable in synthetic materials.[8]

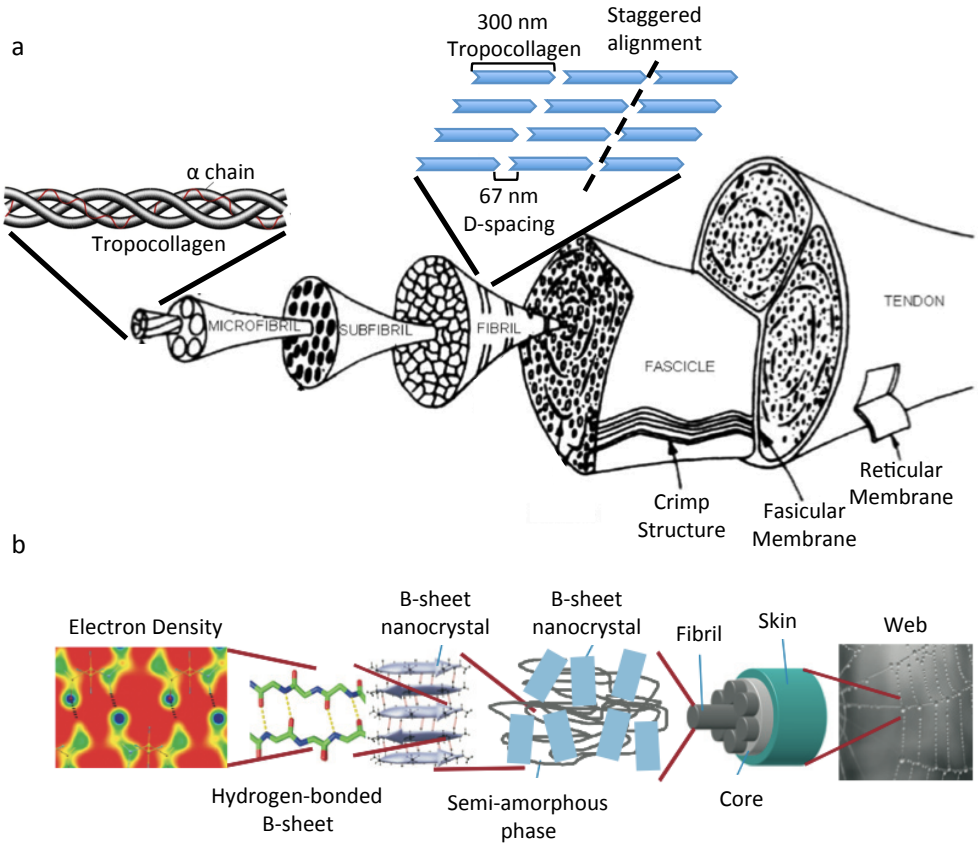

Figure 1.2. Hierarchical structure in collagen and silk. (a) A tendon contains structural hierarchy from the nanoscale, beginning with individual α chains of the collagen triple helix, to the macroscale tendon itself. (b) A spider silk fiber display similar nano-to-macroscale hierarchical ordering. Individual peptides form β-sheets that are interspersed in a semi-amorphous matrix. The composite is spun into fibrils which bundle to form the core of the web filaments. Figures adapted with permission from Meyers et al.[22] and Keten et al.[23]

Example 2: Silk

Silk is widely regarded as the epitome of a proteinaceous material with application-optimized structural properties. Silk's combined stiffness, strength and extensibility rivals even the most robust known natural or man-made fibers. Unlike collagens which are secreted, silks are 'spun' from a specialized organ that consists of a

gland, a duct and a nozzle.[10] Indeed, the silk spinning process is of equal importance to the protein sequence itself in creating a functional silk fiber.

The amino acid sequence of spider dragline silk from *Nephila clavipes* is characterized by three major domains: a loosely conserved six amino acid glycine-rich sequence; a poly-alanine region; and a glycine-glycine-X region in which X represents alanine, tyrosine, leucine or glutamine.[24] The emphasis on small, aliphatic amino acids allows for dense hydrogen bonding to occur in the form anti-parallel β-crystals, between which the protein matrix is less ordered (Figure 1.2b).[23] Theoretically, one can gain insight into the expected properties of a particular silk, by comparing the fraction of ordered versus disordered regions; however, a quick mechanical assay of reconstituted silk versus native silk will demonstrate that poorly processed silk is significantly weaker than its naturally spun analog.[10] Both the nano-structure and microstructure are necessary for silk to function as required.

During processing, the nano- and microscale structure of a silk fiber is created. Prior to spinning, dragline silk is stored in the form of a liquid crystal within a specialized major ampullate gland.[25] The careful control of solvent conditions within the gland and the duct allow for the creation of a particularly strong silk in which there is extensive β-crystal formation. Multiple spinnerets within the duct each create a filament of 100 nm – 200 nm in diameter (Figure 1.2b). These filaments merge together to form silk fibers with diameters of 10 μm – 20 μm, all while preserving the β-crystal secondary structure that was formed within the gland.[10] As the silk is strained, β-crystalline domains are able to share the load, while the less ordered matrix unfolds. The network of β-crystals created during the spinning process allows for very high stresses to be placed on the fiber before

it eventually fractures.[23] This combination of strength and extensibility leads to the aforementioned toughness of silk fibers. A comparison of a spider spinneret to melt spinning, aqueous spinning, or electrospinning, demonstrates nature's superior control over material processing, and the importance of structure and chemistry on material properties.

1.2 BIOLOGICALLY INSPIRED SELF-ASSEMBLING PEPTIDE MATERIALS

Building supramolecular systems from peptides

Supramolecular materials are structures in which the individual building blocks are designed to associate through non-covalent interactions such as hydrogen bonds, metal-coordinate bonds, van der Waals forces and electrostatic interactions. These materials are often simplified analogs of natural materials, such as the collagens and silks mentioned above. By building with repeating units that are stabilized by non-covalent interactions, the resultant material often has nano- or microscale order within the structure. As nanoscale and microscale order is difficult to achieve through top-down processes, supramolecular self-assembly has emerged as a bottom-up synthesis method of substantial interest in materials science. Whether one seeks to develop medically relevant scaffolding materials[26], organic electronics[27], or antibiotics[28], peptide building blocks offer the diversity and ease-of-synthesis necessary to explore a wide-array of potential applications. The following sections will explore four leading self-assembling peptide systems: peptide amphiphiles, amyloids, aromatic dipeptides (diphenylalanine), and D,L-cyclic peptides (DLCPs). Each section will describe the inspiration, structure, assembly,

properties and applications of the system. The field of organic self-assembly is broad and this introduction does not attempt to describe all systems in detail.

Peptide Amphiphiles

Peptide amphiphiles (PAs) are composed of (1) a peptide with both hydrophilic and hydrophobic residues[29], (2) hydrophilic residues coupled to an aliphatic lipid tail[30], or (3) peptide based copolymers.[31] Herein, the predominant focus will be on class (2), hydrophilic peptides coupled to lipid tails.

Synthetic lipid-tailed PAs, first characterized by Dr. Stupp at Northwestern University, are inspired by the siderophores secreted by marine bacteria.[32] Within the natural system, siderophores are used as iron harvesting molecules. They contain a peptide head group coupled to a fatty-acid tail, and they convert from micelles into vesicles in the presence of Fe(III) (Figure 1.3a). These vesicles are then taken up by the bacterial cell and the Fe(III) is harvested for use. This discovery provided information regarding the propensity of PAs to assemble, as well as the utility of specific metal ions as assembly triggers.

The PAs designed by the Stupp Lab contain four major regions: a hydrophobic tail, a stabilizing peptide region, a polar, charged group, and lastly a bioactive epitope (Figure 1.3b). Each component of the peptide amphiphile plays a key role. The hydrophobic tail provides the major impetus for self-assembly in aqueous media, the stabilizing peptide region holds the assembly together through dense hydrogen bonding (often in β-sheets), the charged group ensures the amphiphilic character of the molecule overall, and lastly the bioactive epitope can be used for a broad array of applications.[33]

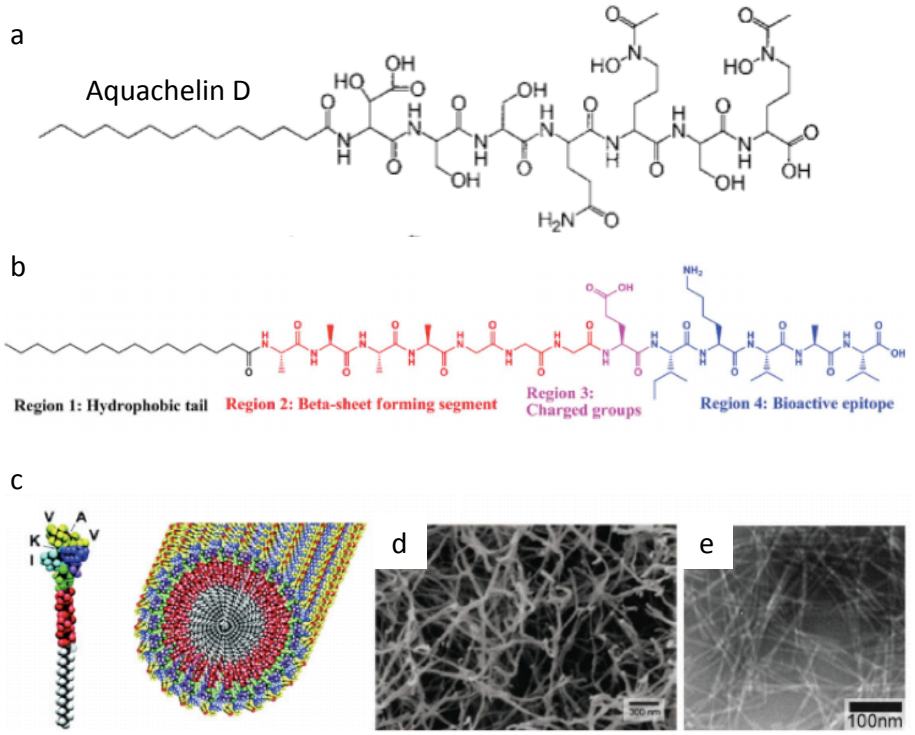

Figure 1.3. Peptide amphiphiles. (a) Aquachelin D is a siderophore from *H. aquamarina* and served as the inspiration for lipid-peptide amphiphiles. (b) Molecular structure of a representative peptide amphiphile with the 4 major domains highlighted. (c) Molecular graphics of IKVAV peptide amphiphile assembling to form a fiber. (d) Scanning electron micrograph of assembled PA fibers. (e) Transmission electron micrograph of PA fibers. Figures adapted with permission from Martinez et al.[32] and Cui et al.[30]

Like many amphiphilic molecules such as surfactants, PAs assemble above a certain critical assembly concentration (CAC).[34] The relationship between the hydrophobic and hydrophilic character of a PA is what determines its propensity to assemble. A system containing hydrophobic chains and small polar head groups will tend towards the formation of micelles, while a system that lacks a hydrophobic tail but contains regions favorable to hydrogen bonding will form β-sheets.[33] Between these two

opposing assemblies, PAs form stable one-dimensional nanofibers in which the peptides are oriented orthogonally to the long axis of the fiber (Figure 1.3c-e).[35] Depending on the head and tail groups chosen, PA fibers can be triggered through changes in pH, temperature, or enzyme concentration.[36]

Peptide amphiphiles have been utilized in a broad set of applications including, but not limited to antimicrobials[37], drug delivery vehicles[38], and materials templating scaffolds.[39] This versatile scaffold holds significant promise for future commercial application within the areas described. Peptide amphiphiles provide an intuitive first-example of the roles of non-covalent interactions in creating supramolecular assemblies and the role of chemistry in determining structure. Indeed, both hydrogen bonding and hydrophobic interactions are the major stabilizing functionalities in amyloid fibrils, aromatic dipeptides, and D,L-cyclic peptides.

Amyloid Fibers

Amyloid fibers, are of particular interest because they can be formed from many different protein sequences.[40] Amyloids were first studied in conjunction with neurodegenerative diseases such as Alzheimers[41], but newly discovered amyloidogenic gene products are increasingly being associated with functional (as opposed to pathogenic) biological performance.[42] Perhaps the most commercially successful self-assembling system, PuraMatrix^{tm}, was inspired by the yeast peptide zuotin. Zuotin, first characterized in Dr. Rich's lab at MIT, is composed of a repeating consensus motif-- n-AEAEAKAKAEAEAKAK-c (Figure 1.4a).[43] In the natural system, zuotin acts as a Z-

DNA binding protein, but researchers found that when synthesized and studied *in vitro* zuotin was able to self assemble into membrane structures.[44]

Amyloids are classified by their fibrillar structure in which *β*-strands associate to form an extended network of supramolecular *β*-sheets perpendicular to the long-axis of the fiber.[18] This structural motif is intriguing in that it is largely defined by the properties of the peptide backbone itself, namely the propensity for hydrogen bonding between carbonyl oxygen and amide hydrogen.[45] In many cases, one face or both faces of the β-sheet contain small, hydrophobic residues such as alanine, to allow for tight packing. In zuotin one finds aliphatic residues on one side of the β-sheet and charged residues on the other, allowing for the pairing of hydrophobic to hydrophobic and the exposure of the hydrophilic pairs to the solvent, thus stabilizing the nanofiber (Figure 1.4 b-c).[46] The general assembly scheme of amyloids allows a variety of different proteins, when subjected to various denaturing and assembly processes, to form amyloid-like structures.[47]

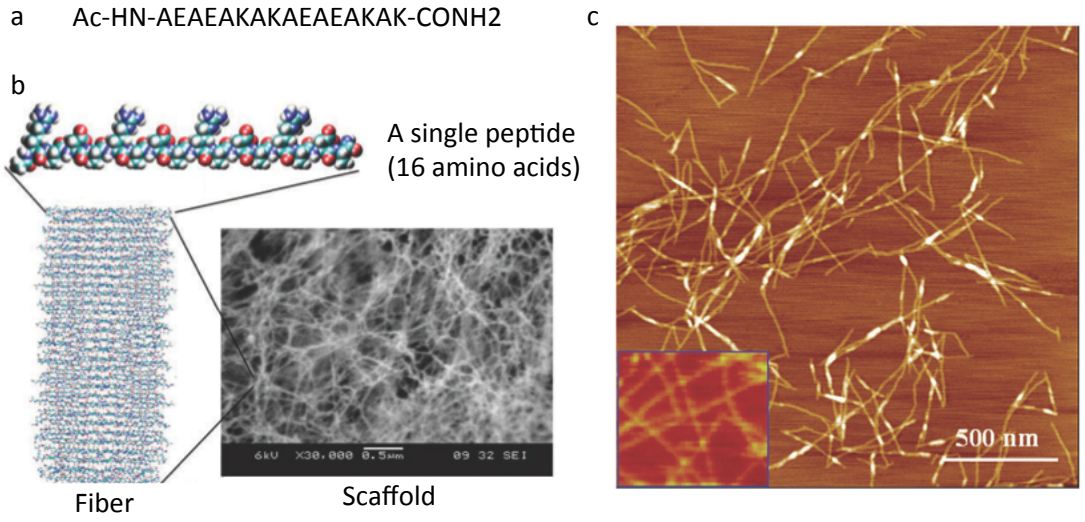

Figure 1.4. Amyloid fibers. (a) The consensus motif from yeast Z-DNA binding proteins that served as the inspiration for charge-alternating amyloid fiber scaffolds such as PuraMatrix[tm]. (b) Hierarchical structure of engineered RADA peptides. Individual peptides stack to form fibers which then extend and tangle to form a scaffold. (c) Atomic force micrographs depict the length, approximate width and morphology of amyloid fibers. Figures adapted with permission from Zhang et al.[43] and Hauser et al.[46]

These nanoscale fibrils continue to grow and form robust fibers with hierarchical order. Indeed, the dense hydrogen bonding and ordered structure of amyloid materials renders them among the most robust known proteinaceous materials with experimentally determined Young's moduli at the nanoscale in the range of 2-4 GPa.[48,49] Amyloids are also solvent and heat resistant. Their stability is what causes pathogenicity in disease, but it also makes amyloids an interesting engineering platform for the creation of self-assembled materials.

The combination of self-assembly, nanoscale order and high stiffness provides a breadth of potential applications including light-harvesting[50], carbon capture[51], drug delivery[52], nanowire fabrication[53], and engineered biofilms.[54,55] Engineering biofilms are

a particularly interesting and novel application for a self assembling system. Peptide amphiphiles, aromatic dipeptides and D,L-cyclic peptides all require *in vitro* synthesis, but amyloids can be completely genetically encoded. This means that one can create living, functional materials with the potential for nanoscale order, robust properties, and designer functionality.

Aromatic Dipeptides (Diphenylalanine)

Aromatic dipeptide structures were discovered in the lab of Dr. Gazit when researchers attempted to find the shortest consensus sequence of an Alzheimer's β-amyloid protein that was able to assemble.[53] Unexpectedly, it was found that only two amino acids were needed to generate supramolecular structures, a pair of phenylalanines (FF) (Figure 1.5 a).

Despite its discovery within an amyloid protein, the structure of the assembly is sufficiently different for it to be considered a new class of self-assembling peptide. Aromatic residues are hydrophobic, yet they also possess an electrostatic interaction that allows them to interact specifically with one another.[56] Upon assembly, FF molecules pack into a porous hexagonal structure in which the peptide backbone forms hydrogen bonds that line the pore and the aromatic side chains interlock with one another between pores (Figure 1.5 b).[57] The resultant structures are hollow tubes with diameters of ~100 nm and lengths on the order of microns (Figure 1.5 c). Interestingly, the addition of a third aromatic group such as a fluorenylmethyloxycarbonyl chloride (FMOC) group, or replacing the dipeptide with D,L-d-2-napthylalanine results in very different assembly states.[58,59] The replacement of FF-NTs with napthylalanine analogues results in structures

that are more fibrous in nature and have a higher polydispersity of sizes. The addition of FMOC to the N-terminus of diphenylalanine results in the formation of a nanofibrous gel, rather than discrete nanotubes. These modifications and resultant structures suggest that freedom to modify FF-NTs while maintaining their structure may be limited.

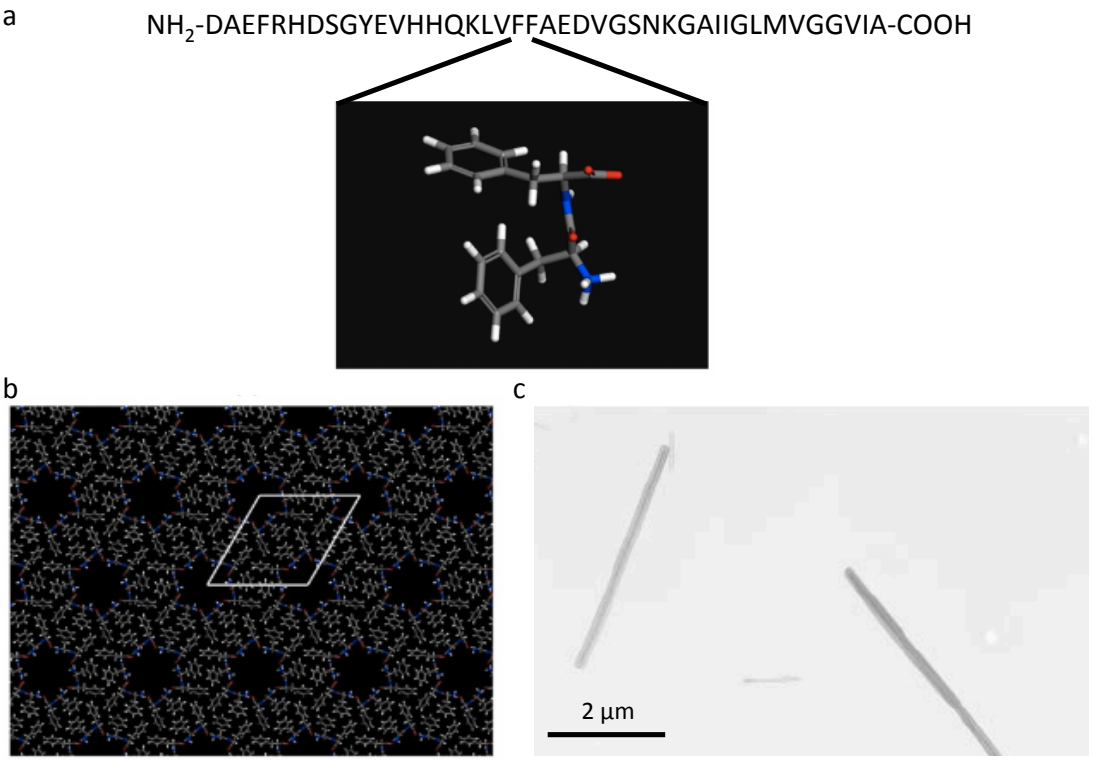

Figure 1.5. Diphenylalanine nanostructures. (a) The central aromatic region that allows for the formation of β-amyloid fibrils. Diphenylalnine is all that is needed for self-assembly. (b) Molecular dynamics model of the packing of diphenylalnine structures into a porous nanotube. The pores are lined by the peptide backbones which undergo hydrogen bonding with one another. Opposite the pores, the aromatic sidechains interlock to form a hydrophobic 'zipper' which stabilizes the structure. (c) Transmission electron micrographs of assembled diphenylalanine nanotubes. Figures adapted with permission from Reches et al.[53] and Azuri et al.[57]

Diphenylalanine nanotubes are among the stiffest measured protein or peptide based systems. A combination of AFM-based point stiffness and bending experiments

establishes the Young's Modulus of FF-NTs to be in the range of 19 GPa – 27 GPa, placing them above their amyloid counterparts and spider silk.[60,61] Similar to amyloids, FF-NTs are stable to high temperatures and a broad array of solvents. Unlike the more reversible peptide-amphiphile system discussed above, amyloids and FF-NTs are difficult to dissolve once assembled.

The rigidity, ease of manufacture, and water solubility of FF-NTs makes them an attractive scaffold for use in engineered materials.[62] FF-NTs have been used to template nanowires[53] and reinforce epoxy resin[63], while FMOC-modified structures have been used in drug delivery and as scaffolds for cell growth.[64]

D,L-Cyclic Peptides

Unlike the systems described above, D,L-cyclic peptides were inspired by tubular peptide assemblies. Within natural systems, there are many examples of tube-forming structures including gramicidins[65,66], coat proteins of the tobacco mosaic virus[67], and lanreotides[68], each evolved to their specific roles (Figure 1.6a). The assembly of synthetic cyclic peptides was first theorized by De Santis et al.[69] and later demonstrated by Dr. Ghadiri with a pH sensitive peptide 8-mer that was found to assemble into large, micron-scale assemblies.[70,71]

The peptide cycles are composed of an even number of amino acids with alternating D- and L-stereochemistry, causing a planar geometry in which the amino acid side chains radiate from the center of the ring and the amide backbone is perpendicular to the plane of the ring (Figure 1.6 b). The initial work was carried out with α-amino acids; however, researchers have expanded the space by testing both β-[72] and γ-amino acids[73],

as well. These adaptations allow the engineer to adjust the rigidity and size of the assembly, including the diameter of the pore.[74]

This geometrical arrangement promotes their assembly into high aspect ratio nano- and microstructures through β-sheet-like hydrogen bonding in which each ring sits flat on the surface of another ring (Figure 1.6c), similar to a 'cyclized amyloid'. However, unlike linear amyloids in which β-sheets are able to slide with respect to one another through stick-slip failure[23], DLCP assemblies are only able to stack directly atop each other. Depending on the sequence of the peptides, the nanotubes may also associate laterally into bundles to create structures that can be microns in width and hundreds of microns in length, significantly larger than the systems described above.[75]

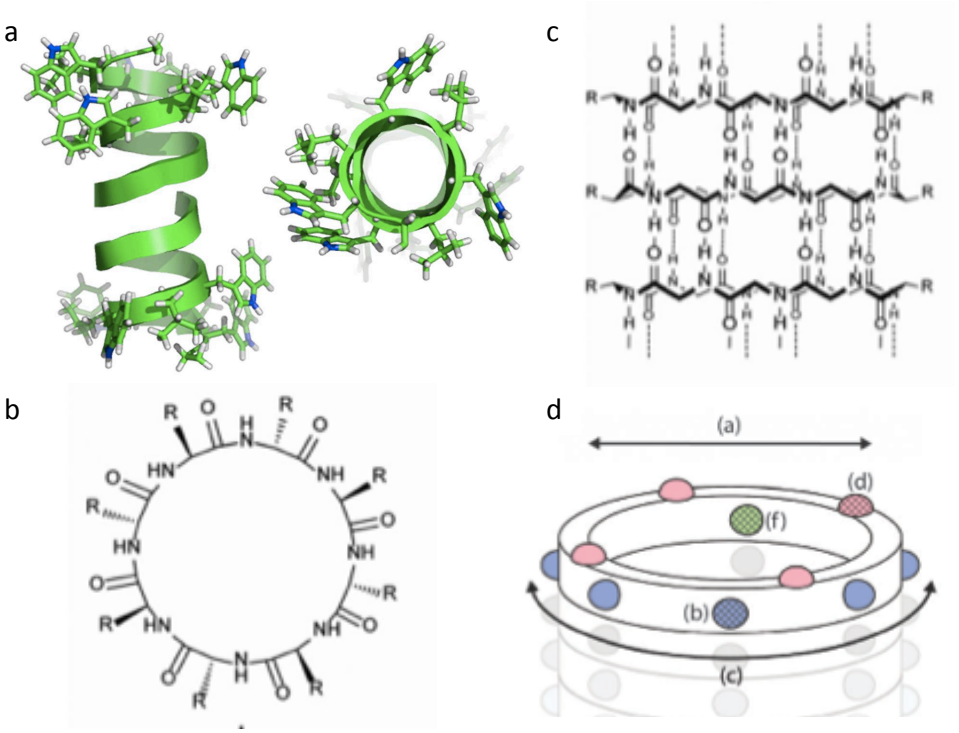

Figure 1.6. D,L-cyclic peptides. (a) Simplified structure of gramicidin A, one of many tube-forming peptides that served as inspiration for D,L-cyclic peptides. (b) Molecular structure of a DLCP 8-mer composed of α-amino acids. (c) Individual monomers stack directly atop one another and are stabilized by favorable β-sheet-like hydrogen bonding. R-groups radiate to the outside of the tube. (d) Schematic of a DLCP demonstrating the tremendous control over chemistry in multiple dimensions. The pore (a), outer surface (b), outer diameter (c), top/bottom (d) and inner surface (f) can each be modified selectively. Figures adapted from Wang et al.[76] Ghadiri et al.[71] and Chapman et al.[74]

D,L-cyclic peptides (DLCPs) share certain characteristics with amyloid fibrils including dense intermolecular hydrogen bonding along the peptide backbone and chemical and mechanical stability. DLCPs also exhibit similarities to FF-NTs in that they are tubular in nature, rather than fibrillar. However, unlike either system, their molecular structure and geometry allow for an enhanced ability to chemically modify the external tube surface, internal pore, internal diameter, top face and bottom face, or to guide

assembly via grafted molecules (Figure 1.6 d).[70,74] Indeed, as DLCPs are synthesized via common solid-state peptide synthesis methods[77], one has the freedom to explore limitless combinations of amino acids and post-synthetic modifications. This versatility has been leveraged to study DLCPs in a variety of applications including structural antibiotics[78], ion channels[79], selective ion transporters[80], and reinforcing agents.[81]

1.3 THESIS STATEMENT AND OUTLINE

The engineer has a choice of building with proteins, peptides, polymers, nucleic acids, lipids, metals and minerals, each class containing tremendous diversity within its category. While the platforms are diverse, they can be unified by a common goal: to engineer nano- and micro-scale order to improve functionality.[82] In doing so, self-assembling systems aim to bring the lessons learned from the order in natural systems[83] into the therapeutics, materials, and electronics that society uses every day. This work is guided by the principle that if one is to build, he or she must understand all aspects of the building material. Therefore, it is important to pair fundamental studies of the materials systems with application-oriented work.

Motivation

D,L-cyclic peptides have been studied for over two decades, but their mechanical properties and their use as a structural component within bulk materials remains largely unexplored. While there appears to be a growing interest in their properties as evidenced by recent computational analyses[84,85,86], there have been no direct measurements. As

amyloids represent some of the stiffest known protein-based materials, we hypothesized that the similarly structured DLCP assemblies will also exhibit high modulus and strength. Furthermore, due to their organic nature they are inherently low density, making them an interesting candidate for fillers in high-performance composites in which weight should be minimized. The unusual ability of DLCPs to position functional groups precisely in space, coupled with their relatively straightforward synthesis, make them well-suited to study the combined effects of geometry and sequence on mechanical properties. Whether the eventual material is to be used for tissue engineering, filtration, ion detection, or any number of other applications, understanding the mechanical impact of incorporating DLCPs as a filler will inform the design decisions.

Hypothesis and Specific Aims

Hypothesis: D,L-cyclic peptides are a mechanically robust class of materials that maintain their stiffness and strength across nano- and micro- length scales. When mixed with a matrix, they are able to act as a mechanical filler, increasing the average stiffness of the bulk material.

Aim 1: To characterize the structure, modulus, and strength of cyclo-[(Gln-D-Leu)$_4$], assemblies across nano- and micro- length scales.

Aim 2: To assess the ability of cyclo-[(Gln-D-Leu)$_4$] assemblies to enhance the elastic modulus of a non-woven mesh of poly-d,l-lactic acid nanofibers.

General Strategy and Outline

Aim 1 will be achieved through the synthesis, assembly, and characterization of cyclo-[(Gln-D-Leu)$_4$] assemblies. Computational modeling, nanoscale depth-sensing indentation, and microscale bending experiments will provide an understanding of the mechanical properties from the atom-scale to the microscale. The structure of the assembly will be characterized through light and electron miscroscopy as well infrared and Raman spectroscopy. The data relating to Aim 1 is presented in Chapter 2.

Aim 2 will be achieved through the electrospinning[87] of composite nanofibers in which poly-d,l-lactic acid forms the matrix and cyclo-[(Gln-D-Leu)$_4$] structures form the filler. Differing weight percentages, sizes, and qualities of filler will be embedded within the fibers. The fibers will be characterized through electron microscopy, infrared spectroscopy, and nanoscale afm-based compressive analysis. To confirm the identity of the peptide filler, fibers are subjected to electron dispersive spectroscopy and are later dissolved so that the peptide filler can be recovered. The data relating to Aim 2 is presented in Chapter 3.

Chapter 4 provides a summary of the results as well as a discussion of future directions. Concluding statements are provided.

1.4 REFERENCES

1. Ashby, M. F.; Gibson, L. J.; Wegst, U., The mechanical properties of natural materials. I. Material property charts. *... of the Royal ...* **1995**.

2. Fratzl, P., *Collagen: Structure and mechanics*. Springer: **2008**.

3. Tao, H.; Kaplan, D. L.; Omenetto, F. G., Silk materials--a road to sustainable high technology. *Advanced materials (Deerfield Beach, Fla.)* **2012,** *24* (21), 2824-2837.

4. Miserez, A.; Li, Y.; Waite, J. H.; Zok, F., Jumbo squid beaks: Inspiration for design of robust organic composites. *Acta Biomaterialia* **2007,** *3* (1), 139-149.

5. Miserez, A.; Weaver, J. C.; Pedersen, P. B.; Schneeberk, T.; Hanlon, R. T.; Kisailus, D.; Birkedal, H., Microstructural and Biochemical Characterization of the Nanoporous Sucker Rings from Dosidicus gigas. *Advanced Materials* **2009,** *21* (4), 401-406.

6. Lin, A. Y.-M.; Chen, P.-Y.; Meyers, M. A., The growth of nacre in the abalone shell. *Acta Biomaterialia* **2008,** *4* (1), 131-138.

7. Broomell, C. C.; Zok, F. W.; Waite, J. H., Role of transition metals in sclerotization of biological tissue. *Acta Biomaterialia* **2008,** *4* (6), 2045-2051.

8. Wegst, U. G. K.; Ashby, M. F., The mechanical efficiency of natural materials. *Philosophical Magazine* **2004,** *84* (21), 2167-2186.

9. Lintz, E. S.; Scheibel, T. R., Dragline, Egg Stalk and Byssus: A Comparison of Outstanding Protein Fibers and Their Potential for Developing New Materials. *Advanced Functional Materials* **2013,** *23* (36), 4467-4482.

10. Porter, D.; Vollrath, F., Silk as a Biomimetic Ideal for Structural Polymers. *Advanced Materials* **2009,** *21* (4), 487-492.

11. Hynes, R. O., The Extracellular Matrix: Not Just Pretty Fibrils. *Science* **2009,** *326* (5957), 1216-1219.

12. Broomell, C. C.; Chase, S. F.; Laue, T.; Waite, J. H., Cutting Edge Structural Protein from the Jaws of Nereis virens. *Biomacromolecules* **2008,** *9* (6), 1669-1677.

13. Amini, S.; Miserez, A., Wear and abrasion resistance selection maps of biological materials. *Acta Biomaterialia* **2013,** *9* (8), 7895-7907.

14. Ulijn, R. V.; Woolfson, D. N., Peptide and protein based materials in 2010: from design and structure to function and application. *Chemical Society Reviews* **2010,** *39* (9), 3349-3350.

15. Keene, E. C.; Evans, J. S.; Estroff, L. A., Matrix Interactions in Biomineralization: Aragonite Nucleation by an Intrinsically Disordered Nacre Polypeptide, n16N, Associated with a β-Chitin Substrate. *Crystal Growth & Design* **2010,** *10* (3), 1383-1389.

16. Rubin, D. J.; Miserez, A.; Waite, J. H., Diverse strategies of protein sclerotization in marine invertebrates: structure–property relationships in natural biomaterials. *Advances in Insect Physiology* **2010,** *38*, 75-133.

17. Pope, F.; Nicholls, A.; Narcisi, P.; Temple, A.; Chia, Y.; Fryer, P.; PAEPE, A.; GROOTE, W.; McEwan, J.; Compston, D., Type III collagen mutations in Ehlers Danlos syndrome type IV and other related disorders. *Clinical and experimental dermatology* **1988,** *13* (5), 285-302.

18. Chiti, F.; Dobson, C. M., Protein misfolding, functional amyloid, and human disease. *Annual Review of Biochemistry* **2006,** *75* (1), 333-366.

19. Kastelic, J.; Galeski, A.; Baer, E., The multicomposite structure of tendon. *Connective tissue research* **1978,** *6* (1), 11-23.

20. Kastelic, J.; Palley, I.; Baer, E., A structural mechanical model for tendon crimping. *Journal of biomechanics* **1980,** *13* (10), 887-893.

21. Caves, J. M.; Kumar, V. A.; Xu, W.; Naik, N.; Allen, M. G.; Chaikof, E. L., Microcrimped Collagen Fiber-Elastin Composites. *Advanced Materials* **2010,** *22* (18), 2041-2044.

22. Meyers, M. A.; Chen, P.-Y.; Lin, A. Y.-M.; Seki, Y., Biological materials: Structure and mechanical properties. *Progress in Materials Science* **2008,** *53* (1), 1-206.

23. Keten, S.; Xu, Z.; Ihle, B.; Buehler, M. J., Nanoconfinement controls stiffness, strength and mechanical toughness of beta-sheet crystals in silk. *Nature Materials* **2010,** *9* (4), 359-367.

24. Xu, M.; Lewis, R. V., Structure of a protein superfiber: spider dragline silk. *Proceedings of the National Academy of Sciences of the United States of America* **1990,** *87* (18), 7120-7124.

25. Vollrath, F.; Knight, D. P., Liquid crystalline spinning of spider silk. *Nature* **2001,** *410* (6828), 541-548.

26. Hartgerink, J. D.; Beniash, E.; Stupp, S. I., Self-Assembly and Mineralization of Peptide-Amphiphile Nanofibers. *Science* **2001,** *294* (5547), 1684-1688.

27. Ashkenasy, N.; Horne, W. S.; Ghadiri, M. R., Design of Self‐Assembling Peptide Nanotubes with Delocalized Electronic States. *Small* **2006,** *2* (1), 99-102.

28. Hamley, I. W., Peptide Nanotubes. *Angewandte Chemie International Edition* **2014,** *53* (27), 6866-6881.

29. Hamley, I., Self-assembly of amphiphilic peptides. *Soft Matter* **2011,** *7* (9), 4122-4138.

30. Cui, H.; Webber, M. J.; Stupp, S. I., Self‐assembly of peptide amphiphiles: From molecules to nanostructures to biomaterials. *Peptide Science* **2010,** *94* (1), 1-18.

31. Kokkoli, E.; Mardilovich, A.; Wedekind, A.; Rexeisen, E. L.; Garg, A.; Craig, J. A., Self-assembly and applications of biomimetic and bioactive peptide-amphiphiles. *Soft Matter* **2006,** *2* (12), 1015-1024.

32. Martinez, J.; Zhang, G.; Holt, P.; Jung, H.-T.; Carrano, C.; Haygood, M.; Butler, A., Self-assembling amphiphilic siderophores from marine bacteria. *Science* **2000,** *287* (5456), 1245-1247.

33. Dehsorkhi, A.; Castelletto, V.; Hamley, I. W., Self-assembling amphiphilic peptides. *Journal of Peptide Science* **2014,** *20* (7), 453-467.

34. Hamley, I. W., *Introduction to soft matter: synthetic and biological self-assembling materials*. John Wiley & Sons: 2008.

35. Paramonov, S. E.; Jun, H.-W.; Hartgerink, J. D., Self-assembly of peptide-amphiphile nanofibers: the roles of hydrogen bonding and amphiphilic packing. *Journal of the American Chemical Society* **2006,** *128* (22), 7291-7298.

36. Löwik, D. W. P. M.; Leunissen, E. H. P.; van den Heuvel, M.; Hansen, M. B.; van Hest, J. C. M., Stimulus responsive peptide based materials. *Chemical Society Reviews* **2010,** *39* (9), 3394.

37. Berkov-Zrihen, Y.; Herzog, I. M.; Feldman, M.; Sonn-Segev, A.; Roichman, Y.; Fridman, M., Di-alkylated paromomycin derivatives: Targeting the membranes of Gram positive pathogens that cause skin infections. *Bioorganic & medicinal chemistry* **2013,** *21* (12), 3624-3631.

38. Cheetham, A. G.; Zhang, P.; Lin, Y.-a.; Lock, L. L.; Cui, H., Supramolecular nanostructures formed by anticancer drug assembly. *Journal of the American Chemical Society* **2013,** *135* (8), 2907-2910.

39. Xu, A.-W.; Ma, Y.; Cölfen, H., Biomimetic mineralization. *Journal of Materials Chemistry* **2007,** *17* (5), 415-449.

40. Knowles, T. P. J.; Buehler, M. J., Nanomechanics of functional and pathological amyloid materials. *Nature Nanotechnology* **2011,** *6* (8), 469-479.

41. Selkoe, D. J., Alzheimer's disease: genes, proteins, and therapy. *Physiological Reviews* **2001,** *81* (2), 741-766.

42. Zganec, M.; Zerovnik, E., Amyloid fibrils compared to peptide nanotubes. *Biochimica et biophysica acta* **2014,** *1840* (9), 2944-2952.

43. Zhang, S.; Lockshin, C.; Herbert, A.; Winter, E.; Rich, A., Zuotin, a putative Z-DNA binding protein in Saccharomyces cerevisiae. *The EMBO journal* **1992,** *11* (10), 3787.

44. Zhang, S.; Holmes, T.; Lockshin, C.; Rich, A., Spontaneous assembly of a self-complementary oligopeptide to form a stable macroscopic membrane. *Proceedings of the National Academy of Sciences* **1993,** *90* (8), 3334-3338.

45. Dobson, C. M., Protein folding and misfolding. *Nature* **2003,** *426* (6968), 884-890.

46. Hauser, C. A. E.; Zhang, S., Designer self-assembling peptide nanofiber biological materials. *Chemical Society Reviews* **2010,** *39* (8), 2780-2790.

47. Adamcik, J.; Jung, J.-M.; Flakowski, J.; De Los Rios, P.; Dietler, G.; Mezzenga, R., Understanding amyloid aggregation by statistical analysis of atomic force microscopy images. *Nature Nanotechnology* **2010,** *5* (6), 423-428.

48. Smith, J. F.; Knowles, T. P. J.; Dobson, C. M.; Macphee, C. E.; Welland, M. E., Characterization of the nanoscale properties of individual amyloid fibrils. *Proceedings of the National Academy of Sciences of the United States of America* **2006,** *103* (43), 15806-15811.

49. Adamcik, J.; Lara, C.; Usov, I.; Jeong, J. S.; Ruggeri, F. S.; Dietler, G.; Lashuel, H. A.; Hamley, I. W.; Mezzenga, R., Measurement of intrinsic properties of amyloid fibrils by the peak force QNM method. *Nanoscale* **2012,** *4* (15), 4426-4429.

50. Channon, K. J.; Devlin, G. L.; Macphee, C. E., Efficient Energy Transfer within Self-Assembling Peptide Fibers: A Route to Light-Harvesting Nanomaterials. *Journal of the American Chemical Society* **2009,** *131* (35), 12520-12521.

51. Li, D.; Furukawa, H.; Deng, H.; Liu, C.; Yaghi, O. M.; Eisenberg, D. S., Designed amyloid fibers as materials for selective carbon dioxide capture. *Proceedings of the National Academy of Sciences* **2014,** *111* (1), 191-196.

52. Maji, S. K.; Schubert, D.; Rivier, C.; Lee, S.; Rivier, J. E.; Riek, R., Amyloid as a depot for the formulation of long-acting drugs. *PLoS biology* **2008,** *6* (2), e17.

53. Reches, M.; Gazit, E., Casting metal nanowires within discrete self-assembled peptide nanotubes. *Science* **2003,** *300* (5619), 625-627.

54. Nguyen, P. Q.; Botyanszki, Z.; Tay, P. K. R.; Joshi, N. S., Programmable biofilm-based materials from engineered curli nanofibres. *Nature communications* **2014,** *5*.

55. Chen, A. Y.; Deng, Z.; Billings, A. N.; Seker, U. O.; Lu, M. Y.; Citorik, R. J.; Zakeri, B.; Lu, T. K., Synthesis and patterning of tunable multiscale materials with engineered cells. *Nature materials* **2014**.

56. Waters, M. L., Aromatic interactions in model systems. *Current opinion in chemical biology* **2002,** *6* (6), 736-741.

57. Azuri, I.; Adler-Abramovich, L.; Gazit, E.; Hod, O.; Kronik, L., Why are diphenylalanine-based peptide nanostructures so rigid? Insights from first principles calculations. *Journal of the American Chemical Society* **2014,** *136* (3), 963-969.

58. SEDMAN, V. L.; CHEN, X.; ALLEN, S.; ROBERTS, C. J.; KOROLKOV, V. V.; TENDLER, S. J. B., Tuning the mechanical properties of self-assembled mixed-peptide tubes. *Journal of Microscopy* **2013,** *249* (3), 165-172.

59. Fichman, G.; Gazit, E., Self-assembly of short peptides to form hydrogels: design of building blocks, physical properties and technological applications. *Acta Biomaterialia* **2014,** *10* (4), 1671-1682.

60. Kol, N.; Adler-Abramovich, L.; Barlam, D.; Shneck, R. Z.; Gazit, E.; Rousso, I., Self-assembled peptide nanotubes are uniquely rigid bioinspired supramolecular structures. *Nano Lett* **2005,** *5* (7), 1343-1346.

61. Niu, L.; Chen, X.; Allen, S.; Tendler, S. J., Using the bending beam model to estimate the elasticity of diphenylalanine nanotubes. *Langmuir* **2007,** *23* (14), 7443-7446.

62. Song, Y.; Challa, S. R.; Medforth, C. J.; Qiu, Y.; Watt, R. K.; Peña, D.; Miller, J. E.; van Swol, F.; Shelnutt, J. A., Synthesis of peptide-nanotube platinum-nanoparticle composites. *Chem. Commun.* **2004,** (9), 1044-1045.

63. Even, N.; Adler-Abramovich, L.; Buzhansky, L.; Dodiuk, H.; Gazit, E., Improvement of the Mechanical Properties of Epoxy by Peptide Nanotube Fillers. *Small* **2011,** *7* (8), 1007-1011.

64. Yan, X.; Zhu, P.; Li, J., Self-assembly and application of diphenylalanine-based nanostructures. *Chemical Society Reviews* **2010,** *39* (6), 1877-1890.

65. Ketchem, R.; Hu, W.; Cross, T., High-resolution conformation of gramicidin A in a lipid bilayer by solid-state NMR. *Science* **1993,** *261* (5127), 1457-1460.

66. Langs, D. A., Three-dimensional structure at 0.86 A of the uncomplexed form of the transmembrane ion channel peptide gramicidin A. *Science* **1988,** *241* (4862), 188-191.

67. Valéry, C.; Paternostre, M.; Robert, B.; Gulik-Krzywicki, T.; Narayanan, T.; Dedieu, J.-C.; Keller, G.; Torres, M.-L.; Cherif-Cheikh, R.; Calvo, P., Biomimetic organization: Octapeptide self-assembly into nanotubes of viral capsid-like dimension. *Proceedings of the National Academy of Sciences* **2003,** *100* (18), 10258-10262.

68. Namba, K.; Pattanayek, R.; Stubbs, G., Visualization of protein-nucleic acid interactions in a virus: Refined structure of intact tobacco mosaic virus at 2.9 Å resolution by X-ray fiber diffraction. *Journal of molecular biology* **1989,** *208* (2), 307-325.

69. De Santis, P.; Morosetti, S.; Rizzo, R., Conformational analysis of regular enantiomeric sequences. *Macromolecules* **1974,** *7* (1), 52-58.

70. Ghadiri, M.; Granja, J.; Milligan, R.; McRee, D.; Khazanovich, N., Self-Assembling Organic Nanotubes Based on a Cyclic Peptide Architecture (Vol 366, Pg 324, 1993). *Nature* **1994,** *372* (6507), 709-709.

71. Ghadiri, M. R.; Granja, J. R.; Milligan, R. A.; McRee, D. E.; Khazanovich, N., Self-assembling organic nanotubes based on a cyclic peptide architecture. *Nature* **1993,** *366* (6453), 324-327.

72. Gademann, K.; Ernst, M.; Hoyer, D.; Seebach, D., Synthesis and Biological Evaluation of a Cyclo - β - tetrapeptide as a Somatostatin Analogue. *Angewandte Chemie International Edition* **1999,** *38* (9), 1223-1226.

73. Amorín, M.; Castedo, L.; Granja, J. R., New cyclic peptide assemblies with hydrophobic cavities: the structural and thermodynamic basis of a new class of peptide nanotubes. *Journal of the American Chemical Society* **2003,** *125* (10), 2844-2845.

74. Chapman, R.; Danial, M.; Koh, M. L.; Jolliffe, K. A.; Perrier, S., Design and properties of functional nanotubes from the self-assembly of cyclic peptide templates. *Chemical Society Reviews* **2012,** *41* (18), 6023-6041.

75. Hartgerink, J. D.; Granja, J. R.; Milligan, R. A.; Ghadiri, M. R., Self-assembling peptide nanotubes. *Journal of the American Chemical Society* **1996,** *118* (1), 43-50.

76. Wang, F.; Qin, L.; Wong, P.; Gao, J., Effects of lysine methylation on gramicidin A channel folding in lipid membranes. *Peptide Science* **2013,** *100* (6), 656-661.

77. McMurray, J. S., Solid phase synthesis of a cyclic peptide using Fmoc chemistry. *Tetrahedron Letters* **1991,** *32* (52), 7679-7682.

78. Fernandez-Lopez, S.; Kim, H. S.; Choi, E. C.; Delgado, M.; Granja, J. R.; Khasanov, A.; Kraehenbuehl, K.; Long, G.; Weinberger, D. A.; Wilcoxen, K. M.; Ghadiri, M. R., Antibacterial agents based on the cyclic D,L-alpha-peptide architecture. *Nature* **2001,** *412* (6845), 452-455.

79. Motesharei, K.; Ghadiri, M. R., Diffusion-limited size-selective ion sensing based on SAM-supported peptide nanotubes. *Journal of the American Chemical ...* **1997,** *119* (46), 11306-11312.

80. Xu, T.; Zhao, N.; Ren, F.; Hourani, R.; Lee, M. T.; Shu, J. Y.; Mao, S.; Helms, B. A., Subnanometer Porous Thin Films by the Co-assembly of Nanotube Subunits and Block Copolymers. *ACS Nano* **2011,** *5* (2), 1376-1384.

81. Rubin, D. J.; Nia, H. T.; Desire, T.; Nguyen, P. Q.; Gevelber, M.; Ortiz, C.; Joshi, N. S., Mechanical Reinforcement of Polymeric Fibers through Peptide Nanotube Incorporation. *Biomacromolecules* **2013,** *14* (10), 3370-3375.

82. Ruokolainen, J.; Mäkinen, R.; Torkkeli, M.; Mäkelä, T.; Serimaa, R.; Ten Brinke, G.; Ikkala, O., Switching supramolecular polymeric materials with multiple length scales. *Science* **1998,** *280* (5363), 557-560.

83. Lakes, R., Materials with structural hierarchy. *Nature* **1993,** *361* (6412), 511-515.

84. Diaz, J. A. C.; Çağin, T., Thermo-mechanical stability and strength of peptide nanostructures from molecular dynamics: self-assembled cyclic peptide nanotubes. *Nanotechnology* **2010,** *21*, 115703.

85. Ruiz, L.; Keten, S., Atomistic modeling and mechanics of self-assembled organic nanotubes. *International Journal of Applied Mechanics* **2011,** *3* (04), 667-684.

86. Ruiz, L.; Keten, S., Multiscale Modeling of Elasticity and Fracture in Organic Nanotubes. *Journal of Engineering Mechanics* **2012,** *140* (3), 431-442.

87. Pham, Q. P.; Sharma, U.; Mikos, A. G., Electrospinning of polymeric nanofibers for tissue engineering applications: a review. *Tissue engineering* **2006,** *12* (5), 1197-1211.

2. Structural, Nanomechanical and Computational Characterization of D,L-Cyclic Peptide Assemblies

Daniel J. Rubin[‡1,2], Shahrouz Amini[‡3,4], Feng Zhou[3], Haibin Su[3], Ali Miserez[3,4,5], *Neel S. Joshi[1,2]

[1]Harvard University, School of Engineering and Applied Sciences

[2]Wyss Institute for Biologically Inspired Engineering

[3]Nanyang Technological University, School of Materials Science and Engineering

[4]Nanyang Technological University, Center for Biomimetic Sensor Science

[5]Nanyang Technological University, School of Biological Sciences

[‡] These authors contributed equally to this work

*njoshi@seas.harvard.edu

The proceeding chapter has been adapted from a study submitted for publication in the journal *ACS Nano*.

2.1 ABSTRACT

The rigid geometry and tunable chemistry of D,L-cyclic peptides make them an intriguing building-block for the rational design of nano- and microscale hierarchically structured materials. Herein, we utilize a combination of electron microscopy, nanomechanical characterization including depth sensing-based bending experiments, and molecular modeling methods to obtain the structural and mechanical characteristics of cyclo-[(Gln-D-Leu)$_4$] (QL4) assemblies. QL4 monomers assemble to form large, rod-like structures with diameters up to 2 μm and lengths of 10s to 100s of μm. Image analysis suggests that large assemblies are hierarchically organized from individual tubes that undergo bundling to form larger structures. With an elastic modulus of 11.3 ± 3.3 GPa, hardness of 387 ± 136 MPa and strength (bending) of 98 ± 19 MPa the peptide crystals are among the most robust known proteinaceous

micro- and nano-fibers. The measured bending modulus of micron-scale fibers (10.5 ± 0.9 GPa) is in the same range as the Young's modulus measured by nanoindentation indicating that the robust nanoscale network from which the assembly derives its properties is preserved at larger length-scales. Materials selection charts are used to demonstrate the particularly robust properties of QL4 including its specific flexural modulus in which it outperforms a number of biological proteinaceous and non-proteinaceous materials including collagen and enamel. The facile synthesis, high modulus, and low density of QL4 fibers indicate that they may find utility as a filler material in a variety of high efficiency, biocompatible composite materials. This study represents the first experimental mechanical characterization of D,L-cyclic peptide assemblies.

2.2 INTRODUCTION

Research into the structure, chemistry and functionality of biomaterials has accelerated in recent years with the goal of creating environmentally benign materials that have optimized physical and mechanical properties[1]. Many of these materials (*e.g.* silks[2,3], collagens[4,5]) derive their properties from protein constituents[6], which form specific secondary structures that assemble into higher order structures with robust yet efficient mechanical behavior.[7] Another class of proteinaceous materials, amyloid fibrils, are particularly interesting because they can be formed from many different protein sequences.[8] Amyloids were first studied in conjunction with neurodegenerative diseases such as Alzheimers[9], but newly discovered amyloidogenic gene products are increasingly being associated with functional (as opposed to pathogenic) biological performance.[10] Amyloids are classified by their fibrillar

structure in which β-strands associate to form an extended network of supramolecular β-sheets perpendicular to the long-axis of the fiber.[11] This structural motif is intriguing in that it is largely defined by the properties of the peptide backbone itself, namely the propensity for hydrogen bonding between carbonyl oxygen and amide hydrogen[12]. This allows a variety of different proteins, when subjected to various denaturing and assembly processes, to form amyloid-like structures.[13] These nanoscale fibrils, self-assembled from individual protein and peptide molecules, continue to grow and form robust fibers with hierarchical order. Indeed, the dense hydrogen bonding and ordered structure of amyloid materials renders them among the most robust known proteinaceous materials with experimentally determined Young's moduli at the nanoscale in the range of 2-4 GPa.[14,15] The combination of self-assembly, nanoscale order and high stiffness provides a breadth of potential applications including light-harvesting[16], carbon capture[17], drug delivery[18], and nanowire fabrication.[19]

D,L-cyclic peptides (DLCPs) share certain characteristics with amyloid fibrils including self-assembly, dense intermolecular hydrogen bonding along the peptide backbone, and chemical and mechanical stability. However, their molecular structure and geometry allow for an enhanced ability to chemically modify the monomers or to guide assembly.[20] The peptide cycles are composed of six to ten amino acids with alternating D- and L-stereochemistry, causing a planar geometry in which the amino acid side chains radiate from the center of the ring and the amide backbone is perpendicular to the plane of the ring. This geometrical arrangement promotes their assembly into high aspect ratio nano- and microstructures through β-sheet-like hydrogen bonding in which each ring sits flat on the surface of another ring (Figure 2.1a). Unlike linear amyloids in which β-sheets are able to slide with respect to one

another[21], DLCP assemblies are only able to stack directly atop each other. Depending on the sequence of the peptides, the nanotubes may also associate laterally into bundles to create structures that can be microns in width and hundreds of microns in length.[22]

The assembly of cyclic peptides was first theorized by De Santis et al.[23] and later demonstrated using a pH sensitive peptide 8-mer that was found to assemble into large, micron-scale fibers.[20] As DLCPs are synthesized via common solid-state peptide synthesis methods[24], one has the freedom to explore limitless combinations of amino acids and post-synthetic modifications. This versatility has been leveraged to study DLCPs in a variety of applications including structural antibiotics[25], ion channels[26], selective ion transporters[27], and reinforcing agents.[28] Additional research has focused on the fundamental properties of cyclic peptides including the thermodynamics of assembly and the breadth of structural flexibility.[29] One area that remains largely unexplored is the utility of cyclic peptides as structural components of composite materials, perhaps because there is little information on the mechanical properties of DLCP structures themselves. While a computational analysis of DLCP structures indicates that they are quite stiff[30], there have been no direct measurements of their mechanical properties. As amyloids represent some of the stiffest known protein-based materials, we hypothesized that the similarly structured DLCP assemblies would also exhibit high modulus and strength. The unusual ability of DLCPs to position functional groups precisely in space, coupled with their relatively straightforward synthesis, make them well suited to study the combined effects of geometry and sequence on mechanical properties. Such a study would provide essential information for downstream applications of DLCPs such as medical devices, and tissue scaffolds.

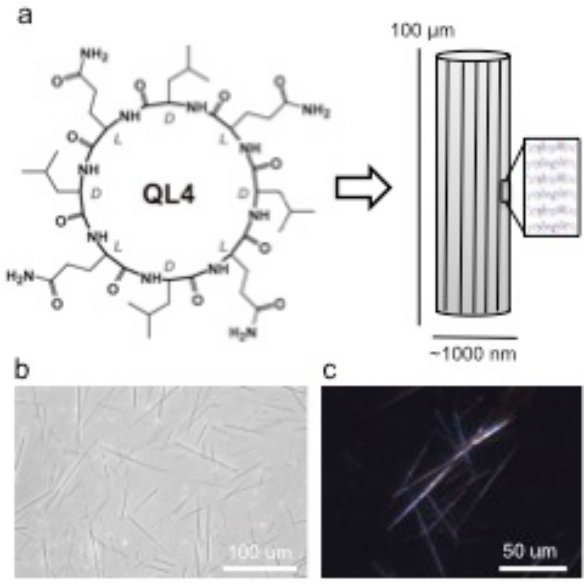

Figure 2.1. QL4 structure and assembly. (a) Chemical structure of QL4 and schematic of QL4 fiber. (b) Optical micrograph of QL4 fibers highlighting the size and rod-like structure. (c) Polarized light micrograph indicating that there is nanoscale order present in large QL4 structures.

In this study we demonstrate that assemblies of the DLCP cyclo-[(Gln-D-Leu)$_4$], abbreviated here as QL4, are among the stiffest and strongest known peptide-based materials. This was accomplished through computational, structural and nanomechanical analyses including molecular dynamics simulations, electron microscopy, nanoindentation, and micro-bending studies. QL4 was selected because it is known to form assemblies, herein referred to as fibers, that are large and stable enough to be probed with accessible nanomechanical probe tools. This particular DLCP has also been shown to increase the elastic modulus of polylactides when incorporated as the filler component of a composite fiber.[28] While previous attempts at molecular dynamics simulations have given clues regarding the elastic modulus of a DLCP assembly,[30] this study represents the first experimental characterization of the mechanical properties of DLCP fibers.

2.3 RESULTS AND DISCUSSION

Synthesis, Assembly and Structure of QL4 Fibers

QL4 was synthesized (Figure 2.2), dissolved in neat trifluoroacetic acid and incubated in the presence of milli-Q water in a closed vessel.

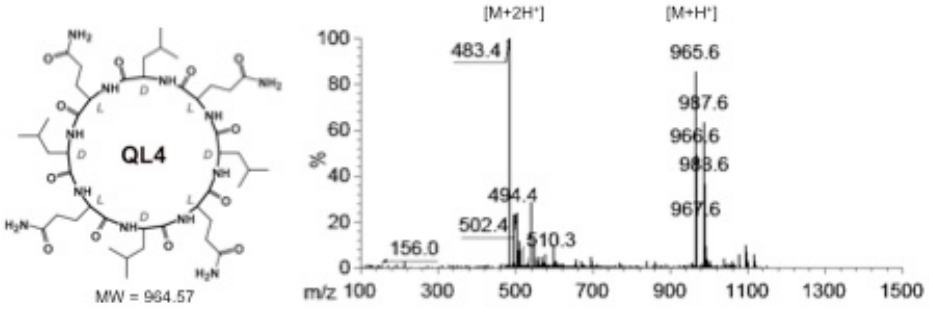

Figure 2.2. Synthesis and confirmation of cyclo-[$(QL)_4$] mass. [left] QL4 structure and molecular weight. [right] A singly charged [$M+H^+$] QL4 ion is visible at 965.6 m/z and the doubly charged [$M+2H^+$] is visible at 483.4 m/z.

Over the course of approximately 72 hours, QL4 assemblies formed at the surface of the solution and were visualized with an optical microscope in bright field mode (Figure 2.1b). Some QL4 fibers reach 100s of microns in length while maintaining nanoscale order, which is indicated by their birefringence demonstrated under cross-polarized light (Figure 2.1c). It is evident from the size of the structures that an individual fiber is composed of thousands of individual nanotubes assembling laterally. The hydrogen-bonded network is apparent through the specific shift in the Amide I band of the Raman spectrum, which is similar to that of β-sheets[22,31] (Figure 2.3).

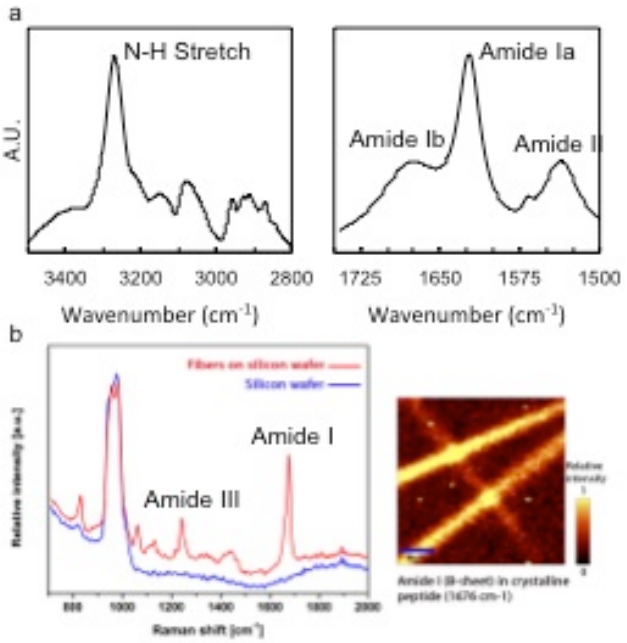

Figure 2.3. FTIR and Raman Spectroscopy of QL4 Fibers. (a) [left] The characteristic N-H stretching frequency at 3278 cm^{-1} indicates a hydrogen bonded network with an average intersubunit distance of 4.7-4.8 Å,[32] providing evidence that QL4 fibers are composed of peptide nanotubes. [right] In concordance with prior literature, Amide 1a, Amide 1b, and Amide II are present at 1629 cm^{-1}, 1688 cm^{-1}, and 1540 cm^{-1}, respectively.[32] (b) [left] Characteristic Raman spectra of an assembled QL4 fiber. Strong peaks at 1242 cm^{-1} and 1676 cm^{-1} correspond to Amide III and Amide I beta sheet signals, respectively.[31] [right] Raman map of peptide assemblies obtained by monitoring the intensity of the amide peak at 1676 cm^{-1}.

SEM analysis of the QL4 fibers indicates that there are two classes of assembled structures, those which are not bundled and have diameters on the order of ~100 nm and those that are bundled and have diameters on the order of a few microns (Figure 2.4a). Present within the larger bundles are striations that indicate a bundle is composed of several ~100 nm assemblies. Furthermore, within larger bundles, one observes gaps in which fibers have broken free as is highlighted in Figure 2.4b, indicating that the ~100 nm assemblies are discrete elements in the larger bundle. We hypothesize that this bundling may occur naturally due to hydrophobic effects between the surfaces of QL4 assemblies in an increasingly aqueous environment

during the assembly process or, alternatively, may be a function of the evaporation necessary in sample preparation. High-resolution TEM micrographs of non-bundled fibers show striations with thicknesses of approximately 2nm along the long-axis of the fiber, providing evidence that the QL4 fibers are composed of individual DLCP nanotubes (Figure 2.4c and d). Taken together, this information suggests that there are three levels of hierarchy in a large QL4 assembly: Individual tube (~ 2nm diameter), fiber (~ 100nm diameter), and bundled fiber (~ 1μm diameter) (Figure 2.4e). While it is possible to verify the existence of the fiber, and bundled fiber, we have not obtained evidence that individual QL4 tubes exist in solution. Prior work has shown that conjugation of polymers to the DLCP side chains can lead to stable assemblies of individual DLCP tubes,[27, 33] however, we have found that without modification, individual tubes continue to grow until a larger fiber or bundled fiber is formed.

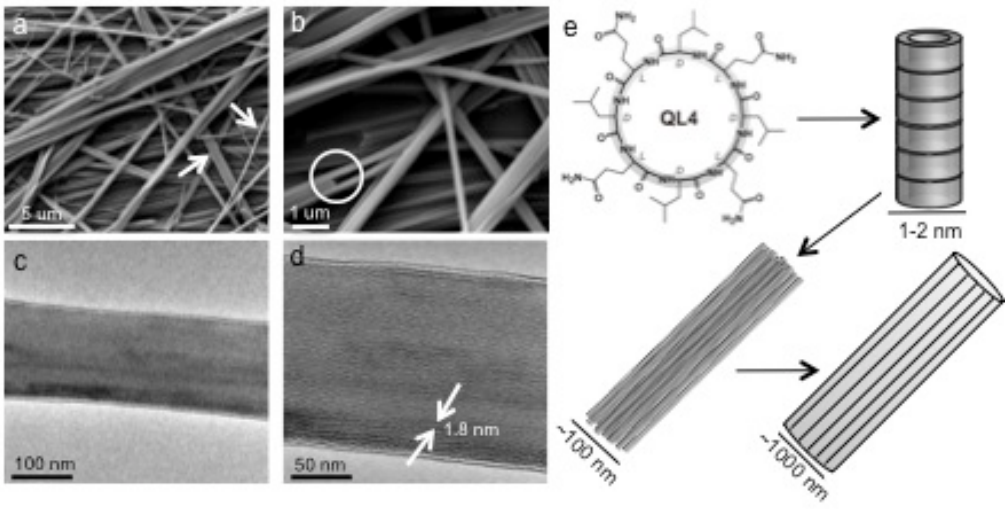

Figure 2.4. Structure of QL4 fibers. (a and b) Scanning electron micrographs highlight two major classes of fibers, single fibers (~100nm diameter) and bundled fibers (~1μm diameter). Bundled fibers have characteristic striations and points of fracture in which a single fiber was removed from the bundle. (c and d) High-resolution transmission electron micrographs indicate that single nanotubes (~2nm diameter) are the building blocks of individual fibers. (e) A schematic representation of the hierarchical order present in a large, bundled QL4 fiber.

Theoretical Structure, Stiffness and Density

Through molecular dynamics simulations, we obtained a theoretically ideal structure for QL4 fibers and used this as a reference for both structural and mechanical analyses. In this work, we employed the COMPASS force field (Condensed-phase Optimized Molecular Potentials for Atomistic Simulation Studies) - developed by H. Sun[34], to optimize the geometry and calculate the energy of all molecules. The COMPASS force field is based on state-of-the-art ab initio and empirical parametrization techniques. The valence parameters and atomic partial charges were supported by ab initio data, and the van der Waals (vdW) parameters were derived by fitting the experimental data of cohesive energies and equilibrium densities.

The convergence tolerance is $2x10^{-5}$ kcal/mol for the energy, 0.001 kcal/mol/Å for the force, 0.001 GPa for the stress and 10^{-5} Å for the displacement. The Ewald method is used for calculating the electrostatic and the van der Waals terms. The accuracy is 10^{-5} kcal/mol. The repulsive cutoff is 6 Å for the van der Waals term. For the periodical structure, the box vectors are also optimized together with the molecules. The Mechanical Properties are calculated by applying strain using static approach. The elastic constants were calculated from a polynomial fit to the calculated stress–strain relation.

Along the longitudinal axis of assembly, QL4 monomers assemble through the creation of 12 hydrogen bonds, 8 along the peptide backbone and 4 mediated by glutamine sidechains, locking the monomers together along the z-axis (Figure 2.5). As discussed above, there is less freedom in the stacking of DLCPs than is present for a linear amyloid molecule. This forces the DLCP monomers to stack directly atop one

another, maximizing the density of hydrogen bonds along the length of the tube. When considering the rotational register of one DLCP monomer to its bonding partner, one finds that they can only stack in four orientations, 0°, 90°, 180°, and 270°. In the case of QL4, this means that glutamine residues are always aligned directly atop other glutamine residues (and likewise for leucine residues).

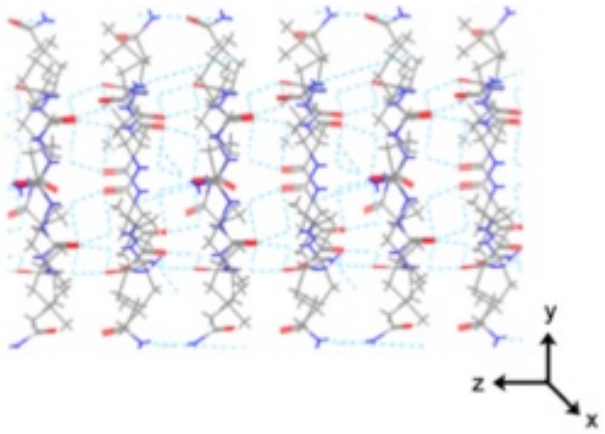

Figure 2.5. Molecular dynamics simulation of assembled QL4 tube. A single nanotube assembles by forming anti-parallel β-sheet-like structures in which each monomer is connected to its neighbor via 8 hydrogen bonds along its peptide backbone. Amino acid side chains are free for lateral (x- and y- axis) and longitudinal (z-axis) interactions.

When considering the lateral assembly (x and y dimensions), two related conformers were examined in parallel. As described in Figure 2.6, Model 1 and Model 2 are both square-packed structures. In Model 1, the amide functional group of glutamine residues point to the center of the structure, while in Model 2, the tubes are each rotated 45 degrees so that leucine side chains are turned toward the center. This shift in structure results in differing free energies and differing mechanical properties. The structure, and theoretical elastic moduli of each model are discussed for both Model 1 and Model 2 below.

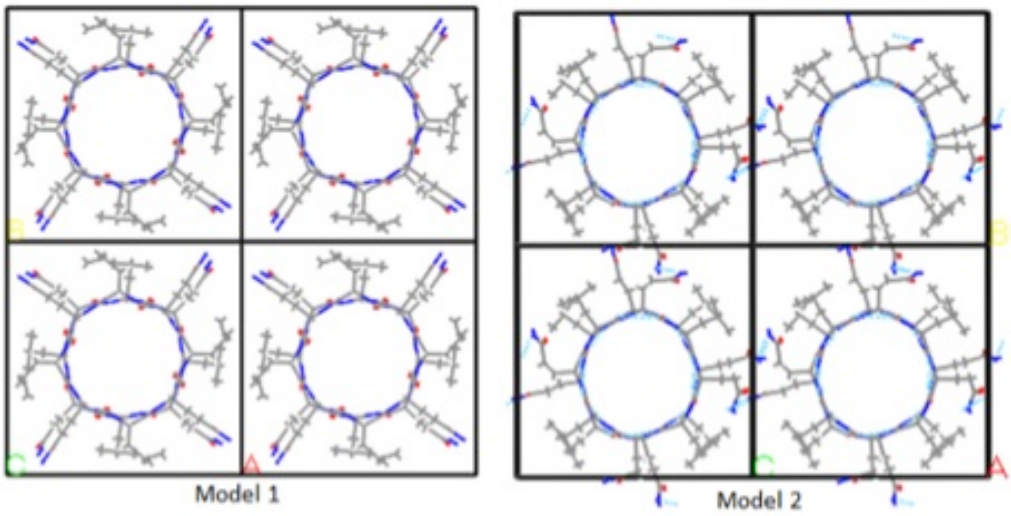

Figure 2.6. Structures of Model 1 and Model 2. Model 1 and Model 2 are closely related, each allows for lateral hydrogen bodning between tubes. In Model 1, these hydrogen bonds occur in the area between the 4 tubes while in Model 2, they interact in side-by-side bonding between neighboring tubes.

A detailed analysis of Model 1 is presented in Figure 2.7. The hydrogen bonded peptide subunits are stacked tightly in an ideal antiparallel β-sheet-like arrangement. Along the z-axis there are eight hydrogen bonds of 2.05-2.10 Å between the backbone of subunits and four hydrogen bonds of 1.98 Å between the sidechains of subunits, this supports the presence of the highly ordered periodicity along the z-axis. The spacing of the unit cell along the Z-axis is calculated to be 9.62 Å. The lateral packing (x and y dimension) is stabilized by both leucine mediated hydrophobic interactions and glutamine mediated hydrogen bonds. The hydrogen bond lengths are 2.30 Å between each of the 4 bonding pairs in the structure. The spacing in the unit cell for both the x and y dimensions is equal to 17.73 Å.

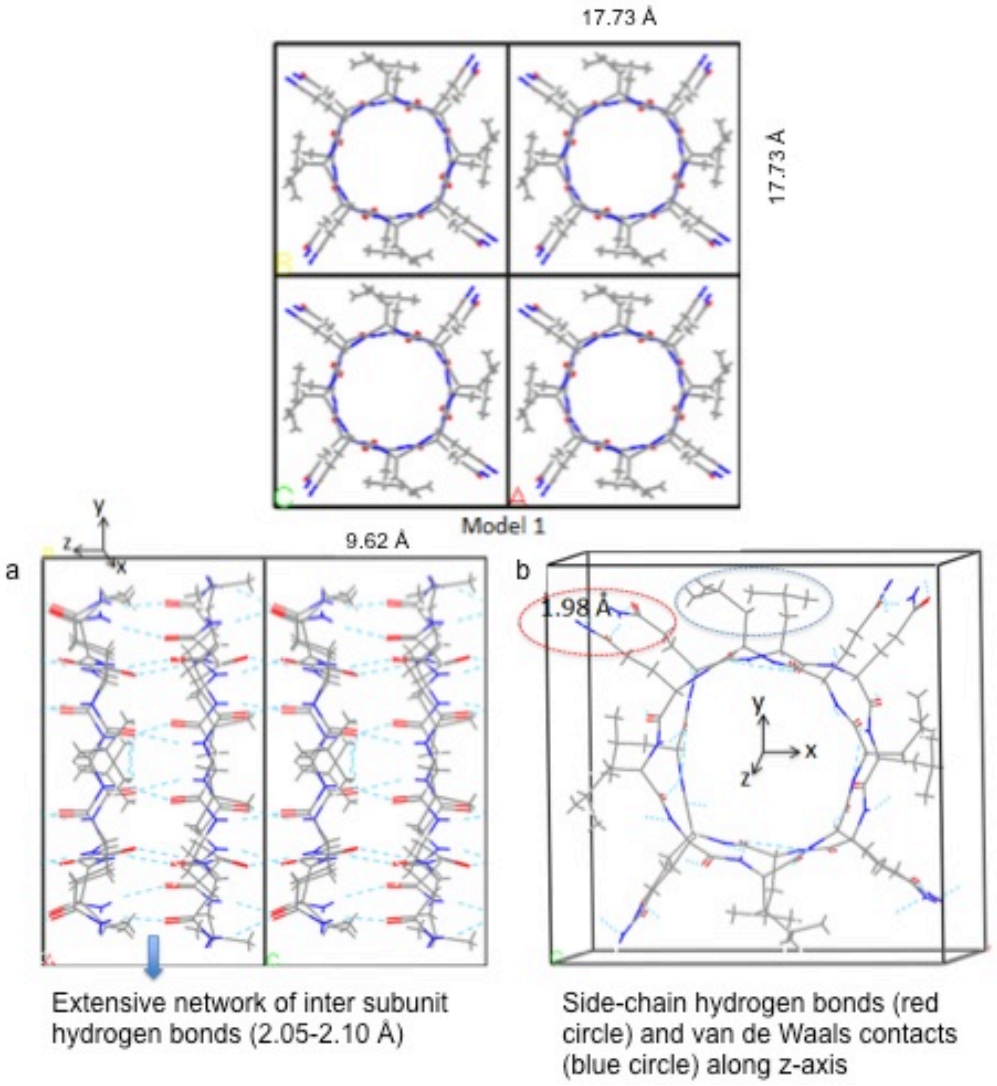

Figure 2.7. Model 1 in detail. [top] Model 1 copied from Figure 2.6. (a) Hydrogen bond orientation and distance between the backbones of peptide cycles. (b) Hydrogen bond orientation between the glutamine sidechains in the longitudinal (z-axis) direction.

Figure 2.8 describes Model 2 in detail. In Model 2, the spacing along the x-, y- and z- axes is changed due to the rotated tube orientation. Along the z-axis, the unit cell is expanded from 9.62 Å to 9.92 Å and the hydrogen bond distance increases by approximately 0.2 Å for both the backbone and sidechain hydrogen bonds. This is a somewhat unexpected result because the longitudinal stacking of the individual

peptide monomers may be assumed to be independent of the lateral assembly, however the model suggests that this is not the case. To minimize the overall energy of the structure, the spacing along the z-axis must change to accommodate the potential for bonding in the x and y planes. Along the x-axis, the unit cell is expanded from 17.73 Å to 17.94 Å. Along the y-axis, the spacing is increased further from 17.73 Å to 18.11 Å. This creates anisotropy between all three axes, x, y and z. Generally speaking, Model 2 is a less compact structure in which hydrogen bonds are weakened due to the increased distance between donor and acceptor pairs along all three assembly axes. This results in a structure that is less stable overall and possesses a total energy calculated to be 67.6 kcal/mol higher than that of Model 1. For each model, the expected density is approximately 1000 kg/m^3, roughly equal to that of water.

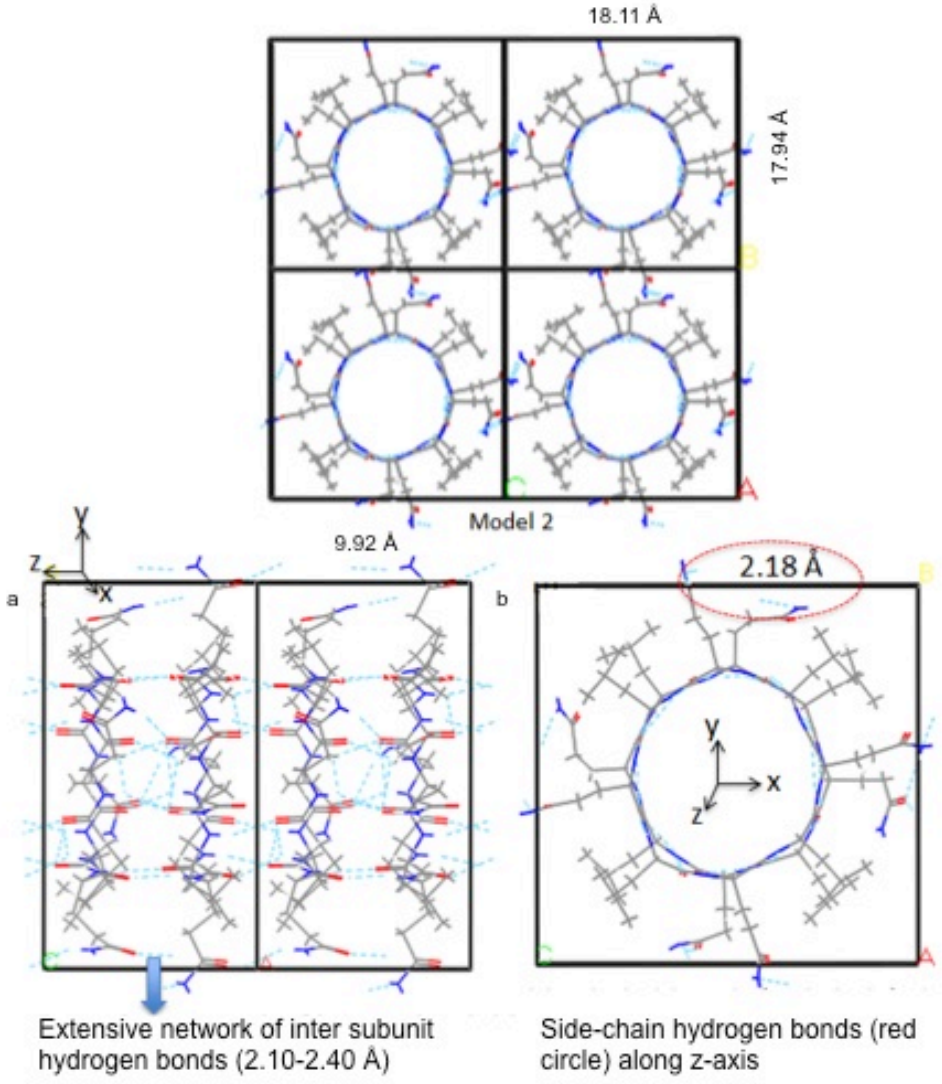

Figure 2.8. Model 2 in detail. [top] Model 2 copied from Figure 2.6. (a) Hydrogen bond orientation and distance between the backbones of peptide cycles. (b) Hydrogen bond orientation between the glutamine sidechains in the longitudinal (z-axis) direction.

A summary of the theoretically ideal packing (Model 1) of QL4 tubes in the x-y plane is shown below in Figure 2.9.

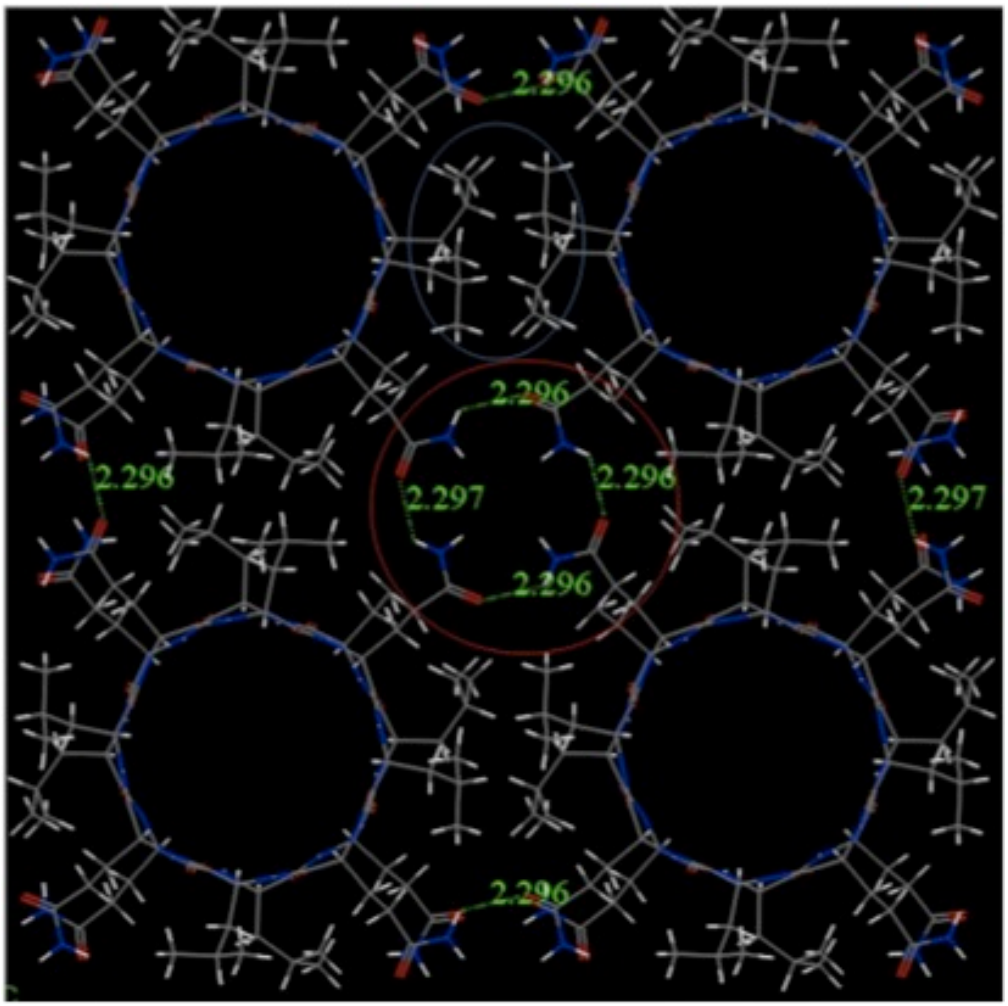

Figure 2.9. The lateral packing of QL4 tub es in a fiber. QL4 fibers are stabilized by interlocking hydrogen bonds and van der Waals interactions. In the ideal structure, glutamine sidechains point towards the center of the unit cell, creating two hydrogen bonds with its neighbors (red circle). Meanwhile, leucine residues are packed tightly together between each pair of tubes, allowing for close contact and favorable van der Waals interactions (blue circle).

One can appreciate a key difference in the geometry of QL4 versus a typical amyloid in that for QL4, hydrophobic interactions are interdigitated with the hydrogen bonds in the lateral direction, while in a typical amyloid fiber, hydrogen bonds and hydrophobic interactions (or other –R group-mediated interactions) are present in two separate, orthogonal planes (Figure 2.10)[35]. We hypothesize that these interlocking interactions are partially responsible for the solvent stability, large size,

and general robustness of the assembled fibers- hydrogen bonds maintain their strength in the presence of hydrophobic solvents while the interspersed leucine residues may act to prevent the ingress of polar solvents.

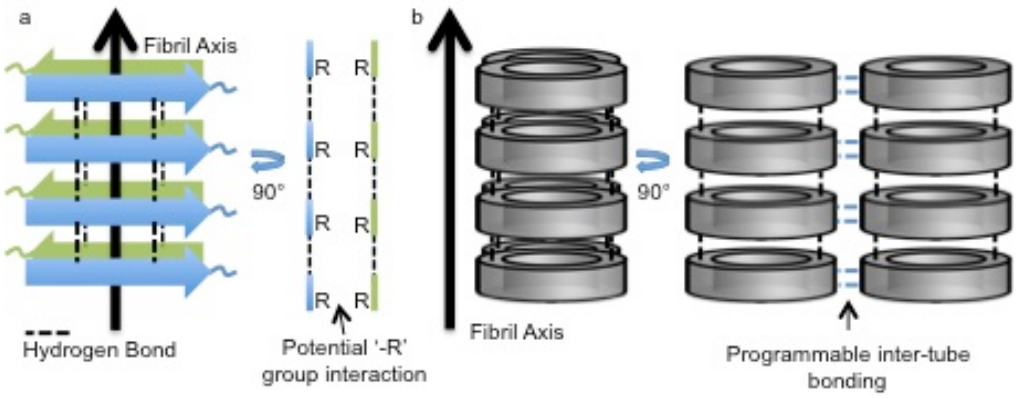

Figure 2.10. Simplified schematic diagram of an amyloid fibril and a DLCP assembly. (a) A typical amyloid fibril assembles by β–sheet formation orthogonal to the principle axis of the fiber. These sheets then bundle together such that side chains may or may not interact in the space between. Often these interactions are hydrophobic in nature and mediated by aromatic amino acids such as phenylalanine.[36] (b) DLCP structures also assemble through backbone β–sheet-like hydrogen bonding. The side chains of the DLCP monomer may be tuned such that specific interactions can occur between individual tubes. For example, a QL4 fiber is stabilized by interlocking hydrogen bonds and hydrophobic interactions as described in Figure 2.9, creating a very stabile, solvent resistant structure.

Returning to the properties of QL4 in Models 1 and 2, both the decreased stability and anisotropy of Model 2 are manifest in the estimated modulus along the x, y and z axes. The values along the z-axis are the highest since the cyclic peptides are assembled by strong H-bonds along the *z* direction. This is the major source for stabilizing the peptide in the nanotube form. The values in the x and y directions are smaller compared with the *z* dimension due to the decrease in hydrogen bond density as well as the comparatively weaker interactions, such as van der Waals and

electrostatic type, among cyclic peptides in the x-y plane. Hence, the anisotropy of the system is manifested by the more rigid character in the *z* direction.

Comparing the models, starting with the z-axis, the expected theoretical modulus for Model 1 is 22.62 GPa versus 20.21 GPa for Model 2. It is worth noting that these values are both very high for non-mineralized proteinaceous materials. Turning to the x and y axes for Model 1, one sees that the theoretical modulus is 2.72 GPa in both dimensions. This is expected due to the symmetry present along these axes. With equal unit cell spacing and equal bond distances, one would expect the stiffness to be equal as well.

Similarly, the elastic moduli for Model 2 along the x and y axes also reflects the symmetry, or lack thereof, in the structure. The theoretical modulus along the x-axis is 4.43 Gpa, while the modulus along the y-axis is 1.36 Gpa. Despite the longer bond lengths, the more optimal geometric orientation of hydrogen bond donors and acceptors help to create a relatively high stiffness along the x-axis. A summary of the theoretical moduli for Model 1 and Model 2 are represented in Table 2.1.

Axis	Model 1 Stiffness (GPa)	Axis	Model 2 Stiffness (GPa)
x	2.72	x	4.43
y	2.72	y	1.36
z	22.62	z	20.21

Table 2.1. Elastic constants of cyclic peptide nanotubes. Model 1 exhibits a higher modulus along the z-axis and intermediate moduli in the x- and y-axis. Model 2 demonstrates the anisotropy in all three dimensions with three unique modulus values. Along the z-axis the modulus is slightly below Model 2, and along the x- and y-axis the modulus values are higher and lower, respectively.

The high modulus along all three dimensions likely contributes to the large size and rod-like morphology of the assembled structures. The high aspect ratio can be inferred from the particularly high modulus (which reflects general stability) along the z-axis of assembly. It is worth noting that even in the comparatively compliant axes, our model suggests that QL4 assemblies possess a stiffness in the range of 2-4 GPa, equal to the measured value in amyloid fibers. Along the stiff axis, the theoretical modulus of 22.6 GPa is significantly higher than what has been measured at the nanoscale for amyloid or other protein-based fibrils.

Nano- and Micromechanical Analysis

The direct mechanical characterization of QL4 fibers was performed experimentally through both nanoindentation and micro-scale bending experiments, which were conducted using a depth-sensing nanoindenter. Both analyses were performed on large QL4 assemblies with widths ranging from 1-2 μm. For each indent, the modulus and hardness were calculated from the load versus depth curve generated with the indenter in load-controlled mode using the classical Oliver-Pharr analysis (Figure 2.11).[37] When the probe penetrates the surface, both plastic and elastic deformation occur. The point of maximal depth at a given load provides the measurement of hardness, while the elastic recoil in the surface upon removal of the tip allows for the calculation of the elastic modulus. A standard curve of varying indentation areas versus depth within a fused quartz susbtrate was used to standardize the data.

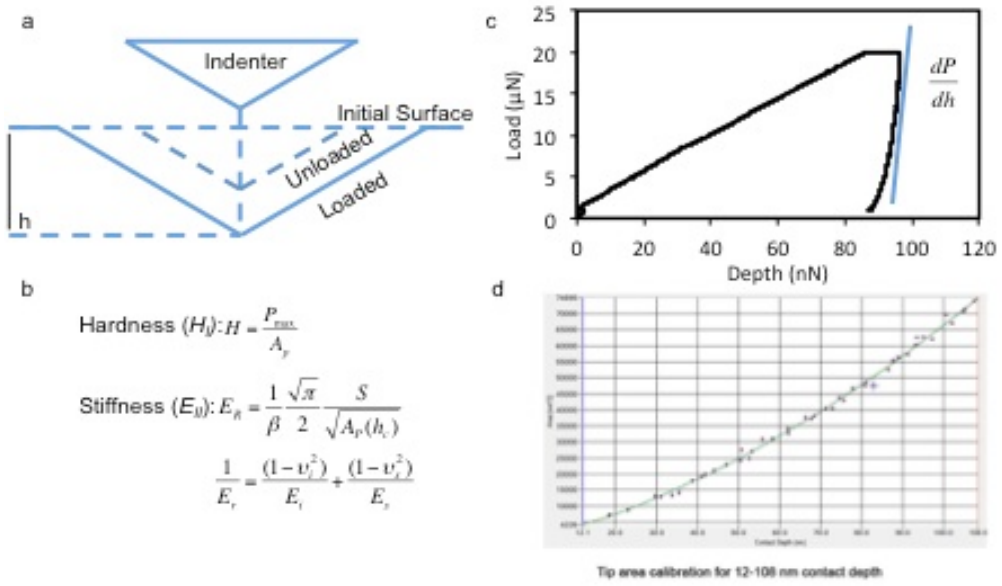

Figure 2.11. Nanoindentation of QL4 fibers (1). (a) A schematic representation of a single indent depicting the loaded and unloaded surface. Elastic energy stored in the material is responsible for the surface recoil and is used to calculate the elastic modulus. (b) Calculation of the hardness and the elastic modulus (stiffness) of a QL4 fiber. (c) A load versus depth curve from an individual indent. As the tip is withdrawn, the slope of the resulting curve (*dP/dh*) is used to calculate the material stiffness. (d) In order to process the data, a standard curve was created in which depths of 12-100 nm were probed and the corresponding indent-area was calculated.

In indentation studies, QL4 samples were deposited on a fused quartz substrate and probed with a cube corner diamond tip (Figure 2.12a). The position of each indent was accurately defined in the Scanning Probe Microscopy (SPM) mode and multiple indents were performed along the length of several crystals (Figure 2.12b). To confirm that indents occurred directly on the center of the fibers, FESEM micrographs were obtained after testing (Figure 2.12d). The average elastic modulus and hardness of a large QL4 fiber were determined to be 11.3 ± 3.3 Gpa and 387 ± 136 Mpa, respectively. It is intriguing to note that the average modulus (measured perpendicular to the fiber axis) is significant larger than the computed moduli in the x and y directions (2.72 Gpa). We attribute this discrepancy to two factors. First, the

indentation stress field beneath the indenter is complex and characterized by principal tensile stresses whose direction lay almost perpendicular to the direction of indentation[38], namely along the fiber axis. Since the computed modulus along the fiber axis is high (22.6 Gpa), the results may be a consequence of some peptide nanotube sustaining tensile stresses during indentation, resulting in a higher apparent modulus. Second these results may also be a result of the strong lateral interactions between the individual peptide nanotubes, leading to increased mechanical stability, a hypothesis that is also supported by the micro-bending experiments presented next. Despite the large size of the fibers tested here, the measured modulus and hardness of QL4 fibers are also significantly higher than those measured for individual amyloid fibers by AFM-based methods.

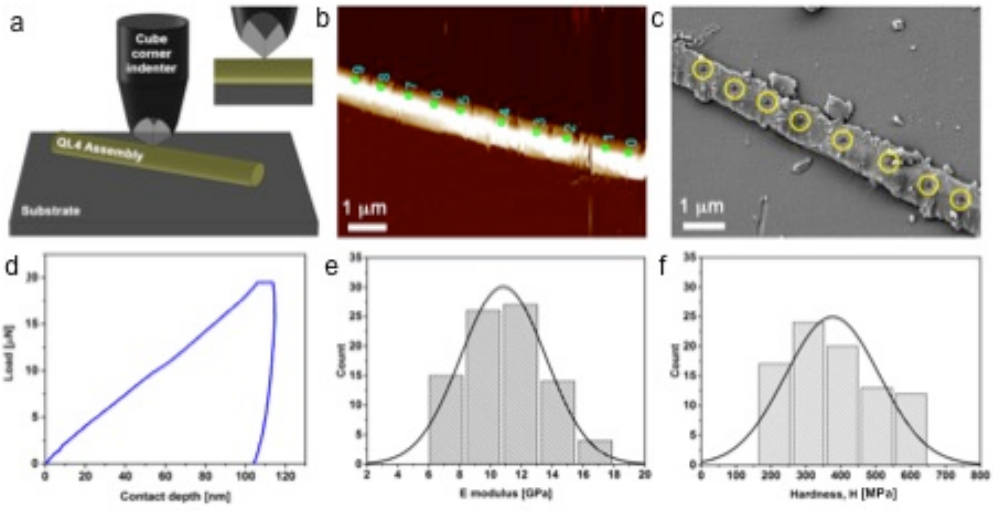

Figure 2.12. Nanoindentation of QL4 fibers (2). (a) QL4 fibers were deposited on a fused quartz substrate and probed directly with a cube corner indenter tip. (b) Scanning probe microscopy (SPM) was used to select multiple points to test along an individual fiber. (c) Residual indents were verified by FESEM analysis to confirm the spatial accuracy of each indent. (d) An individual load versus depth curve for a single indent. (e,f) The elastic modulus and hardness of over 100 individual indents were used to calculate the average values.

To elucidate the fracture strength of QL4 fibers and to gain a deeper understanding of the fiber modulus, fibers were subjected to a micro-scale bending analysis (Figure 2.13). QL4 fibers were deposited on uncoated molybdenum TEM grids with 40 μm circular pores (Figure 2.14a). After locating individual fibers spanning pores in the grid, the fiber was bent, orthogonal to the long axis, by a cono-spherical tip with a 5 μm nominal radius. To confirm that fiber loading neither compressed the fiber nor bent the grid, the same force was applied to fibers on a flat surface and the measured displacement was negligible. Because the fibers are very long in comparison to the grid pore, and because the ends of the fiber did not appear to move during or after the experiment, we have used a clamped beam as a model for our calculations (Figure 2.13). It is worth noting that the clamped beam model is highly sensitive to both the suspended length as well as the geometric area of a cross-section. For these results, a circular cross-section was used and the diameter was measured from FESEM micrographs.

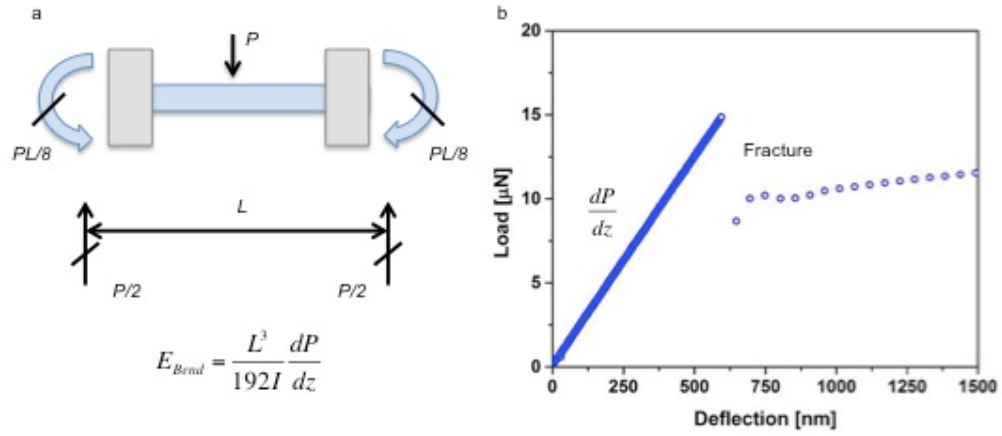

Figures 2.13. Bending analysis of QL4 fibers (1). (a) Schematic representation of a cylindrical clamped beam in bending. (b) A load versus deflection curve of an individual bending experiment highlighting the initial slope and fracture of a single fiber.

The bending modulus and strength, 10.5 ± 0.9 GPa and 97.8 ± 18.8 MPa, respectively, were calculated from individual force versus displacement curves (Figure 2.14e and f). In the displacement curve, partial fracture is indicated by sudden decreases in the measured load (Figure 2.14d). We hypothesize that these micro-fractures occur as individual fibers within the larger bundle are broken and/or delaminated from one another (Figure 2.13c). It is worth noting that microscale modulus values via bending analysis are nearly identical to those obtained through nanoindentation perpendicular to the fiber axis. Unlike many other molecularly self-assembled systems, QL4 DLCPs are able to grow to such large sizes that direct nano- and micro-scale measurements can be obtained on the same samples and compared, providing an understanding of the mechanical properties across higher length scales.

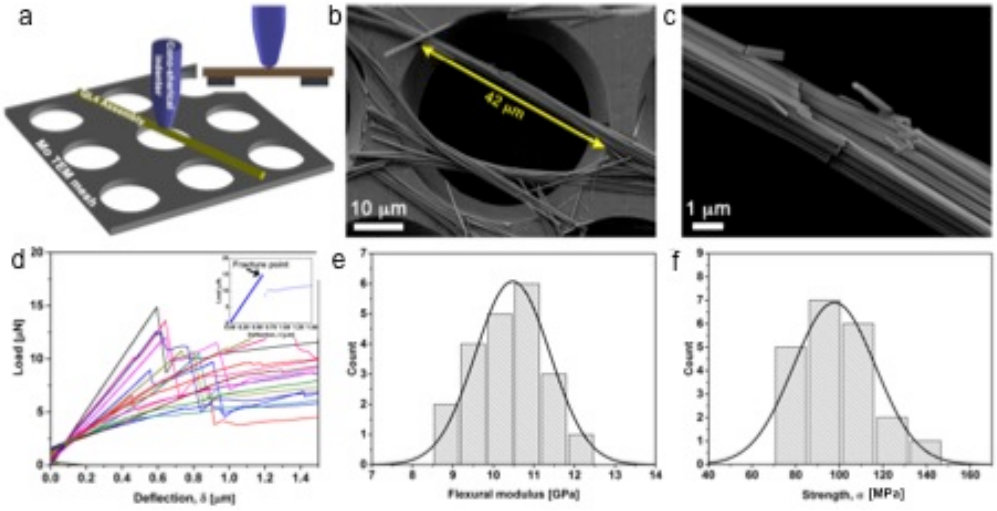

Figure 2.14. Bending analysis of QL4 fibers (2). (a) A 5 μm spherical tip was used to bend individual and bundled fibers over pores in a Mo grid. (b) A large QL4 bundled fiber bridges the pore of a Mo grid. (c) High magnification shows individual fracture events that occurred during the bending experiment. (d) Combined raw bending data for individual tubes. Curves exhibit a linear elastic region followed by a series of fracture events. A fracture point is presented at the inset image. (e-f) The bending modulus and fracture strength of QL4 fibers.

Prior bending analyses of other tube-based assemblies including single-walled carbon nanotube ropes and microtubules have shown that the shear modulus of the bundle is much weaker than the axial (Young's) modulus.[39,40] This is due primarily to a lack of inter-tube interaction within the bundle, which leads to bending and flexing as tubes slide with respect to one another. Conversely, QL4 fibers contain a dense network of inter-tube hydrogen bonds, mediated by glutamine side chains that act to stabilize each tube with respect to its neighbors (Figure 2.9). We suggest that these lateral interactions are directly responsible for the robust flexural and Young's moduli because they lead to more efficient load transfer between the tubes, which is also in line with the high modulus measured by nanoindentation. Indeed high load transfer will enhance the development of a continuum-like stress field beneath the indenter that results in regions of the fibers to be under tensile stresses, as discussed above. Furthermore these interactions contribute to the remarkably rigid, rod-like morphology of QL4 fibers. The overall rigidity, characterized by the persistence length ($l_p = EI/k_bT$), where I is the moment of inertia of the fibers, is on the order of meters (assuming a circular cross-section), which explains the lack of any noticeable bending within the fibers observed to date. This brings to light an interesting lever with which one may be able to tune the properties of DLCP structures. By tuning the side chain chemistry of the individual DCLP monomer that composes the fiber, one may be able to tune the flexural modulus and control the general morphology and properties of the assembled fiber to be more rod-like or more flexible in nature. A summary of the mechanical results for both the computational and experimental analyses is presented in Figure 2.15.

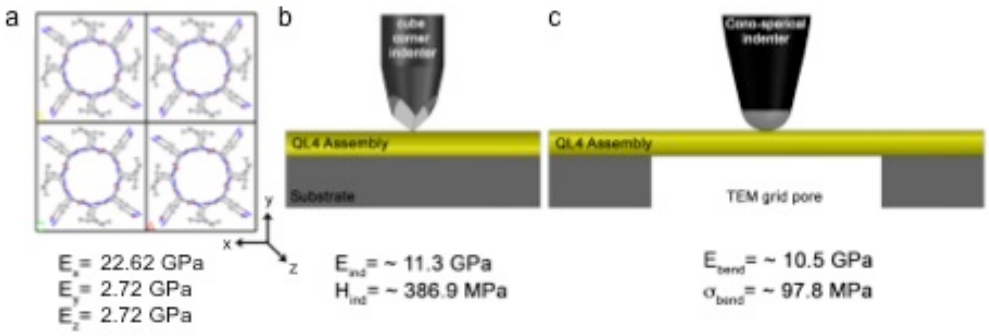

Figure 2.15**.** Summary of mechanical analyses and deformation modes. (a) Molecular dynamics simulations suggest that the elastic modulus parallel to the long axis of a fiber is 22.62 GPa. In the 'weak' directions, the elastic modulus is 2.72 GPa. (b) Nanoindentation experiments and (c) bending experiments confirm a ~11 GPa modulus across length scales.

In order to place the modulus and strength of QL4 within the context of other natural and synthetic materials, we have constructed two material selection charts (Ashby plots): one modulus *vs*. density plot (Figure 2.16a), with the density inferred from the computational modeling, and one modulus *vs*. strength plot (Figure 2.16b). Guidelines drawn on the modulus *vs*. density plot allows one to compare the specific performance of materials in tension (given by E/ρ) or in bending (given by $E^{1/2}/\rho$).[7, 41] One sees that the efficiency of QL4 fibers in tension outpaces a variety of materials including, collagen, tendon, cancellous and compact bone. The material outperformance is more significant when considering the material efficiency in bending, where QL4 fibers also outperform enamel and even steel. The relatively facile synthesis, high aspect ratio, high modulus, and low density of QL4 fibers indicate that they may find utility as a filler material in a variety of high efficiency, biocompatible composite materials.

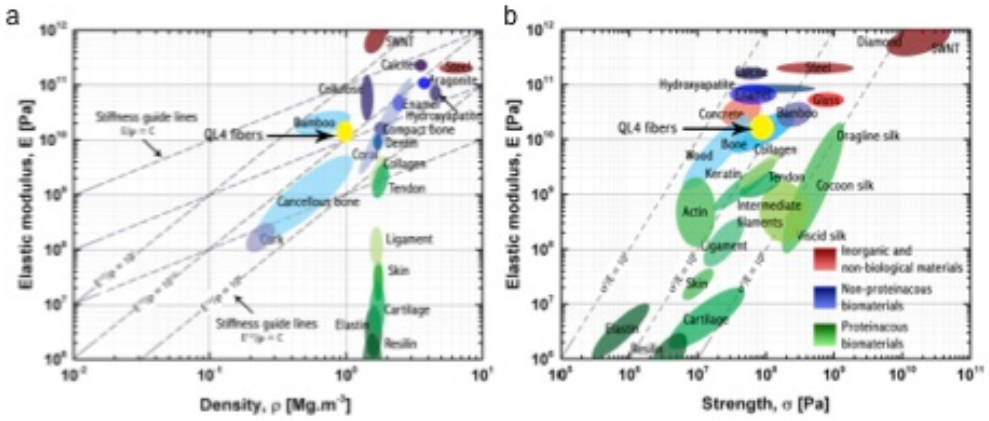

Figure 2.16**.** Comparison of materials properties. Figures adapted from Wegst et al. and Buehler et al.[7, 41] (a) Young's modulus versus density of a variety of materials. Tie lines represent the efficiency of materials in tension (E/ρ) and bending ($E^{1/2}/\rho$). QL4 fibers are among the stiffest known protein-based materials and surpass collagen, tendon, and compact bone in density-adjusted flexural modulus. (b) Young's modulus versus strength for a variety of materials. Tie lines represent the ability of a material to store elastic energy (σ_f^2/E). In comparing the stiffness and strength, it is evident that QL4 fibers exhibit similar behavior to bone and that their modulus is on par with the stiffest known proteinaceous materials including spider dragline silk.

The stiffness vs. strength selection chart of QL4 (Figure 2.16b), together with the materials index σ_f^2/E (guidelines with slope of 2) allows one to compare the materials performance in terms of their ability to store elastic energy prior to fracture.[7, 41] In both stiffness and strength, QL4 fibers are most directly comparable to bone. The stiffness of QL4 fibers exceed that of all but the most robust known proteinaceous materials such as spider dragline silk. Although the elastic energy to failure of silks is superior, as evidenced by their location along the far-right guideline in Figure 2.16b, QL4 fibers exhibit a performance metric on par with commonly known biological materials such as collagen, tendon and keratin. Perhaps unexpectedly, Figure 2.16a and 2.16b support the claim that the mechanical response of QL4 fibers is more similar to 'light' bone than to other protein based materials.

2.4 CONCLUSION

Our multi-scale mechanical analysis of QL4 fibers by nanoindentation and micro-bending demonstrates that DLCP assemblies are comparable to the most robust known protein and peptide materials. Indeed, the properties exceed those of amyloid fibrils and are on par with those of silks, suckerins[42,43], and diphenylalanine nanotubes[44], the most robust known self-assembling peptide based materials. Furthermore, they maintain those properties even at the micron length scale. This is a noteworthy feature given that the larger scale assembly is not stabilized by covalent, electrostatic, or coordination bonds between the individual monomers. In terms of stiffness and strength, QL4 is similar to bone, despite being roughly half the density. We hypothesize that the stiffness in both indentation and flexural deformation modes is supported by the rigid geometry as well as the density of hydrogen bonds in the lateral and longitudinal axes within the fibers, leading to the high persistence length and rod-like morphologies observed. Looking forward, there are a number parameters worth considering in order to modulate the properties of the assembled fiber including modifying the primary sequence, inducing covalent linkages, and assembling structures *in situ* within other materials to form nano-composites. The simple synthesis, ease of modification, potential for biocompatibility, rod-like morphology, and robust mechanical properties of DLCPs make them a promising class of peptides for further exploration in materials science, chemistry and biology, particularly as mechanical fillers in low-weight, high-stiffness composite materials. Looking to the future, the versatility provided by the self-assembling DLCP structures may prove useful for applications beyond traditional mechanical reinforcement. These applications include including actuating, self-healing, conductive and filtration materials.

2. 5 Materials and Methods

Chemicals and Reagents Acetone, dichloromethane, dimethylformamide, diisopropylamine, and piperidine were purchased from Sigma Aldrich. Dichloromethane and dimethylformamide were dried over molecular sieves. The following chemicals were used as provided: Acetone, trifluoroacetic acid, 2-(1H-benzotriazol-1-yl)-1,1,3,3-tetramethyluronium hexafluorophosphate (HBTU), and (benzotriazol-1-yl-oxytripyrrolidinophosphonium hexafluorophosphate) (PyBOP) (Sigma Aldrich). All amino acids and Rink Amide-MBHA resin were purchased from AAPPTEC, Louisville Kentucky.

Cyclic Peptide Synthesis and Assembly D,L-cyclic peptides were synthesized in accordance with the procedure of McMurray.[24] Fmoc-Glu-OAll was coupled to a Rink Amide-MBHA resin through the side-chain carboxylate. When cleaved, this residue is converted to a Gln. Standard Fmoc synthesis produced an uncyclized 8-mer which was cyclized through a PyBop assisted coupling reaction. Peptides were cleaved from the resin with 95% TFA, 2.5% water and 2.5% triisopropylsilane. To isolate the peptide, the TFA solution was concentrated by evaporation and dropped into cold diethyl ether causing precipitation. The mixture was centrifuged, re-suspended in TFA and precipitated again to increase purity. Cyclic peptide identity was verified by liquid chromatography electrospray ionization mass spectroscopy. Self-assembly was achieved by dissolving 2.5 mgs/ml of QL4 in a mixture of 60% TFA and 40% water. The assembly occurred in a glass vial over 48-72 hours at which point microcrystals could be seen by eye. Assemblies were harvested by diluting the assembly with a mixture of acetone and dichloromethane and pelleting the crystals by centrifugation.

Light Microscopy QL4 samples were deposited on glass slides and viewed on a Zeiss Axio Observer inverted microscope. Assembled fibers were suspended in water, deposited on a slide, allowed to dry and were viewed under both brightfield and cross-polarized light conditions.

Field emission scanning electron microscopy of QL4 assemblies QL4 samples were deposited on a quartz substrate and sputter coated to a projected thickness of ~5nm. All samples were sputter-coated with Au/Pd and then imaged on a Zeiss FE-SEMSupra55VP (Carl Zeiss, Oberkochen, DE) in SE2 mode. After indentation observations were performed using a FESEM (JEOL, 7600 F) at a 5 kV accelerating voltage using a lower secondary electron detector (LEI) to prevent surface charging.

Transmission electron microscopy of QL4 assemblies A suspension of QL4 assemblies in water was spotted on a quantifoil TEM grid, wicked away, and stained with uranyl acetate. Sample was viewed on a JEOL2100 TEM at 200kV. For higher resolution images, spots were selected in which the assembly was overlapping a pore in the quantifoil. Attention was paid to finding particularly narrow fibers that overlaid channels to ensure that striations could be visualized. Larger, bundled fibers obscured the individual nanotubes.

Molecular dynamics simulation of QL4 structure and stiffness We employed the COMPASS force field (Condensed-phase Optimized Molecular Potentials for Atomistic Simulation Studies) - developed by H. Sun[34], to optimize the geometry and calculate the energy of all molecules. The COMPASS force field is based on state-of-the-art ab initio and empirical parametrization techniques. The valence parameters and atomic partial charges were supported by ab initio data, and the van der Waals

(vdW) parameters were derived by fitting the experimental data of cohesive energies and equilibrium densities. For more details, please refer to the supplemental information.

Nanoindentation and Bending of QL4 assemblies QL4 assemblies were suspended in water and dropped onto a fused-quartz substrate. The droplet was wicked away, leaving numerous assemblies along the surface. A Triboindenter TI-950 Nanomechanical tester (Hysitron, Minneapolis, MN, USA) equipped with a 2D standard transducer and a 50nm cube-corner tip was used to do SPM imaging and indent along the length of individual structures. The tip was calibrated using a standard fused quartz sample. For indentation studies, a 50nm cube-corner tip was to indent the QL4 assemblies directly atop a fuesd-quartz substrate. Multiple indents were made on each fiber. For bending studies, QL4 assemblies were deposited on a Mo TEM grid with circular pores of 40 μm diameter. Assemblies overlapping pores were bent using a 5μm cono-spherical indenter tip. The force and displacement curves were used to identify the modulus and strength as well as the nature of fracture of the material.

2.6 ACKNOWLEGEMENT

N.S.J. acknowledges funding support from the Harvard MRSEC, the Army Research Office STIR program under award no. ARO-167836, the IMI Program of the National Science Foundation under award no. DMR 08-43934, and the Center for Nanoscale Systems (CNS) at Harvard University, a member of the National Nanotechnology Infrastructure Network (NNIN), which is supported by the National

Science Foundation under NSF award no. ECS-0335765. A.M thanks the support of the Singapore National Research Foundation (NRF) though a NRF Fellowship.

2.7 REFERENCES

1. Zhao, N.; Wang, Z.; Cai, C.; Shen, H.; Liang, F.; Wang, D.; Wang, C.; Zhu, T.; Guo, J.; Wang, Y.; al., e., Bioinspired materials: from low to high dimensional structure. *Advanced materials* **2014,** *26* (41), 6994-7017.

2. Winkler, S.; Kaplan, D. L., Molecular biology of spider silk. *Reviews in Molecular Biotechnology* **2000,** *74* (2), 85-93.

3. Tao, H.; Kaplan, D. L.; Omenetto, F. G., Silk materials--a road to sustainable high technology. *Advanced materials (Deerfield Beach, Fla.)* **2012,** *24* (21), 2824-2837.

4. van der Rest, M.; Garrone, R., Collagen family of proteins. *FASEB journal : official publication of the Federation of American Societies for Experimental Biology* **1991,** *5* (13), 2814-2823.

5. Fratzl, P., *Collagen: Structure and mechanics*. Springer: 2008.

6. Hu, X.; Cebe, P.; Weiss, A. S.; Omenetto, F.; Kaplan, D. L., Protein-based composite materials. *Materials Today* **2012**.

7. Wegst, U. G. K.; Ashby, M. F., The mechanical efficiency of natural materials. *Philosophical Magazine* **2004,** *84* (21), 2167-2186.

8. Knowles, T. P. J.; Buehler, M. J., Nanomechanics of functional and pathological amyloid materials. *Nature Nanotechnology* **2011,** *6* (8), 469-479.

9. Selkoe, D. J., Alzheimer's disease: genes, proteins, and therapy. *Physiological Reviews* **2001,** *81* (2), 741-766.

10. Zganec, M.; Zerovnik, E., Amyloid fibrils compared to peptide nanotubes. *Biochimica et biophysica acta* **2014,** *1840* (9), 2944-2952.

11. Chiti, F.; Dobson, C. M., Protein misfolding, functional amyloid, and human disease. *Annual Review of Biochemistry* **2006,** *75* (1), 333-366.

12. Dobson, C. M., Protein folding and misfolding. *Nature* **2003,** *426* (6968), 884-890.

13. Adamcik, J.; Jung, J.-M.; Flakowski, J.; De Los Rios, P.; Dietler, G.; Mezzenga, R., Understanding amyloid aggregation by statistical analysis of atomic force microscopy images. *Nature Nanotechnology* **2010,** *5* (6), 423-428.

14. Smith, J. F.; Knowles, T. P. J.; Dobson, C. M.; Macphee, C. E.; Welland, M. E., Characterization of the nanoscale properties of individual amyloid fibrils. *Proceedings of the National Academy of Sciences of the United States of America* **2006,** *103* (43), 15806-15811.

15. Adamcik, J.; Lara, C.; Usov, I.; Jeong, J. S.; Ruggeri, F. S.; Dietler, G.; Lashuel, H. A.; Hamley, I. W.; Mezzenga, R., Measurement of intrinsic properties of amyloid fibrils by the peak force QNM method. *Nanoscale* **2012,** *4* (15), 4426-4429.

16. Channon, K. J.; Devlin, G. L.; Macphee, C. E., Efficient Energy Transfer within Self-Assembling Peptide Fibers: A Route to Light-Harvesting Nanomaterials. *Journal of the American Chemical Society* **2009,** *131* (35), 12520-12521.

17. Li, D.; Furukawa, H.; Deng, H.; Liu, C.; Yaghi, O. M.; Eisenberg, D. S., Designed amyloid fibers as materials for selective carbon dioxide capture. *Proceedings of the National Academy of Sciences* **2014,** *111* (1), 191-196.

18. Maji, S. K.; Schubert, D.; Rivier, C.; Lee, S.; Rivier, J. E.; Riek, R., Amyloid as a depot for the formulation of long-acting drugs. *PLoS biology* **2008,** *6* (2), e17.

19. Reches, M.; Gazit, E., Casting metal nanowires within discrete self-assembled peptide nanotubes. *Science* **2003,** *300* (5619), 625-627.

20. Ghadiri, M.; Granja, J.; Milligan, R.; McRee, D.; Khazanovich, N., Self-Assembling Organic Nanotubes Based on a Cyclic Peptide Architecture (Vol 366, Pg 324, 1993). *Nature* **1994,** *372* (6507), 709-709.

21. Keten, S.; Xu, Z.; Ihle, B.; Buehler, M. J., Nanoconfinement controls stiffness, strength and mechanical toughness of beta-sheet crystals in silk. *Nature Materials* **2010,** *9* (4), 359-367.

22. Hartgerink, J. D.; Granja, J. R.; Milligan, R. A.; Ghadiri, M. R., Self-assembling peptide nanotubes. *Journal of the American Chemical Society* **1996,** *118* (1), 43-50.

23. De Santis, P.; Morosetti, S.; Rizzo, R., Conformational analysis of regular enantiomeric sequences. *Macromolecules* **1974,** *7* (1), 52-58.

24. McMurray, J. S., Solid phase synthesis of a cyclic peptide using Fmoc chemistry. *Tetrahedron Letters* **1991,** *32* (52), 7679-7682.

25. Fernandez-Lopez, S.; Kim, H. S.; Choi, E. C.; Delgado, M.; Granja, J. R.; Khasanov, A.; Kraehenbuehl, K.; Long, G.; Weinberger, D. A.; Wilcoxen, K. M.; Ghadiri, M. R., Antibacterial agents based on the cyclic D,L-alpha-peptide architecture. *Nature* **2001,** *412* (6845), 452-455.

26. Motesharei, K.; Ghadiri, M. R., Diffusion-limited size-selective ion sensing based on SAM-supported peptide nanotubes. *Journal of the American Chemical …* **1997,** *119* (46), 11306-11312.

27. Xu, T.; Zhao, N.; Ren, F.; Hourani, R.; Lee, M. T.; Shu, J. Y.; Mao, S.; Helms, B. A., Subnanometer Porous Thin Films by the Co-assembly of Nanotube Subunits and Block Copolymers. *ACS Nano* **2011,** *5* (2), 1376-1384.

28. Rubin, D. J.; Nia, H. T.; Desire, T.; Nguyen, P. Q.; Gevelber, M.; Ortiz, C.; Joshi, N. S., Mechanical Reinforcement of Polymeric Fibers through Peptide Nanotube Incorporation. *Biomacromolecules* **2013,** *14* (10), 3370-3375.

29. Chapman, R.; Danial, M.; Koh, M. L.; Jolliffe, K. A.; Perrier, S., Design and properties of functional nanotubes from the self-assembly of cyclic peptide templates. *Chemical Society Reviews* **2012,** *41* (18), 6023-6041.

30. Diaz, J. A. C.; Çağin, T., Thermo-mechanical stability and strength of peptide nanostructures from molecular dynamics: self-assembled cyclic peptide nanotubes. *Nanotechnology* **2010,** *21*, 115703.

31. Movasaghi, Z.; Rehman, S.; Rehman, I. U., Raman Spectroscopy of Biological Tissues. *Applied Spectroscopy Reviews* **2007,** *42* (5), 493-541.

32. Hartgerink, J.; Granja, J.; Milligan, R.; Ghadiri, M., Self-assembling peptide nanotubes. *J. Am. Chem. Soc* **1996,** *118* (1), 43-50.

33. Couet, J.; Samuel, J. D. J. S.; Kopyshev, A.; Santer, S.; Biesalski, M., Peptide-Polymer Hybrid Nanotubes. *Angewandte Chemie International Edition* **2005,** *44* (21), 3297-3301.

34. Sun, H., COMPASS: an ab initio force-field optimized for condensed-phase applications overview with details on alkane and benzene compounds. *The Journal of Physical Chemistry B* **1998,** *102* (38), 7338-7364.

35. Volpatti, L. R.; Knowles, T., Polymer physics inspired approaches for the study of the mechanical properties of amyloid fibrils. *Journal of Polymer Science Part B: …* **2014**.

36. Azuri, I.; Adler-Abramovich, L.; Gazit, E.; Hod, O.; Kronik, L., Why are diphenylalanine-based peptide nanostructures so rigid? Insights from first principles calculations. *Journal of the American Chemical Society* **2014,** *136* (3), 963-969.

37. Pharr, W. C. O. G. M., Measurement of hardness and elastic modulus by instrumented indentation: Advances in understanding and refinements to methodology. **2004**, 1-18.

38. Fischer-Cripps, A. C., *Nanoindentation*. Springer: 2011; Vol. 1.

39. Kis, A.; Kasas, S.; Babić, B.; Kulik, A.; Benoît, W.; Briggs, G.; Schönenberger, C.; Catsicas, S.; Forró, L., Nanomechanics of Microtubules. *Physical Review Letters* **2002,** *89* (24), 248101.

40. Salvetat, J. P.; Briggs, G.; Bonard, J. M.; Bacsa, R. R., Elastic and shear moduli of single-walled carbon nanotube ropes. *Physical Review Letters* **1999**.

41. Ashby, M. F.; Gibson, L. J.; Wegst, U., The mechanical properties of natural materials. I. Material property charts. *… of the Royal …* **1995**.

42. Guerette, P. A.; Hoon, S.; Ding, D.; Amini, S.; Masic, A.; Ravi, V.; Venkatesh, B.; Weaver, J. C.; Miserez, A., Nanoconfined β-sheets mechanically reinforce the supra-biomolecular network of robust squid Sucker Ring Teeth. *ACS Nano* **2014,** *8* (7), 7170-7179.

43. Guerette, P. A.; Hoon, S.; Seow, Y.; Raida, M.; Masic, A.; Wong, F. T.; Ho, V. H. B.; Kong, K. W.; Demirel, M. C.; Pena-Francesch, A.; Amini, S.; Tay, G. Z.; Ding, D.; Miserez, A., Accelerating the design of biomimetic materials by integrating RNA-seq with proteomics and materials science. *Nature Biotechnology* **2013,** *31* (10), 908-915.

44. Kol, N.; Adler-Abramovich, L.; Barlam, D.; Shneck, R. Z.; Gazit, E.; Rousso, I., Self-assembled peptide nanotubes are uniquely rigid bioinspired supramolecular structures. *Nano Lett* **2005,** *5* (7), 1343-1346.

Chapter 3: Mechanical Reinforcement of Polymeric Fibers Through Peptide Nanotube Incorporation

Daniel J. Rubin[1,2], Hadi T. Nia[3], Thierry Desire[4], Peter Q. Nguyen[2], Michael Gevelber[4], Christine Ortiz[3], *Neel S. Joshi[1,2]

[1]Harvard University, School of Engineering and Applied Sciences

[2]Wyss Institute for Biologically Inspired Engineering

[3]Massachusetts Institute of Technology, Department of Materials Science and Engineering

[4]Boston University, Department of Mechanical Engineering

* njoshi@seas.harvard.edu

The proceeding chapter has been adapted from the following published study: Rubin, D. J.; Nia, H. T.; Desire, T.; Nguyen, P. Q.; Gevelber, M.; Ortiz, C.; Joshi, N. S., Mechanical Reinforcement of Polymeric Fibers through Peptide Nanotube Incorporation. *Biomacromolecules* **2013,** *14* (10), 3370-3375.

3.1 ABSTRACT

High aspect ratio nanotubular assemblies can be effective fillers in mechanically reinforced composite materials. However, most existing nanotubes used for structural purposes are limited in their range of mechanical, chemical, and biological properties. We demonstrate an alternative approach to mechanical reinforcement of polymeric systems by incorporating synthetic D,L-cyclic peptide nanotube bundles as a structural filler in electrospun poly D-, L-lactic acid fibers. The nanotube bundles self-assemble through dynamic hydrogen bonding from synthetic cyclic peptides to yield structures whose dimensions can be altered based on processing conditions, and can be up to hundreds of microns long and several hundred nanometers wide. With 8 wt% peptide

loading, the composite fibers are >5-fold stiffer than fibers composed of the polymer alone, according to AFM-based indentation experiments. This represents a new use for self-assembling cyclic peptides as a load-bearing component in biodegradable composite materials.

3.2 INTRODUCTION

Materials whose mechanical and physical properties can be precisely tuned are critical for the fabrication of effective tissue engineering scaffolds,[1] wound dressings,[2] medical sutures, filtration devices, and textiles.[3] Increasingly, a composite design in which a high-aspect ratio filler material is incorporated within a less-structured matrix is employed in order to match the specific combination of high-performance properties required by the structure. For example, carbon nanotubes (CNTs)[4] and cellulose nanowhiskers[5] have been investigated extensively to increase the stiffness and strength of synthetic polymer fibers. Mathematical models and empirical studies of composite materials have suggested that there are four key factors that affect their mechanical properties: 1) the Young's modulus of the filler material, 2) the strength of the molecular interactions between the filler material and the surrounding polymer matrix, 3) the filler material aspect ratio, and 4) the orientation of the supporting material with respect to the fiber long axis.[6] Both CNTs and cellulose nanowhiskers make for effective filler materials in some composites because they exhibit high Young's moduli and high aspect ratios. However, due to their methods of synthesis they both exhibit limited capabilities in terms of controlling the spatial complexity of possible surface modifications, accessing a wide range of dimensions, and inducing assembly and disassembly. Both materials are

generally regarded as non-biodegradable, raising questions about their ultimate fate after incorporation into biological systems.[7] Although cellulose nanowhiskers are thought to be biocompatible, toxicity remains an ongoing hurdle for CNTs.[8]

Materials created through self-assembly may provide alternative reinforcement systems that exhibit a combination of biocompatibility and biodegradability, enable the formation of nanostructures with controllable dimensions, allow for rapid exploration of complex surface chemistries, and provide refined methods for stimulus responsive and self-healing materials. Specifically, due to their straightforward synthesis and customizability[9], engineered peptides have emerged as a powerful way to create nanostructures and larger scale materials with highly tunable properties.[10] However, the vast majority of these systems are designed such that short linear amino acid sequences assemble to form porous networks composed of entangled supramolecular fibers.[11] In order to create peptide-based filler materials that can mimic the mechanical stability of conventional fillers, a supramolecular system capable of forming rigid assemblies is required.

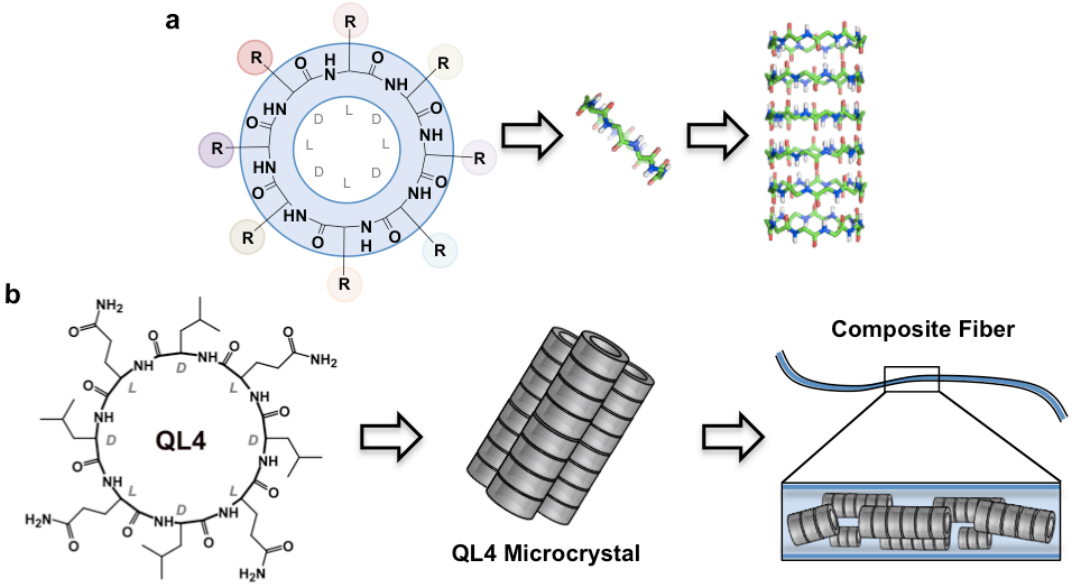

Figure 3.1. D,L-cyclic peptide composite fibers: chemistry and fabrication (a) Schematic of an 8-amino acid D,L-cyclic peptide. R = sidechain. Individual monomers stack atop one another in antiparallel β-sheets, resulting in peptide nanotubes and larger crystals. (b) Chemical structure of QL4, schematic of QL4 microcrystal, and QL4-Polymer composite structure.

We have developed a bottom-up approach to synthesizing filler materials for composite reinforcement based on the self-assembly of D-, L-cyclic peptides (DLCPs). Originally selected for use as membrane-disrupting antibiotics due to their unique structure, customizable surface chemistry, and potential for biocompatibility,[12] DLCPs have since been underutilized in biomaterials applications. The peptide cycles are composed of eight amino acids with alternating D- and L-stereochemistry, causing a planar geometry in which the amino acid side chains radiate from the center of the ring and the amide backbone is perpendicular to the plane of the ring, promoting their assembly into high aspect ratio nano- and microstructures through β-sheet-like hydrogen bonding (Figure 3.1a).[13] Depending on the sequence of the peptides, the nanotubes may also associate longitudinally into bundles to create structures that can be hundreds of

microns in length. In the previous Chapter, the data confirm that the Young's modulus of DLCP assemblies is comparable to the stiffest known self-assembled organic systems.[14] Thus, the self-assembled structures exhibit many of the desirable structural features for filler materials in composites – they are mechanically rigid, they have high aspect ratios, and their surface chemistry can be customized to maximize filler-matrix interactions. Most importantly, since DLCP nanotubes are created through bottom-up self-assembly, they represent an intriguing dynamic scaffold whose physical properties can be changed based on assembly state, allowing for future work in stimulus responsive and self-healing materials.

We demonstrate the mechanical reinforcement of synthetic polymer fibers using DLCP-NTs by AFM-based indentation experiments. This was accomplished through the fabrication of composite fibers where the major component was poly(D-, L-lactic acid) (PDLLA) and the minor component was DLCP-NTs (Figure 3.1b). While aliphatic polyesters such as PDLLA are convenient to use because they are commercially available and have been deemed safe for human implantation by the FDA, their mechanical and physical properties are sub-optimal for applications in which they must replace or augment load bearing tissues.[15] PDLLA was selected for this study, because: 1) it is commonly used in the fabrication of implantable biomedical materials[3], 2) its amorphous structure prevents the creation of nanocrystalline irritants upon biodegradation[16], yet 3) it is less stiff than its crystalline analogs, and 4) it is unstable when subjected to a static load.[17] Despite the extensive study of self-assembled peptide systems for various applications, there have been few examples[18] of their use as mechanical reinforcement agents. We have accomplished the controlled synthesis of DLCP-NT bundles, their

incorporation into electrospun PDLLA fibers, and the mechanical characterization of this system. This represents the first demonstration of DLCPs as mechanically stabilizing components of a composite material.

3.3 RESULTS AND DISCUSSION

Synthesis, Assembly and Processing of DLCP Structures

DLCPs were synthesized on the solid phase using previously published protocols.[13] For this study, we used cyclo-[$(QL)_4$], which we abbreviate as QL4 (Figure 3.2). This sequence was chosen because of its known tendency to assemble into large, stable bundles of tubes, which here we call fibers, assemblies or structures.[13] In this case, assembly was accomplished by dissolving the DLCPs in trifluoroacetic acid (TFA) and adding pure water until a concentration of 40:60 water was reached. Formation of DLCP-NT bundles (microcrystals) proceeded over the course of 48 hours. SEM analysis of the fibers revealed that they exhibited a range of dimensions.

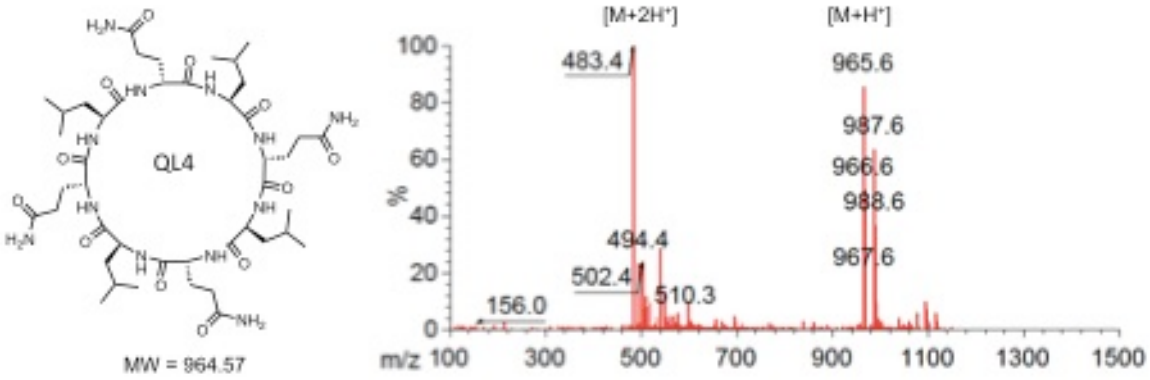

Figure 3.2. Verification of cyclo-[(QL)$_4$]. [left] Structure of QL4. [right] Verification of peptide monoisotopic mass by electrospray ionization mass spectrometry. The singly charged [M+H$^+$] ion is visible at 965.6 m/z and the doubly charged [M+2H$^+$] is visible at 483.4 m/z.

The largest observed structures had diameters of several hundred nanometers and reached 10-50 μm in length (Figure 3.3a). Given that a single nanotube of stacked DLCPs is only a nanometer in diameter, this indicates that the microcrystals are composed of thousands of laterally associated DLCP-NTs. Previous reports of QL4 assemblies have suggested that this bundling is mediated by hydrogen bonding between glutamine residues[13], which was since confirmed in Chapter 2. Importantly, the microcrystals were quite robust once assembled, being able to withstand centrifugation and vortexing. However, upon ultrasonication the microcrystals were shortened, presumably by transverse fracture, since the average lengths decreased from 14 ± 12 μm to 3 ± 2 μm while the average widths remained largely unchanged (Figure 3.3b). Over the course of multiple syntheses and assemblies we did not observe any smaller nanostructure being

formed. It appears that QL4 assembles very rapidly once it is nucleated and strongly favors structures on the size scale presented here.

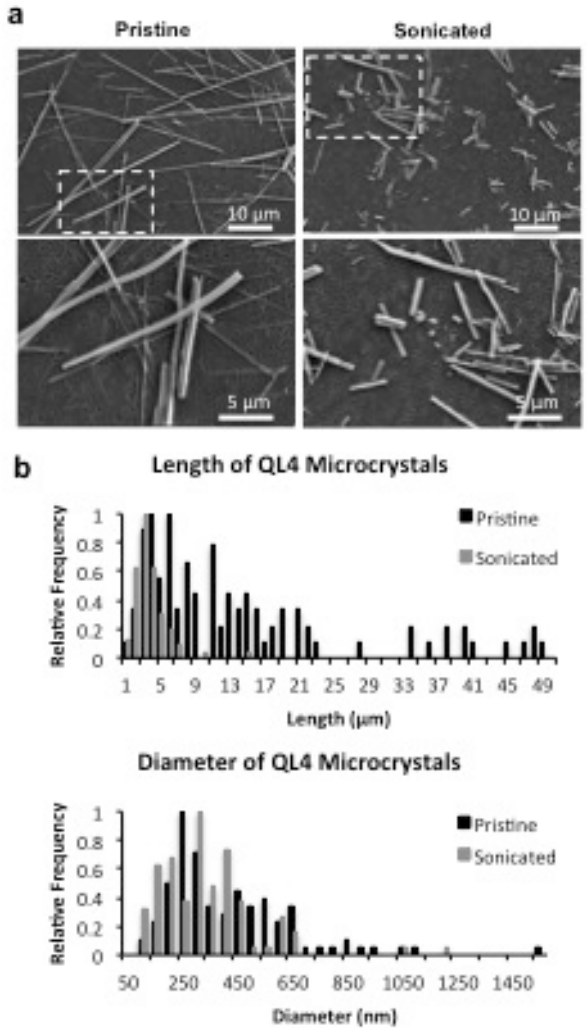

Figure 3.3. Size characterization of QL4 fibers (a) SEM images of microcrystals before and after sonication. White dashed boxes indicate region that is magnified in the lower images (b) Length and width distributions of microcrystals indicating that sonication causes transverse fracture but does not alter the width of the fibers.

Lyophilization also led to DLCP-NT disassembly and aggregation to varying degrees (Figure 3.4). We hypothesize that when QL4 assemblies are allowed to dry completely, the intermolecular and intertube interactions become sufficiently strong to

prevent the re-solubliziation of assemblies upon resuspension. Attempts at resuspension and removal from vessel surfaces result in the aggregation and disassembly described in Figure 3.4.

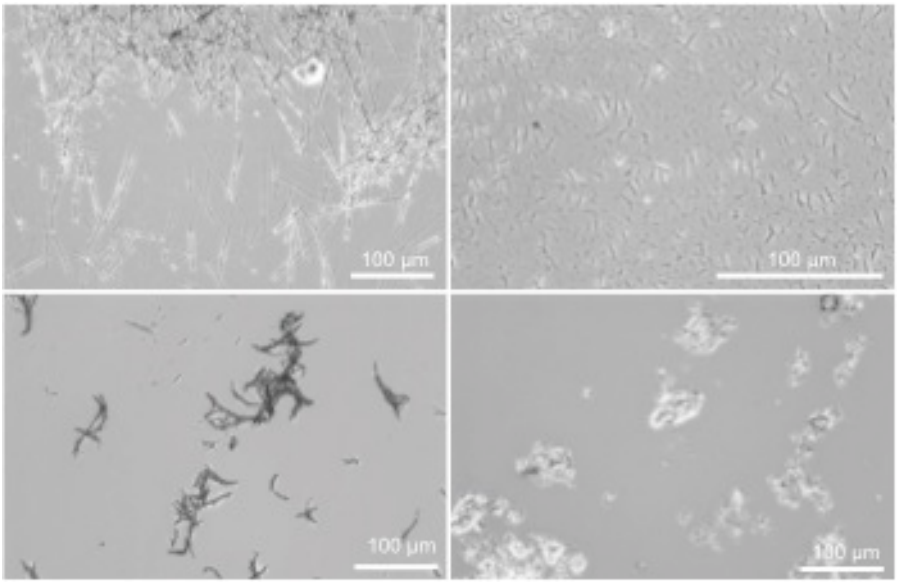

Figure 3.4. Optical micrographs of pristine and disassembled QL4 fibers. [Top left] pristine, [top right] sonicated, [bottom left] partially disassembled, and [bottom right] extensively disassembled.

Materials Processing and Structural Analysis

To prepare the spinning solution, the DLCP-NTs were mixed with PDLLA in 3:1 acetone/dichloromethane. As QL4 is generally hydrophobic, yet has a high density of hydrogen bonding moieties, it was expected to interact favorably with PDLLA. In order to probe the dispersion of DLCPs into the polymer matrix, droplets of the spinning solution were placed on glass slides and allowed to dry. Optical micrographs of the dried droplets revealed that the intact DLCP-NTs at 1%, 4% and 8% loading were evenly dispersed inside the polymer matrix (Figure 3.5). Indeed, in a polymer droplet it appears as though DLCP-NTs are able to interact within the matrix, creating the potential for an

interpenetrating network. In contrast, DLCP-NTs that were poorly mixed, or disassembled did not disperse evenly and formed clumps within the dried spinning solution (Figure 3.5). These highly irregular dispersions create a significant amount of variation between samples. Due to the large size of QL4 assemblies, dispersion is imaged at the micron scale.

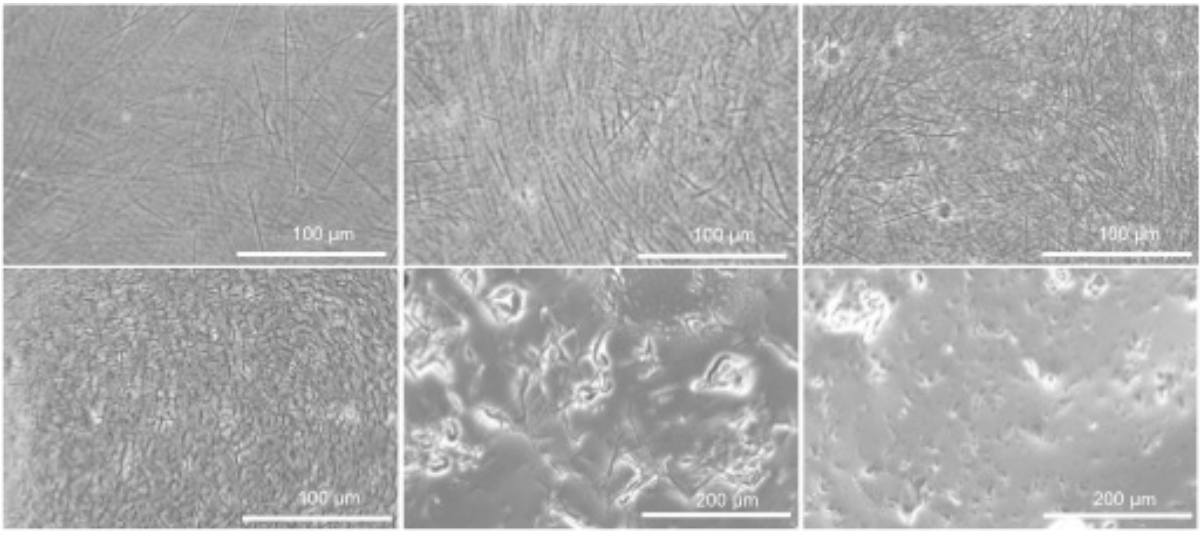

Figure 3.5. Bright field images of dried polymer droplets containing QL4 dopant. [Top, left to right] pristine 1%, 4% and 8% loading. [Bottom, left to right] Sonicated, partially disassembled and extensively disassembled with 8% loading. Partially and extensively diassembled/aggregated filler materials appear to clump within the polymer droplets.

Electrospinning experiments confirmed that composite nanofibers could be obtained with varying concentrations of PDLLA and microcrystals. A noteworthy observation is that solutions containing pure PDLLA formed lightly beaded fibers at and below a polymer concentration of 8% by weight (Figure 3.6).

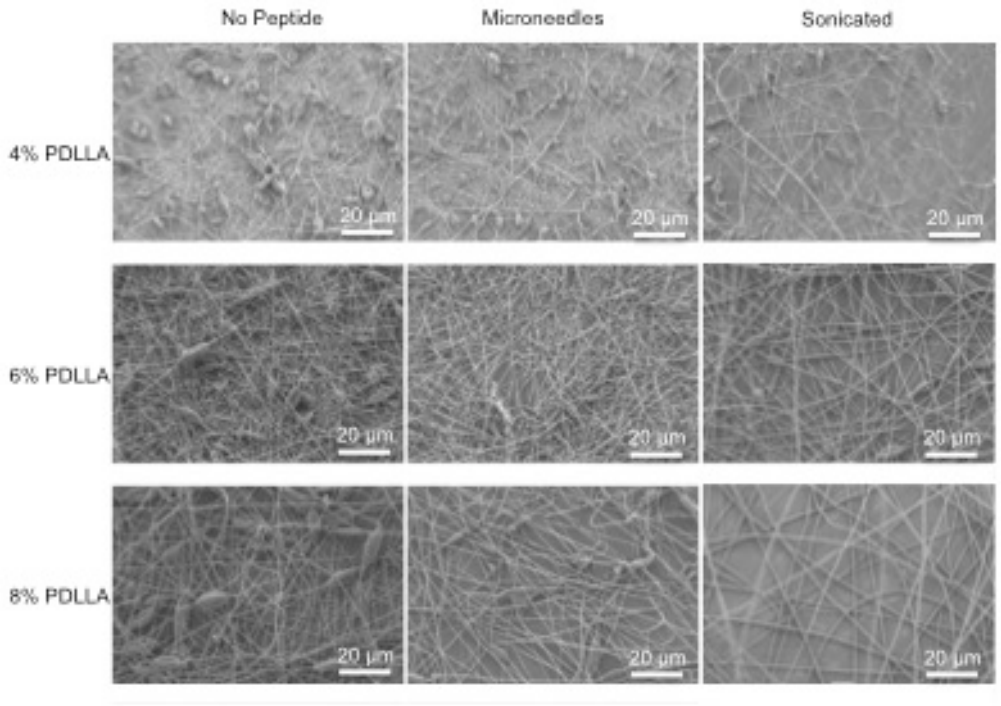

Figure 3.6. Composite fiber morphology and beading. The addition of QL4, at one weight percent (with respect to the mass of PDLLA), decreases the propensity of fibers to bead. The decrease in beading is more pronounced when QL4 assemblies are sonicated before fiber incorporation, likely due to more efficient mixing, increased homogeneity and increased microcrystal-polymer interactions.

However, when QL4 microcrystals were added to the spinning solutions, little to no beading was observed at an 8% polymer concentration. As beading can be caused by inefficient polymer entanglement[13], it is possible that favorable polymer-microcrystal interactions promote increased effective entanglement during the spinning procedure. Like the fibers composed of pure PDLLA, those containing DLCP-NTs exhibited smooth morphologies, suggesting that the microcrystals were aligned with and fully encapsulated by a polymeric sheath (Figure 3.7a). If the microcrystals exhibited alternative alignments, they would be visibly protruding from the fiber, which is not observed in any of the SEM images.

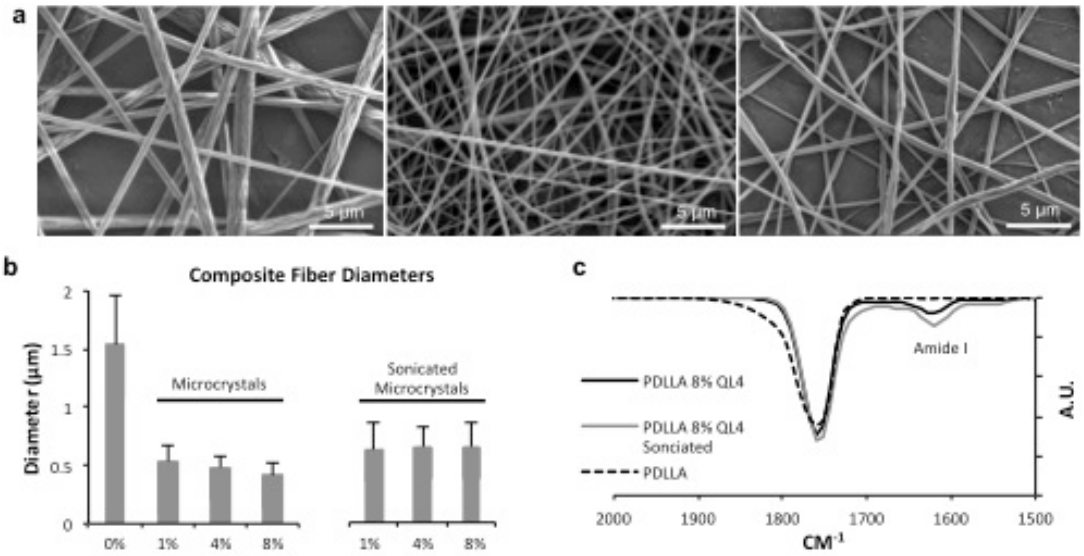

Figure 3.7. Characterization of composite fibers. (a) Representative SEM images of electrospun fibers with 0% (left), 8% pristine (center), and 8% sonicated (right) DLCP-NTs. (b) Average fiber diameter. (c) FTIR spectra of composite fiber mats in which (dashed) corresponds to pure PDLLA and (black) and (gray) correspond to pristine microcrystals and sonicated microcrystals respectively. Amide C=O stretch peak near 1620 cm^{-1} indicates the presence of DLCP-NTs in the fibers.

Fibers spun with intact microcrystals consistently exhibited smaller diameters (~0.5 µm) compared to those composed of pure PDLLA (~1.5 µm) (Figure 3.7b). This observation is in accordance with previous publications on nanocomposite fibers, which have attributed it to increased conductivity or changes in viscosity of the spinning solution upon addition of the nanofiller.[19] The resultant nanofiber mats were self-standing and sufficiently strong to be lifted from their collection surface for further characterization. The presence of QL4 DLCP-NTs within the fiber was confirmed by Fourier-transform infrared spectroscopy (FTIR) (Figure 3.7c). The Amide I (1625 cm^{-1}) peak, which is characteristic of proteins and peptides, is present only for fibers containing DLCP-NTs. The IR absorbance peak at 1750 cm^{-1}, which is present in all three samples,

corresponds to the carbonyl stretching frequency of the PDLLA matrix. Furthermore, the position of the amide N-H stretch at 3278 cm^{-1} (Figure 3.8) matches previously reported values[13], which were correlated with the presence of a tightly hydrogen bonded network with an inter- peptide distance of 4.7 – 4.8 Å, according to a Krimm's analysis[20], indicating that the microcrystals are ordered and composed of nanotubes.

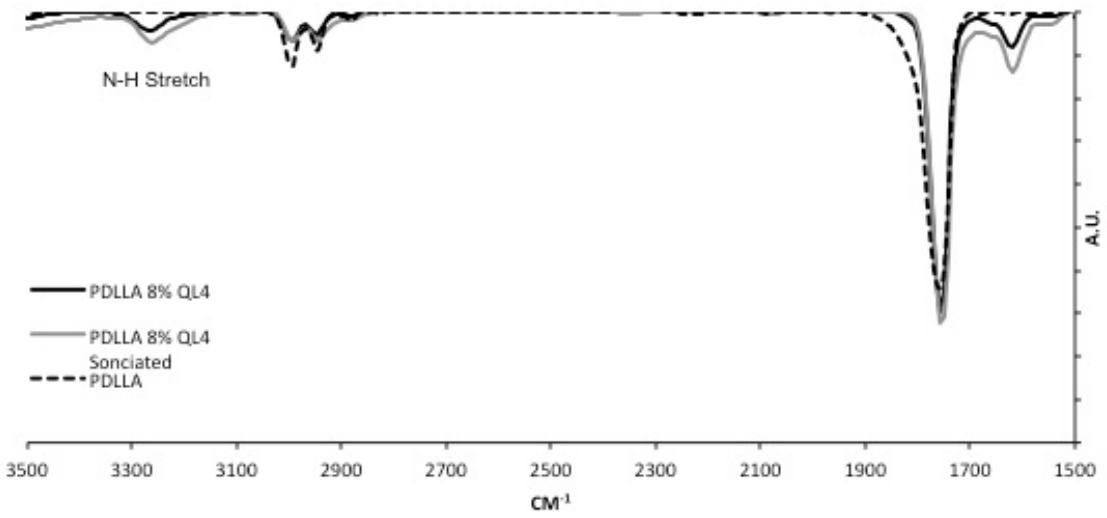

Figure 3.8. FT-IR spectra of composite nanofiber with 8% peptide loading. The characteristic N-H stretching frequency at 3278 cm^{-1} indicates a hydrogen bonded network with an average intersubunit distance of 4.7-4.8 Å**[13],** providing evidence that microcrystals are composed of peptide nanotubes, and that peptide nanotubes are not compromised by electrospinning.

The next step in understanding the general structure of the fiber is to confirm the dispersion and identity of the component generating the amide signal. To accomplish this, electron microscopy was used to image the fibrous mat at high resolution (Figure 3.9). The general morphology of the mat is uniform, but there are places in which bulges suggest that peptide crystals may be embedded. These spaces are marked with blue rectangles.

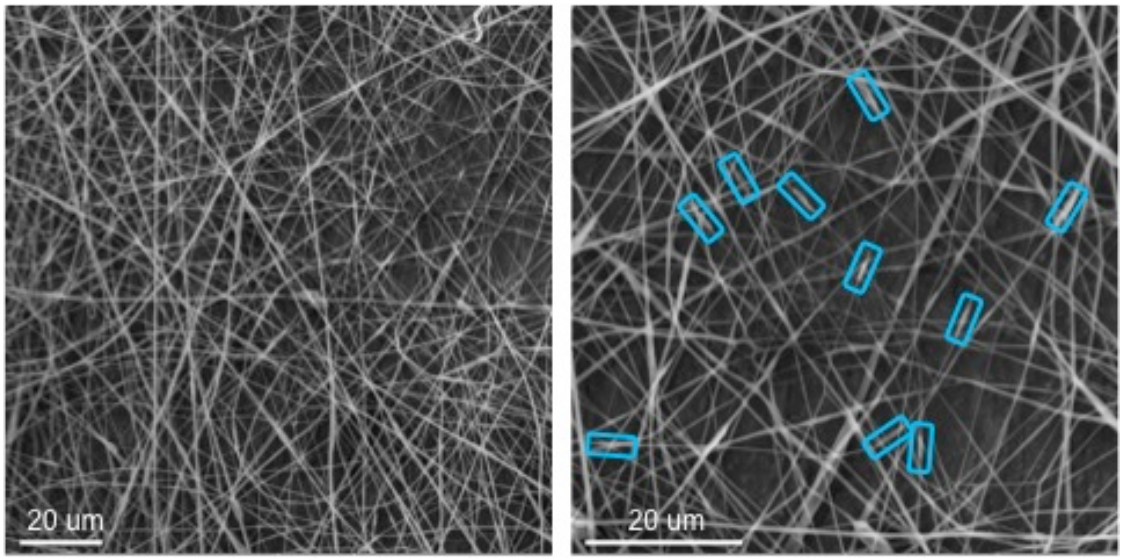

Figure 3.9. Characterization of DLCP dispersion within composite fibers. [Left] A composite fibrous mat containing dispersed, sonicated DLCP assemblies. [Right] An expanded image of the mat with DLCP assemblies highlighted in blue. DLCP assemblies are well dispersed throughout the fiber mesh.

Fibers were then subjected to analysis by electron dispersive spectroscopy (EDS), which allows one to probe the particular atomic components present at a point in the field of view. Figure 3.10 depicts 2 such spectra, one in which there is a peptide microcrystal present (blue) and one in which there is no crystal present (red). Although there are many peptide crystals present within the fiber mesh, this result supports the claim that there are also many places within the mesh that are devoid of any reinforcing element. We hypothesize that this is due to the similar diameters of the peptide microcrystals and composite fibers. The final step in confirming the identity of the DLCP microcrystals was to dissolve the fiber mat by solvating with acetone and dichloromethane (the same solution used for fiber fabrication). After dissolving the mesh and centrifuging the solution, samples were placed on TEM grids for imaging. Figure 3.10c shows intact

pristine and sonicated microneedles that have been ‘extracted’ from dissolved composite fibers. This confirms the presence of DLCP assemblies throughout the fibrous mesh.

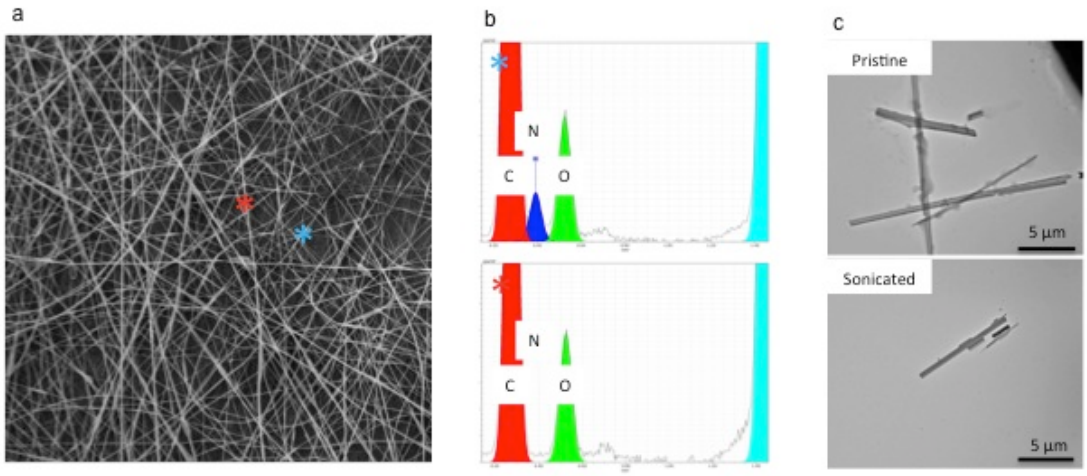

Figure 3.10. Confirmation of DLCP identity within fiber mesh. (a) A fibrous mat containing sonicated DLCP microcrystals. The red and blue asterisks correspond to spots in the mesh in which a DLCP microcrystal is (blue asterisk) or is not (red asterisk) (b) Electron dispersive spectroscopy (EDS) analysis of the fiber mesh at the position of the asterisks. [Top] a nitrogen peak suggests that there are peptides present at this point. [Bottom] A lack of nitrogen signal allows us to conclude that there are no peptides present at this point. (c) Composite fibers were digested in 3:1 acetone/dichloromethane allowing the extraction of peptide structures. [Top] Extracted pristine microcrystals. [Bottom] Extracted sonicated microcrystals.

AFM-Based Nanomechanical Characterization

In order to probe the mechanical stabilization conferred by QL4, individual fibers were subjected to nanoindentation experiments using an atomic force microscope with a glass microbead (40 µm diameter) affixed to the cantilever tip. The deflection and z-piezo measurements of each indentation were converted from volts to nanometer to calculate the indentation depth. The force was obtained as the product of the measured spring constant of the cantilever and the deflection. The force-displacement curves were then

used to obtain Young's modulus of each fiber. Average force displacement curves were generated for dried fibers on silicon backing with the following four fiber compositions: 0%, 1%, 4%, 8% by weight DLCP-NTs (Figure 3.11). Fibers containing pristine microcrystals were compared to those containing sonicated microcrystals as well as those that had been either partially or extensively disassembled by lyophilization.

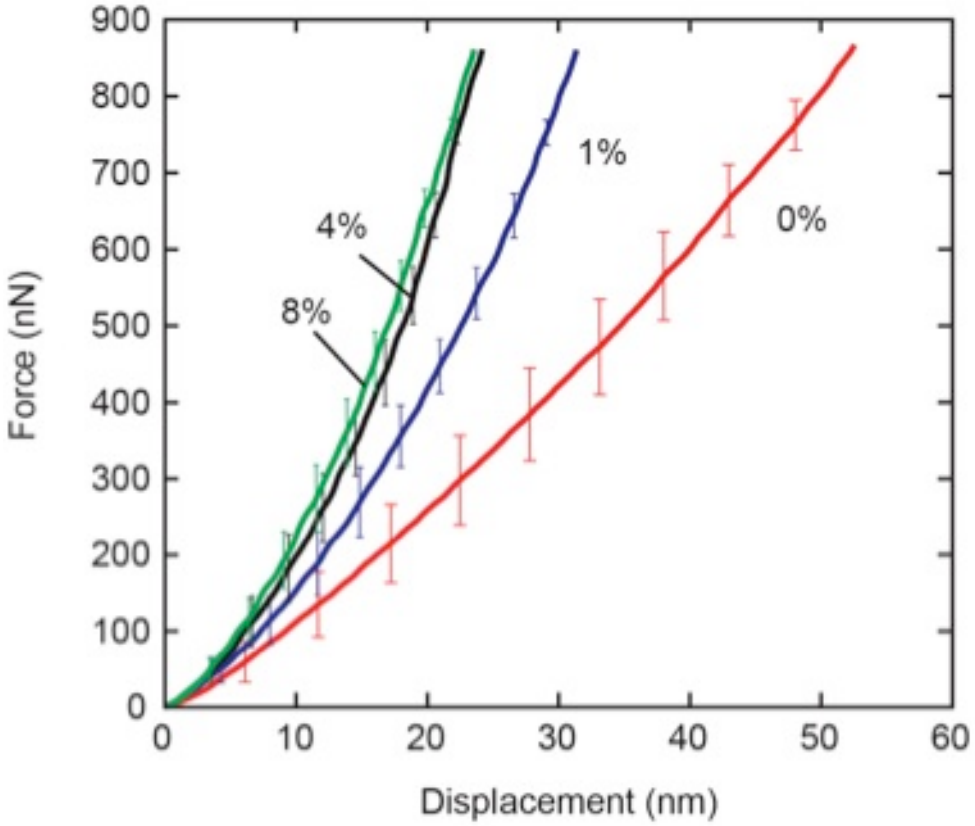

Figure 3.11. Force/Displacement of composite fibers. A representative example of force displacement curves generated through AFM-based compression testing. It is evident that with increasing peptide concentration, the slope of the curve increases, indicating a stiffer material. The increase in stiffness begins to plateau after 4% loading, likely due to peptide aggregation in the spinning dope used to fabricate the fiber.

For each indentation curve the modulus was obtained by fitting a Hertzian contact model. We utilized the contact model between two elastic bodies with curved surfaces for

which an analytical solution exists. The model consists of two perpendicular cylinders approximating the spherical indenter and the cylindrical fibers.[21] Since the diameter of the spherical probe (D ~ 40 μm) is much larger than the diameter of each fiber (d ~ 0.8 μm), the approximation of two cylindrical bodies describes the indentation contact geometry closely. According to the Hertzian contact model of ellipsoidal contact area:

$$F = \alpha \frac{4}{3} E^* R^{1/2} \delta^{3/2} \tag{1}$$

where F is the indentation force and δ is the indentation depth. The modulus E^* is obtained from the following relationship

$$E^* = \frac{E}{1 - \nu^2} \tag{2}$$

where the Poisson's ratio υ is assumed to be 0.3 and E is the Young's modulus of the fiber. The effective Gaussian radius of curvature R in Eq. (1) is obtained from

$$R = \sqrt{R_1 R_2} \tag{3}$$

where R_1 is the radius of the spherical probe, R_1 ~ 20 μm, and R_2 is the average radius of the fiber, R_2 ~ 0.4 μm. The coefficient α is a correction constant that is found by finite element simulation of the spherical indentation of cylindrical fibers and accounts for the contact geometry between the cylindrical fibers and the flat substrate.

The finite element model was implemented using the commercial finite element software ABAQUS (Version 6.9, SIMULIA, Providence, RI) for the configuration shown in Figure 3.14a. Because of the symmetry of the problem, we modeled half of the fiber from the apex of the indenter. The probe tip is modeled as rigid sphere of radius ~ 20 μm and the substrate were modeled as a rigid surface since they are much stiffer than the fibers. The fibers are modeled as elastic cylinders of radius ~ 0.4 μm and half-length of 3 μm, which is much larger than the contact distance between the special probe and sample. The probe tip as assigned a displacement of 40 nm, close to the experimental indentation depth. The coefficient α is calculated to be $\alpha = 0.56$ by comparing the analytical expression in Eq. 1 with the force-displacement curve that is obtained from the finite element simulation (Figure 3.12). Young's modulus *E* at each indentation site is obtained by curve fitting of Eq. (1) to the experimental indentation curves (Figure 3.13).

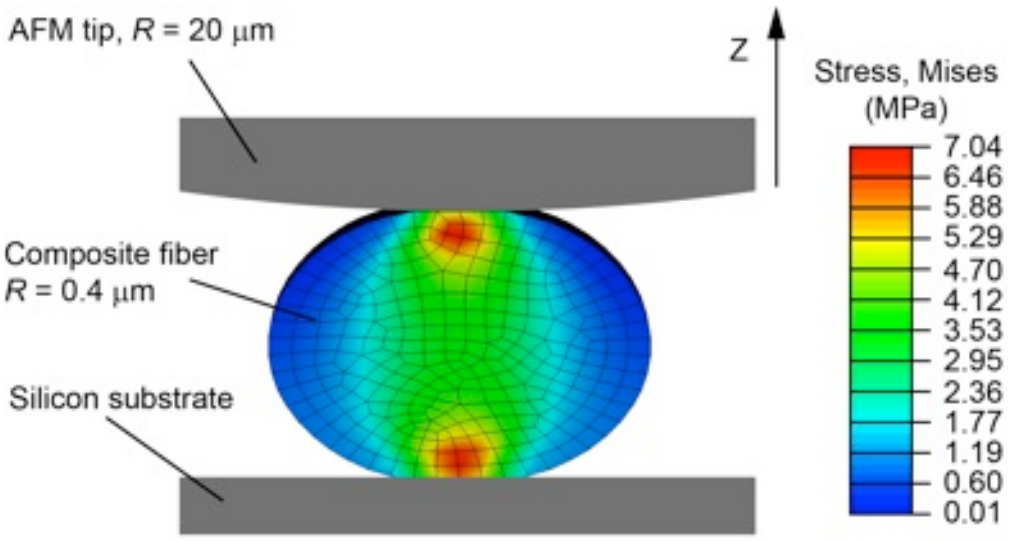

Figure 3.12. Finite element model of compression geometry. Finite element model of the contact between rigid spherical AFM tip, elastic composite fiber and rigid flat substrate has been implemented to find the correction coefficient α to the analytical expression for Hertzian contact between two cylindrical elastic bodies in Eq. 1. Stress distribution is shown at the cross section of the fiber for a typical indentation depth of 40 nm and E = 100 MPa.

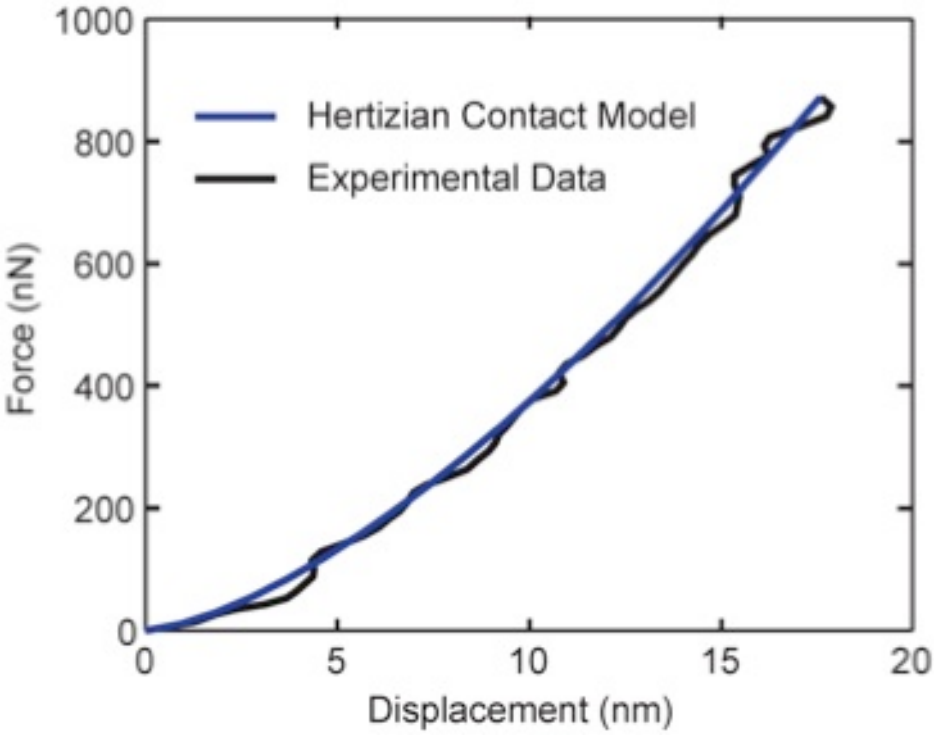

Figure 3.13. Hertzian contact model. Hertzian contact model (in blue) has been fitted to the experimental indentation curves (in back) to obtain the elastic modulus of each fiber. Here typical curves are shown for a fiber with 4% nanotubes.

When comparing the average modulus between fibers with varying loadings of sonicated and pristine peptide assemblies, one recognizes a dose-dependent increase in fiber modulus, with the highest QL4 loading (8%) leading to the highest modulus values for each fiber type. Furthermore, we observed significantly decreased reinforcement for the samples in which the DLCP-NTs had been disassembled partially and a further decrease in reinforcement when the DLCP-NTs had been disassembled extensively. Composite fibers reinforced with sonicated microcrystals exhibited the highest stiffness values, despite the fact that their average length was smaller than microcrystals in the pristine sample. We believe that this is likely due to their narrower length distribution (Figure 3.3b), which allows for more homogeneous mixing in the pre-spinning solution,

and consequently more contact area with the surrounding polymer matrix and better stress transfer from microcrystal to polymer after fiber formation. Due to the decrease in the regularity of the structure of disassembled microcrystals, it was not possible to compare their average lengths to the pristine or sonicated sample-sets. Fibers containing sonicated microcrystals at a loading of 8% exhibited a Young's modulus of ~595 MPa, corresponding to a >5-fold increase in stiffness over fibers composed of PDLLA alone. Fibers containing pristine microcrystals at a loading of 8% were the next best performer with a Young's modulus of ~465 MPa, roughly 4-fold higher than the control sample. A student's t-Test was performed on the calculated Young's modulus *E*. In all the tests, a p-value of <0.05 was taken as statistically significant.

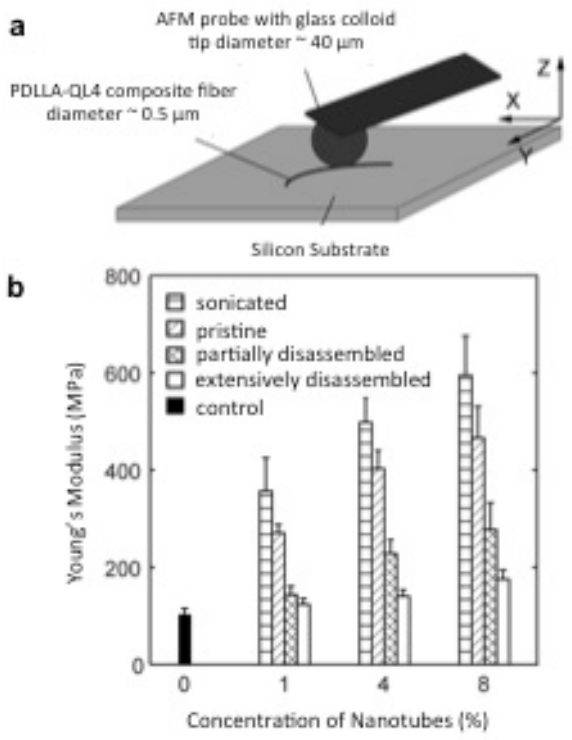

Figure 3.14. Nanomechanical characterization of composite fibers. (a) Schematic of AFM probe with a spherical colloidal tip used for testing. (b) Average Young's modulus of fibers plotted against DLCP-NT concentration for sonicated, intact, partially disassembled, and extensively disassembled microcrystals (N = 16; N = 48 for control). The stiffest measured samples are composites containing sonicated QL4 fillers with a loading of 8% by weight.

It is theoretically possible that variations in fiber diameter across the samples could affect the fiber mechanics. However, based on an analysis of modulus vs. fiber diameter for the experimental sample set, it is apparent that the amount and identity of the filler material are the main contributors to the increased stiffness values (Figure 3.15). One sees that there are cases in which the fiber diameter remained constant, while the Young's Modulus changed in parallel with the increased filler composition (Sonicated), as well as cases in which the Young's Modulus remained stable while the diameter of the

fiber varied greatly (Control). Furthermore, it is typical to observe increased stiffness when fibers possess diameters below the 500nm diameter shown here .

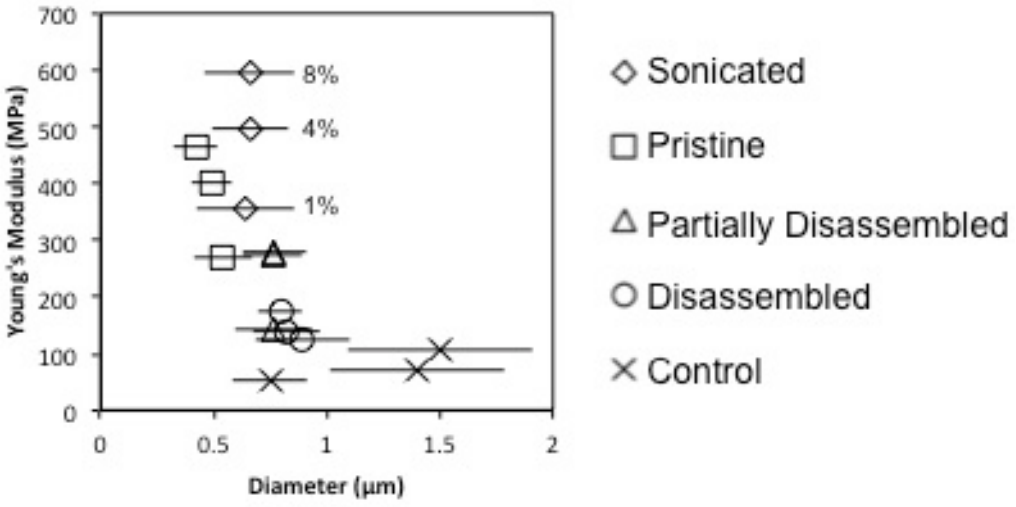

Figure 3.15. Correlation between fiber modulus and fiber diameter depicted for each of the experimental conditions: sonicated (*diamonds*), pristine (*squares*), partially disassembled (*triangles*), extensively disassembled (*circles*), and control (*exes*). Each data point within each series corresponds to a different loading of DLCP microcrystal, however, only the sonicated series is labeled for clarity. Note that for control samples (0% peptide loading), large changes in diameter result in no change in modulus, however for sonicated and pristine microcrystals, large increases in stiffness occur without a corresponding change in diameter, implicating filler quantity and state as the primary determinants in reinforcement. Each data point represents 16 measurements at a given condition.

The measurements of average moduli suggest that the composite fiber mesh is generally more robust than the control mesh, however, reporting the average values of the modulus does not convey a complete story. Figure 3.16 depicts a series of point-stiffness measurements from which the averages were calculated, as well as a schematic structure of the internal structure of the fiber. Analysis of the system by SEM, EDS and FT-IR suggests that there are regions within the fiber that do not contain peptide reinforcers.

Within a given section of fiber, one can imagine indenting in an area with an embedded structure at the core of the fiber, at the surface of the fiber, or with no embedded peptide at all. Depending on the area that is tested, the point stiffness will appear significantly higher or lower. This leads to highly variable point stiffnesses.

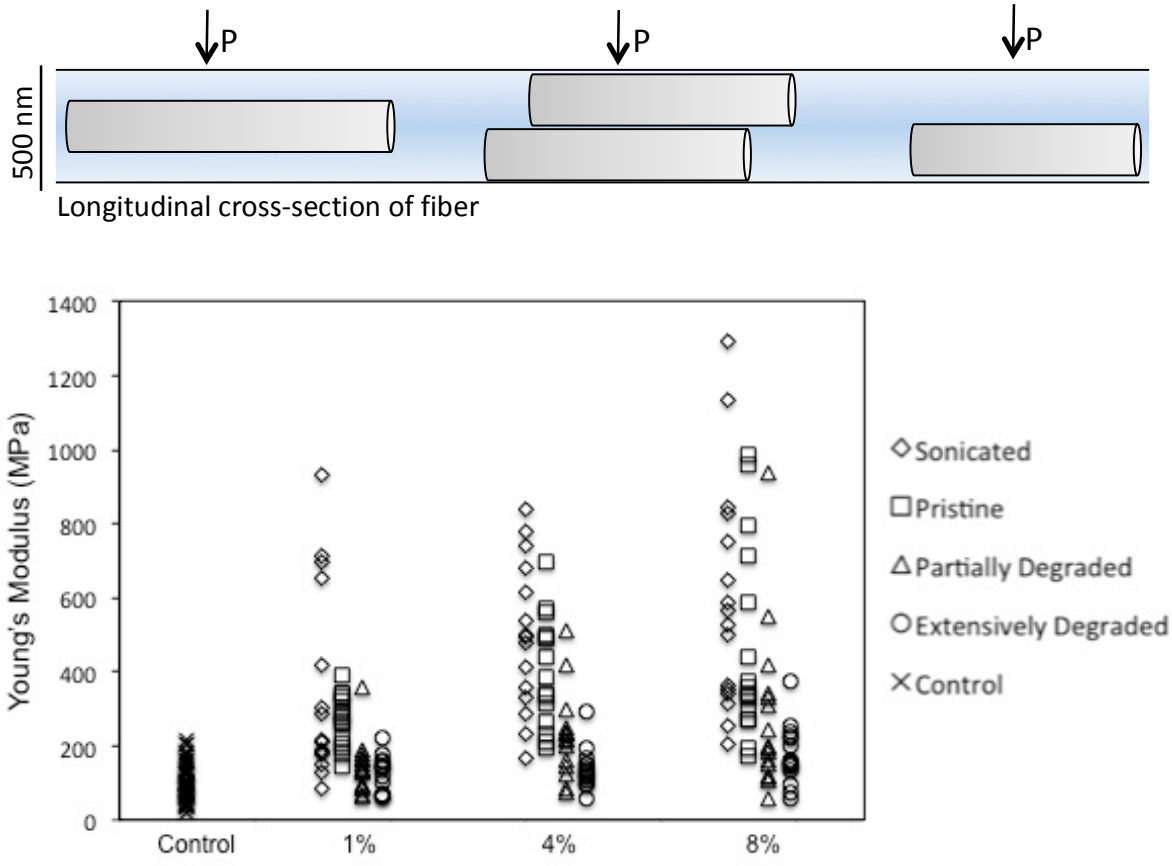

Figure 3.16. Composite fiber structure and distribution of point-stiffnesses. [Top] SEM, EDS and FT-IR based structural analysis suggests that the internal structure of the fiber is inhomogenous, likely due to the similar diameters between peptide assemblies and the fiber in which they are embedded. This lends itself toward a material with very disperse point stiffnesses depending on where the force (P) is applied. [Bottom] Distribution of modulus values from individual force-displacement experiments for all composite fiber samples. Variance suggests that point-stiffness is a function of proximity to a microcrystal.

Control fibers that do not contain any peptide have a consistent point stiffness below 200 MPa. As peptide is added to the system, pristine or otherwise, the individual point stiffness measurements begin to increase. The higher the loading percentage of filler material, the more likely one is to probe an area that is influenced by the peptide filler and therefore there are an increased fraction of measurements that fall above the control baseline. The stiffest measured areas have elastic moduli of 1-1.4 GPa, representing approximately a 10-fold increase in stiffness as compared to the average value of the control. These maximum stiffness measurements are on par with well characterized biomaterials such as collagen and tendon. [22, 23] This indicates that with increased loading, one can expect to continue to reinforce the scaffold so long as the composite fiber is able to maintain a similar morphology. It is worth noting that the geometry of the mechanical test described herein is an unusual method to probe fibers. Fibers, by definition, are anisotropic structures in which the long axis is strong and the axes orthogonal to that are relatively weak. Despite sample loading along the weak axis, the composite fibers described here are able to approach the properties of robust biomaterials. This raises an interesting consideration for the use of DLCP-NTs as a filler element that helps stabilize the 'weak' axis of fibers.

Complete tables of average moduli and statistical significance are presented in Figures 3.17 and 3.18. At just 1% loading by weight, pristine and sonicated DLCP-NTs were able to generate roughly 3-fold increase in the average modulus of the tested fibers. Indeed, with the exception of completely disassembled peptide filled fibers, all peptide fillers generated statistically significant reinforcement at 1% loading by weight. Due to

the plateauing reinforcement effect detected herein, there is a decrease in statistical separation between conditions as one moves from 1% to 4% and from 4% to 8% loading.

Average Young's Modulus (MPa)				
	Sonicated	Pristine	Partially Disassembled	Extensively Disassembled
1%	356 ± 68	270 ± 18	143 ± 18	123 ± 13
4%	497 ± 53	402 ± 38	227 ± 30	139 ± 14
8%	594 ± 78	465 ± 66	278 ± 55	175 ± 19

Figure 3.17. The average Young's modulus and corresponding standard errors of composite fibers. The most significant reinforcement occurs when sonicated QL4 microcrystals act as the filler material.

Statistical Significance in Young's Modulus Values												
	1% Sonic	4% Sonic	8% Sonic	1% Pris.	4% Pris.	8% Pris.	1% P. Dis.	4% P. Dis.	8% P. Dis.	1% E. Dis.	4% E. Dis.	8% E. Dis.
0%	*	*	*	*	*	*	*	*	*	ns	*	*
	1% Sonic	ns	*	1% Pris.	*	*	1% P. Dis.	*	*	1% E. Dis.	ns	*
		4% Sonic	ns		4% Pris.	ns		4% P. Dis.	ns		4% E. Dis.	ns
			8% Sonic			8% Pris.			8% P. Dis.			8% E. Dis.

Figure 3.18. The statistical significance (student's t-test, $p < 0.05$) between, denoted by (*), is presented between each sample set and the control, as well as within a given sample set. All sample sets, excluding disassembled microcrystals, are statistically significant with respect to the control at 1 weight percentage incorporation.

3.4 CONCLUSION

In summary, we demonstrated that electrospun PDLLA fibers can be reinforced by incorporation of self-assembled cyclic peptide nanotubes. At only 1% peptide loading by weight, both pristine and sonicated DLCP-NTs were able to reinforce the PDLLA fiber mesh by a factor of ~3. Higher concentrations of uniform microcrystals led to

higher stiffness values, with the stiffest fibers obtained with 8% by weight loading of sonicated DLCP microcystals exhibiting a modulus value of 595 MPa, representing a >5-fold increase in modulus as compared to the control. We also demonstrated that DLCP-NTs are able to withstand the high energy conditions associated with electrospinning, potentially establishing DLCP-NTs as a compatible filler component in a variety of other material processing techniques. Nano- and micro-structures assembled from DLCPs possess a unique combination of customizable surface chemistry and rigidity that are absent in most high aspect ratio nano-scale materials. However, examples of DLCP incorporation into macroscopic materials have heretofore been limited. The versatility provided by the self-assembling DLCP structures makes them a potentially useful alternative to those restricted by covalent bonding when considered for applications in high-performance and self-healing materials.

3.5 MATERIALS AND METHODS

Chemicals and Reagents Acetone, dichloromethane, dimethylformamide, diisopropylamine, and piperidine were purchased from Sigma Aldrich. Dichloromethane and dimethylformamide were dried over molecular sieves. The following chemicals were used as provided: Acetone, trifluoroacetic acid, 2-(1H-benzotriazol-1-yl)-1,1,3,3-tetramethyluronium hexafluorophosphate (HBTU), and (benzotriazol-1-yl-oxytripyrrolidinophosphonium hexafluorophosphate) (PyBOP) (Sigma Aldrich). All amino acids and Rink Amide-MBHA resin were purchased from AAPPTEC, Louisville Kentucky.

Cyclic Peptide Synthesis D,L-cyclic peptides were synthesized in accordance with the procedure of McMurray.[24] Fmoc-Glu-OAll was coupled to a Rink Amide-MBHA resin through the side-chain carboxylate. When cleaved, this residue is converted to a Gln. Standard Fmoc synthesis produced an uncyclized 8-mer which was cyclized through a PyBop assisted coupling reaction. Peptides were cleaved from the resin with 95% TFA, 2.5% water and 2.5% triisopropylsilane. To isolate the peptide, the TFA solution was concentrated by evaporation and dropped into cold diethyl ether causing precipitation. The mixture was centrifuged, resuspended in TFA and precipitated again to increase purity. Cyclic peptide identity was verified by liquid chromatography electrospray ionization mass spectroscopy.

Self-Assembly Self-assembly was achieved by dissolving 2.5 mgs/ml of QL4 in a mixture of 60% TFA and 40% water. The assembly occurred in a glass vial over 48-72 hours at which point microcrystals could be seen by eye. Crystals were harvested by diluting the assembly with a mixture of acetone and dichloromethane and pelleting the crystals by centrifugation. Crystals were rinsed 3 times with acetone/dichloromethane before characterization and incorporation in PDLLA.

Electrospinning Nanofibers were produced by traditional electrospinning methods. Solutions containing 8% poly-D,L-lactide and varying amounts of QL4 microcrystals ranging from 0 wt% to 8 wt% in 3:1 acetone to dichloromethane were vortexed to promote mixing. The solutions were then electrospun at a flow rate of 0.07 ml/min, 25 kV and at 30cm from the collecting plate. Samples were collected on aluminum foil and silicon wafers and stored for later use.

FE-SEM Imaging of Fibers and DLCP Nanotubes Electrospun fiber samples deposited on aluminum foil were cut and mounted onto SEM stubs using carbon adhesive. For the recovery of DLCPs from non-woven mats, nanofibers were incubated in acetone, selectively dissolving the polymer while leaving QL4 microcrystals intact. Once the PDLLA had dissolved, QL4 was pelleted by centrifugation and washed 3 times with acetone, before resuspension in water. This suspension was applied to a Nuclepore filter under low vacuum, the filters were allowed to dry under vaccum, and then mounted onto SEM stubs as above. All samples were sputter-coated with Au/Pd and then imaged on a Zeiss FE-SEMSupra55VP (Carl Zeiss, Oberkochen, DE) in SE2 mode.

Fourier-Transform Infrared Spectroscopy A Bruker Hyperion 3000 FTIR microscope (Bruker Optics Inc, Billerica, MA) was used to confirm the presence of DLCPs in the composite fibers. Electrospun fibers, with aluminum foil backing, were placed under the objective and measurements were taken in reflectance mode.

Mechanical Characterization An Asylum MFP3D AFM (Asylum Research, Santa Barbara, CA) was used to perform the nanoindentation on single fibers atop a silicon wafer in the dry state. A glass spherical probe tip (Polysciences, Warrington, PA), diameter ~ 40 um, was attached to the tipless cantilever with nominal spring constant k ~ 30 N/m (Budget Sensors, Sofia, Bulgaria). The thermal oscillation method was applied to determine the cantilever spring constant for each probe tip [25]. The indentation was performed under force control scheme, with maximum force ~ 900 nN. The axial (z direction) displacement of tip is calculated as the z-piezo subtracted by the vertical deflection of the cantilever. All data reported in this manuscript is based on axial loading of fibers.

3.6 ACKNOWLEGEMENTS

This work was funded by a seed grant from the Harvard MRSEC, the Army Research Office (ARO - 167836) STIR program, and the Center for Nanoscale Systems (CNS) at Harvard University, a member of the National Nanotechnology Infrastructure Network (NNIN), which is supported by the National Science Foundation under NSF award no. ECS-0335765

3.7 REFERENCES

1. Freed, L. E.; Engelmayr, G. C.; Borenstein, J. T.; Moutos, F. T.; Guilak, F., Advanced Material Strategies for Tissue Engineering Scaffolds. *Advanced Materials* **2009,** *21* (32-33), 3410-3418.

2. (a) Zahedi, P.; Rezaeian, I.; Ranaei-Siadat, S.-O.; Jafari, S.-H.; Supaphol, P., A review on wound dressings with an emphasis on electrospun nanofibrous polymeric bandages. *Polymers for Advanced Technologies* **2009**, n/a-n/a; (b) Cai, Z.-X.; Mo, X.-M.; Zhang, K.-H.; Fan, L.-P.; Yin, A.-L.; He, C.-L.; Wang, H.-S., Fabrication of Chitosan/Silk Fibroin Composite Nanofibers for Wound-dressing Applications. *IJMS* **2010,** *11* (9), 3529-3539.

3. Tian, H.; Tang, Z.; Zhuang, X.; Chen, X.; Jing, X., Biodegradable synthetic polymers: Preparation, functionalization and biomedical application. *Progress in Polymer Science* **2012,** *37* (2), 237-280.

4. Ma, W.; Liu, L.; Zhang, Z.; Yang, R.; Liu, G.; Zhang, T.; An, X.; Yi, X.; Ren, Y.; Niu, Z.; Li, J.; Dong, H.; Zhou, W.; Ajayan, P. M.; Xie, S., High-Strength Composite Fibers: Realizing True Potential of Carbon Nanotubes in Polymer Matrix through Continuous Reticulate Architecture and Molecular Level Couplings. *Nano Letters* **2009,** *9* (8), 2855-2861.

5. Wang, T.; Drzal, L. T., Cellulose-Nanofiber-Reinforced Poly(lactic acid) Composites Prepared by a Water-Based Approach. *ACS Applied Materials & Interfaces* **2012,** *4* (10), 5079-5085.

6. (a) Velasco-Santos, C.; Martinez-Hernandez, A.; Castano, V., Carbon nanotube-polymer nanocomposites: The role of interfaces. *Composite Interfaces, 11* **2005,** *8* (9), 567-586; (b) Young, K.; Blighe, F.; Vilatela, J.; Windle, A.; Kinloch, I.; Deng, L.; Young, R.; Coleman, J., Strong Dependence of Mechanical Properties on Fiber Diameter for Polymer– Nanotube Composite Fibers: Differentiating Defect from Orientation Effects. *ACS nano*.

7. Dugan, J. M.; Gough, J. E.; Eichhorn, S. J., Bacterial cellulose scaffolds and cellulose nanowhiskers for tissue engineering. *Nanomedicine* **2013,** *8* (2), 287-298.

8. Van Der Zande, M.; Junker, R.; Walboomers, X. F.; Jansen, J. A., Carbon Nanotubes in Animal Models: A Systematic Review on Toxic Potential. *Tissue Engineering Part B: Reviews* **2011,** *17* (1), 57-69.

9. Boyle, A. L.; Woolfson, D. N., De novo designed peptides for biological applications. *Chemical Society reviews* **2011,** *40* (8), 4295.

10. Matson, J. B.; Zha, R. H.; Stupp, S. I., Peptide Self-Assembly for Crafting Functional Biological Materials. *Current opinion in solid state & materials science* **2011,** *15* (6), 225-235.

11. (a) Zhang, S., Fabrication of novel biomaterials through molecular self-assembly. *Nature Biotechnology* **2003,** *21* (10), 1171-1178; (b) Jung, J.; Gasiorowski, J.; Collier, J., Fibrillar peptide gels in biotechnology and biomedicine. *Peptide Science* **2010,** *94* (1), 49-59.

12. Fernandez-Lopez, S.; Kim, H.-S.; Choi, E. C.; Delgado, M.; Granja, J. R.; Khasanov, A.; Kraehenbuehl, K.; Long, G.; Weinberger, D. A.; Wilcoxen, K. M., Antibacterial agents based on the cyclic D, L-α-peptide architecture. *Nature* **2001,** *412* (6845), 452-455.

13. Hartgerink, J.; Granja, J.; Milligan, R.; Ghadiri, M., Self-assembling peptide nanotubes. *J. Am. Chem. Soc* **1996,** *118* (1), 43-50.

14. Diaz, J.; Çağin, T., Thermo-mechanical stability and strength of peptide nanostructures from molecular dynamics: self-assembled cyclic peptide nanotubes. *Nanotechnology* **2010,** *21*, 115703.

15. Peltoniemi, H.; Ashammakhi, N.; Kontio, R.; Waris, T.; Salo, A.; Lindqvist, C.; Grätz, K.; Suuronen, R., The use of bioabsorbable osteofixation devices in craniomaxillofacial surgery. *Oral Surgery, Oral Medicine, Oral Pathology, Oral Radiology, and Endodontology* **2002,** *94* (1), 5-14.

16. Böstman, O.; Pihlajamäki, H., Clinical biocompatibility of biodegradable orthopaedic implants for internal fixation: a review. *Biomaterials* **2000,** *21* (24), 2615-2621.

17. Felfel, R. M.; Ahmed, I.; Parsons, A. J.; Rudd, C. D., Bioresorbable screws reinforced with phosphate glass fibre: Manufacturing and mechanical property characterisation. *Journal of the Mechanical Behavior of Biomedical Materials* **2013,** *17*, 76-88.

18. Even, N.; Adler-Abramovich, L.; Buzhansky, L.; Dodiuk, H.; Gazit, E., Improvement of the Mechanical Properties of Epoxy by Peptide Nanotube Fillers. *Small* **2011,** *7* (8), 1007-1011.

19. (a) Changsarn, S.; Mendez, J. D.; Shanmuganathan, K.; Foster, E. J.; Weder, C.; Supaphol, P., Biologically Inspired Hierarchical Design of Nanocomposites Based on Poly(ethylene oxide) and Cellulose Nanofibers. *Macromolecular Rapid Communications* **2011,** *32* (17), 1367-1372; (b) Liao, G.-Y.; Zhou, X.-P.; Chen, L.; Zeng, X.-Y.; Xie, X.-L.; Mai, Y.-W., Electrospun aligned PLLA/PCL/functionalised multiwalled carbon nanotube composite fibrous membranes and their bio/mechanical properties. *Composites Science and Technology* **2012,** *72* (2), 248-255.

20. Bandekar, J.; Krimm, S., Normal mode spectrum of the parallel-chain β-sheet. *Biopolymers* **1988,** *27* (6), 909-921.

21. Popov, V. L., *Contact mechanics and friction*. Springer: 2010.

22. Ashby, M. F.; Gibson, L. J.; Wegst, U., The mechanical properties of natural materials. I. Material property charts. *… of the Royal …* **1995**.

23. Wegst, U. G. K.; Ashby, M. F., The mechanical efficiency of natural materials. *Philosophical Magazine* **2004,** *84* (21), 2167-2186.

24. McMurray, J. S., Solid phase synthesis of a cyclic peptide using Fmoc chemistry. *Tetrahedron Letters* **1991,** *32* (52), 7679-7682.

25. Hutter, J. L.; Bechhoefer, J., Calibration of Atomic Force Microscope tips. *Review of Scientific Instruments* **1993,** *64*, 1868.

Chapter 4: Summary and Future Directions

4.1 SUMMARY

Biologically Inspired Self-Assembling Materials: Inspiration, Structure and Properties

In Chapter 1, examples of natural materials, descriptions of biologically inspired self-assembling peptides, and the guiding hypotheses of this work were provided. Nature has evolved a diverse toolkit from which it creates the inspiring materials synthesized by plants and animals. In many cases, these materials are composites and demonstrate hierarchical structures organized from the nano- to the macroscale. Collagen[1] and silk[2], the two examples discussed in Chapter 1, are both well characterized and serve as inspiration to materials engineers.

When considering a self-assembling platform for the design of a material, one must take into account the chemistry of the monomer in order to determine the system's properties. These properties include, but are not limited to, the ability to modify the self-assembling building block, the size and structure of the assembly, the dynamic or static nature of the assembly, and the mechanical and chemical stability of the assembly. The breadth of systems that have been engineered to date is evidence of the difficulty in designing a 'winning' system that can become a technology of choice across application areas. While some systems excel in their stability, others are easier to modify, and others may be best for dynamic materials applications.

D,L-cyclic peptides were chosen as the centerpiece of this research because they combine unparalleled chemical flexibility with a high persistence length an distinct rod-like morphology that is not apparent in other peptide systems. The size and morphology

of DLCP assemblies serve as indicators of their stability. Despite recent interest in mechanical analyses, there was little experimental evidence to support expectations that D,L-cyclic peptides actually had the properties necessary to enable bio-engineered real-world applications. This work was undertaken to more fully characterize the fundamental mechanical properties of DLCP assemblies so that engineers could make better informed decisions about their potential as a nanoscale construction material.

Structure and Mechanical Properties of D,L-Cyclic Peptides

In Chapter 2, the structure and mechanical properties of bundled fibers, assembled from QL4, were examined in detail. Through electron microscopy and computational modeling of assemblies it was revealed that QL4 forms large structures on the order of 100nm-2μm in diameter and up to 10μm-100μm long. The structures are hierarchically organized from individual tubes that form fibers, which then bundle to form the large fibers used in mechanical testing. We hypothesize that the size and stability of QL4 assemblies is a factor of two characteristics. First, by cyclizing the peptide, the degrees of conformational freedom are limited and the potential for intermolecular interactions is similarly constrained. This necessitates that QL4 monomers stack directly atop one another when bonding and prevents freedom to slip in the x- or y-plane orthogonal to the long axis of assembly. Second, the presence of symmetric glutamine residues on the peptide cycle allows for dense, favorable packing between tubes (inter-tube associations), with alternate leucine residues providing a secondary stabilizing effect in the structure. Together, these factors result in a distinctly large and rod-like morphology that is not found in other organic self-assembling systems.

Bundled fibers were subjected to nanoindentation and depth-sensing-based bending over micron-scale channels. The density adjusted stiffness (specific modulus) was found to be superior to collagen and tendon[3], as well as amyloid fibrils measured at the nanoscale by similar methods.[4,5,6] The density adjusted flexural modulus of QL4 fibers is more pronounced, outperforming both enamel and steel. The strength of QL4 fibers (measured in flexion) is similar to collagen, tendon, bone and enamel.[3] Together, this data indicates that QL4 fibers behave similarly to what one expects from 'light' bone, rather than a typical peptide material.

Due to the high stiffness, particularly in flexion, and the low density of QL4 fibers, they have interesting potential for use as mechanical fillers in low-density, high-performance composites. When one considers the potential for dynamic assembly, disassembly, and tunable surface chemistry, it is evident that D,L-cyclic peptides could be an intriguing scaffold for a variety of composite materials applications.

D,L-Cyclic Peptides as Filler Materials in Biodegradable Composite Fibers

In Chapter 3, bundled QL4 fibers were utilized as a structural filler material within poly-d,l-lactic acid (PDLLA) fibers. Peptide assemblies were incorporated in four different forms: pristine, sonicated, partially disassembled, and fully disassembled. Upon sonication, the average length of a bundle decreased from ~20 μm to ~3 μm. Fibers were disassembled/aggregated by lyophilization followed by scraping from the sides of vessels and resuspension. Each type of peptide filler was incorporated at 1, 4, and 8 weight percentage loadings into PDLLA solution.

Peptide-doped PDLLA solutions were electrospun into nanofibers using a traditional electrospinning apparatus.[7] Pristine and sonicated peptide fillers disperse well within the polymer solution while disassembled/aggregated fillers tend to clump, leaving significant areas within the polymer solution devoid of peptide reinforcing elements. The resultant composite fibers were smooth, indicating the peptide assemblies were aligned with the long axis of the fiber. Fibers were analyzed by SEM, FTIR and EDS in order to characterize their internal structure. Unlike a true nano-composite, the peptide assemblies are similar in diameter to the fiber diameter, resulting in fibers with gaps between filler elements.

The elastic moduli of the composite fiber meshes was tested using AFM-based indentation methods. In these tests, fibers were indented perpendicular to their long axis. This method allowed for the determination of average properties of the fiber mesh based on a series of 'point' stiffness measurements. Composite fibers containing 8% by weight sonicated peptide filler exhibited the highest average modulus, roughly 6-fold higher than the control samples. The performance of sonicated peptide fillers was followed by pristine, partially disassembled, and fully disassembled peptide fillers. The results indicate that the nature of the peptide filler, whether due to internal structure or potential for dispersion, determines the potential for reinforcement.

Self-assembled DLCP structures possess a unique combination of customizable chemistry and rigidity that are absent in most high aspect ratio nano-scale materials and self-assembled peptide materials. This is the first example of DLCP incorporation into a bulk material. The versatility provided by the self-assembling DLCP structures may

prove useful for applications beyond traditional mechanical reinforcement, including actuating and self-healing materials.

4.2 FUTURE DIRECTIONS

Systematic Characterization of DLCP Structures with Alternative Bonding Modalities

The preceding studies describe a first foray into the mechanical characterization of D,L-cyclic peptides. QL4 was selected for these studies due to its large size, stability, and ease of synthesis. While QL4 has proven to be an interesting model system, the true potential of DLCPs is in their nearly limitless chemical diversity. As discussed in Chapter 1, DLCPs are somewhat unique in their ability to tolerate side-chain modification while still assembling into supramolecular structures.[8] If one considers natural amino acids, unnatural amino acids, heterocyclic peptides and post-translational modifications, it is evident that DLCPs are a high-potential engineering platform with a broad array of applications.

Filtering the potential peptide candidates to discern reasonable monomers for future experiments can be a challenge. Focusing exclusively on disentangling the range of modulus, strength and densities that one can achieve with a simple DLCP 8-mer, it would be beneficial to explore other bonding modalities, particularly metal-coordinate bonds, salt-bridges, and covalent linkages. Metal-coordinate chemistry is found throughout natural systems, perhaps most notably in the oxygen-carrying hemoglobin protein. However, metal coordinate chemistry is used by nature in the reinforcement of materials as well. The jaw of the marine polychaetes *Nereis virens*, and *Glycera*

dibranchiata are loaded with Zn and Cu, respectively.[9, 10, 11] In each case, nature has chosen protein-mediated metal-coordinate bonds as a means to retain hardness, wear resistance, and stiffness within an aqueous environment.[12] When one considers the potential medical uses of DLCPs, particularly in the form of composites, it may be relevant to imbue the DLCP filler with similar water-tolerant chemistry. The natural ability of histidine residues to chelate metals could prove to be an affective component of a DLCP tailored to this use.

As a point of comparison, synthesizing DLCPs that are capable of salt-bridging will provide an alternate stabilization mechanism that is of interest. Pioneering work in DLCP synthesis and characterization led by Dr. Ghadiri explored the use of cyclo-[(L-Glu-D-Leu)$_4$] and cyclo-[(L-Lys-D-Leu)$_4$] as a co-assembly pair.[13] A computational and mechanical analysis of this bridged co-assembly would provide an interesting counterpoint to the other non-covalent assemblies, H-bond mediated and metal-coordinate mediated. Furthermore, by utilizing a salt-bridging pair, one could begin to explore self-assembly in-situ within an aqueous environment, a hurdle that is insurmountable with the extremely hydrophobic, insoluble QL4 peptide.

Lastly, to test the upper limits of stiffness and strength, one could explore the use of covalent bonding pairs. An experimentally tractable starting point may be to utilize cysteine-mediated covalent capture as is described in the peptide amphiphile system designed by the Stupp Lab.[14] While disulfide bonds are less stable than carbon-carbon or amide bonds, they have the added benefit of external control through modulation of redox conditions within the solution.[15] This would provide a method for testing covalent linkages without compromising the dynamic nature of the material.

The direct comparison of hydrogen bond, metal-coordinate, salt-bridge, and covalent stabilization will provide significant breadth in our understanding of the DLCP as a structural material. An area yet to be discussed is the anisotropy of bonding within the aforementioned materials. Along the long axis of assembly, all structures will be stabilized through hydrogen-bonds as was the case with QL4 fibers. However, in addition to backbone-mediated bonding the side chain chemistry may impact both longitudinal and lateral assembly. Further experimentation with the chemistries described above will expand the potential utility of DLCPs to include stronger, more wear-resistance, and water-tolerant composites.

Preliminary results of the synthesis of cyclo-[$(ELKL)_2$] its structural characterization are presented in Appendix A.

Controlling the Size and Shape of DLCP Assemblies

The end goal of supramolecular self-assembly is to build intricate, functional structures with nano- and microscale dimensions, from the bottom up.[16] Even a cursory analysis of a natural system will inspire one's innate curiosity to understand how such ordered diversity can be created from such simple building blocks. While DLCPs provide a vehicle to create tremendous diversity, it is a scaffold that has proven difficult to control.[8] For DLCPs to realize their full potential, we must develop methods for controlling the diameter and length of cyclic peptide nanotubes and fibers.

Current techniques to control peptide length and diameter are limited to appending polymer chains from DLCPs and utilizing layer-by-layer deposition techniques.[17,18,19,20] The pioneering work by Dr. Biesalski demonstrated that by

conjugating polymer chains of varying lengths to DLCPs, one could prevent lateral aggregation and control the length of the assembly within the range of ~50 nm – 150 nm.[19] Mizrahi, et al. have also demonstrated control over DLCP nanotube length by layering alternately charged DLCP monomers on a gold surface.[20] These results stand in stark contrast to the comparatively massive structures formed by QL4 that can reach above 100 μm in length.[21] While these methods provide control, they are very labor intensive and are not particularly scalable. Taking these data points to represent the smallest and largest structures that can be formed from DLCPs, it is evident that there is a wide range, representing multiple orders of magnitude, within which one can seek to control both length and diameter.

It has been reported that DLCPs assemble by a cooperative mechanism in which there is a slow nucleation step followed by a rapid elongation step.[22] Therefore, controlling the initiation of assembly and time of assembly may allow one to exert some control over the length and diameter of structures. One option to consider would be to 'seed' the assembly with partially disassembled DLCP structures. The addition of the seeds bypasses the nucleation step, and the overall size of assembly may be controlled by the ratio of seed to monomer. A secondary control mechanism of interest is an on-demand assembly trigger. By using a photo-cleavable protecting group such as 2-nitroveratryl[23], one could prevent the assembly of the DLCP until the proper conditions are achieved, affording both nucleation control and prevention of premature assembly. To date, methods for the control of DLCP assemblies have been limited, however it is a necessary focus if cyclic peptides are to become a practical, functional scaffold for materials engineering.

Preliminary results describing seeded DLCP assemblies are presented in Appendix B.

Utilizing DLCP Fibers as Polymer Stabilizers

Due to the high cost of synthesis and processing, it is unlikely that DLCPs will find a use as a pure, bulk material. Rather, DLCPs may find their niche as a minority, functional component within a larger, less costly matrix. These functional composites could find utility as filters[24], ion sensors[20], or responsive polymers.[25] One area that is yet to be explored is the use of DLCP fibers or DLCP nanotubes as reinforcing elements for polymer materials subjected to static loads, such as resorbable orthopedic implants.

Resorbable materials are of interest in medicine because they obviate the need for post-operative surgery and can enhance healing by preventing stress shielding that may otherwise occur.[26] Indeed, over the last fifty years, research in biodegradable polymers for application in therapeutic structural materials has yielded many clinically relevant devices including sutures, plates and screws.[27] Due to their high yield-stress and modulus, polymers based on lactic acid (PLA), glycolic acid (PGA), or blends of the two (PLGA), have come into favor for applications in which the material must bear significant loads.[28] Despite their high elastic modulus, it was discovered that over time, under static loading conditions such as is present in the spine, these devices would fail before the body was able to fully heal.

While a solid polymer material appears rigid and stable, molecular rearrangements within the bulk can still occur. These rearrangements are never observed because without an outside stimulus, the time scale and degree of movement is virtually zero.[29] However,

as soon as a stress is applied to the system, the polymer chains begin to flow. In the case of a polymer structure undergoing a slow deformation, the forces exerted on the bulk material are transferred to individual molecular chains, which flow with respect to one another, allowing the material to stretch significantly. If one considers placing a material under static load, rather than a fixed strain rate, it is evident that over long enough time scales, the structure will still deform, and eventually fail.[28]

There are several ways to imagine engineering around the mechanical failure of polylactides/glycolides. Traditional approaches include, but are not limited to, reengineering the polymer itself, crosslinking the structure, and using a polymer blend. An alternate approach to consider is the integration of a nanoscale filler such as a DLCP nanotube or fiber. By incorporating peptide-based nanostructures of complimentary surface chemistry to the polymer, one may be able to increase the overall stability. Namely, the nanostructures will associate closely with the polymer, decreasing its flexibility, acting as 'side chains', and increasing favorable interactions within the melt, all of which act to decrease the free volume, and increase the glass transition temperature and time-to-failure.[30] Due to the potential for control over size, dimensions and surface chemistry, one can imagine a suite of DLCP-fillers, specifically tuned for use in a variety of load-bearing, resorbable materials.

An area concern for any application of DLCPs *in vivo* is their biocompatibility, or lack thereof. Research by the Ghadiri Lab suggests that the toxicity (as measured by hemolysis) of amphipathic DLCPs varies with sequence but is quite low.[31] Early work within the Joshi Lab suggests that assembled QL4 fibers, when mixed with media, do not cause cell death in fibroblasts. Together, these analyses represent two potential toxicity

extremes, monomers and very large fibers. For a complete study, the analysis of a variety of DLCP monomers, assemblies, and large assemblies should be tested *in vitro* and *in vivo*.

Preliminary results of the fabrication, structural characterization and mechanical analysis of cyclo-[$(QL)_4$]-loaded PDLLA films is presented in Appendix C.

DLCP Assemblies as Toughening Agents

Materials toughness is defined as the total amount of energy that can be absorbed by a material before failure. Biomaterials, particularly silks, have remarkable toughness that surpasses similar synthetic materials. [2,32] Often this toughness is achieved by synthesizing a composite in which one component is held together through 'sacrificial' bonds that are able to break, and possibly reform, upon stress. This allows the material to absorb a huge amount of energy. If one considers the example of a spider web trapping a flying insect, it is clear that if the material must withstand the momentum of the insect by dissipating the energy. Otherwise the insect would be more likely to break through, or bounce off. Both strength and extensibility are necessary.

As DLCPs are supramolecular in nature, they may prove to be interesting 'crosslinking-nodes' within composites. By crosslinking the stiff DLCP assembly into a softer, more elastic matrix it may be possible to approximate the overall structure of silk. Rather than β-crystals, the material would have DLCP fibers. As stresses are imposed on the matrix, forces will be transferred to the DLCP structures are able to

come apart. This will allow for the continued deformation of the material as a whole but will also provide stiffness and strength. Upon relaxation of the material, one may find that DLCP structures are able to reattach to one another, allowing the material to self heal between deformations.

The focus in Chapters 2 and 3 was on the model system of QL4, however to analyze the toughening potential of DLCP crosslinkers one would need to synthesize a peptide with more readily available crosslinking handles. The options include amine or carboxylic containing amino acids such as glutamate, aspartate and lysine, as well as sulfhydryl containing amino acids such as cysteine. Of course, unnatural amino acids could be included as well.

Preliminary results of the fabrication, structural characterization and mechanical analysis of ELKL2/Elastin films is presented in Appendix D.

4.3 Conclusions

Self-assembled peptide systems allow for the creation of hierarchically structured materials with broad functionality. However, building with peptides is not without its share of difficulties. Specifically, self-assembling peptides lack the programmability of nucleotide-based structures and therefore the assembly process is very difficult to control. This is observed in peptide amphiphiles, amyloid fibrils, aromatic dipeptides, and D,L-cyclic peptides.

Within the field, D,L-cyclic peptides possess their own specific challenges including difficulties in synthesis/cyclization, unpredictable solubility, uncontrolled assembly/disassembly, and concerns over biocompatibility. First, amino acid conjugation

during synthesis can be a challenge with certain sequences. For efficient coupling, the peptide end should be fully exposed to the surrounding solvent. Repeated amino acids with flexible structures, such as glycine, can lead to a hidden reactive site that decreases the overall coupling efficiency. Cyclization may be inhibited by a flexible backbone, or by a backbone that is overly constrained due to the presence of bulky side-chains or post-translational modifications.

Solubility varies greatly between DLCPs of similar chemistry. For example, the peptide QL4, which has been described extensively herein, is soluble only in trifluoroacetic acid. The replacement of a single leucine with a lysine residue causes the peptide to be soluble in all aqueous media and polar organics. Peptides with oppositely charged functional groups such as glutamates and lysines are insoluble in aqueous media, despite the addition of salts and manipulation of pH.

With unpredictable solubility comes difficulty in assembly. First, peptides lack the obvious base-pair mediated programmability of nucleotide-based self-assembling systems. Therefore, DLCPs must be assembled by controlling external factors such as solvent, solute concentration, pH, and temperature. QL4 assembles to form robust structures, but it is not easily controlled. Conversely, the majority of other peptides that were investigated failed to assemble at all. This suggests that DLCP assembly tends to be an, ‘all or nothing’ phenomenon in which the peptides either assemble until the point of precipitation, or fail to assemble.

Lastly, the potential biocompatibility for DLCPs remains a concern. The chemistry of DLCP monomers, the aggregate chemical behavior of the assembled DLCP structure, and the size and shape of the DLCP structure must all be considered. While

individual monomers may be sufficiently small to be passed through the body, one must ensure that the chemistry in the crystalline form, and in the monomer, is not directly toxic and does not generate an immune response. Perhaps more subtle is the concern over the physical structure of DLCPs. Taking QL4 as an example, it is quite similar in size and shape to asbestos. This suggests that toxicity could be a function of shape and size.

Many of the aforementioned complications can be mitigated through the conjugation of other molecules to the DLCP ring. Solubility, assembly, and biocompatibility may all be controlled through the conjugation of molecules with known solubilities and biocompatibilities to a basic DLCP backbone. The Xu and Biesalski labs have pioneered this approach and it has shown promise in the control of assembly. However, to my knowledge, a detailed biocompatibility study has not been completed.

4.4 REFERENCES

1. Fratzl, P., *Collagen: Structure and mechanics*. Springer: 2008.

2. Keten, S.; Xu, Z.; Ihle, B.; Buehler, M. J., Nanoconfinement controls stiffness, strength and mechanical toughness of beta-sheet crystals in silk. *Nature Materials* **2010,** *9* (4), 359-367.

3. Wegst, U. G. K.; Ashby, M. F., The mechanical efficiency of natural materials. *Philosophical Magazine* **2004,** *84* (21), 2167-2186.

4. Adamcik, J.; Lara, C.; Usov, I.; Jeong, J. S.; Ruggeri, F. S.; Dietler, G.; Lashuel, H. A.; Hamley, I. W.; Mezzenga, R., Measurement of intrinsic properties of amyloid fibrils by the peak force QNM method. *Nanoscale* **2012,** *4* (15), 4426-4429.

5. Adamcik, J.; Jung, J.-M.; Flakowski, J.; De Los Rios, P.; Dietler, G.; Mezzenga, R., Understanding amyloid aggregation by statistical analysis of atomic force microscopy images. *Nature Nanotechnology* **2010,** *5* (6), 423-428.

6. Knowles, T. P. J.; Buehler, M. J., Nanomechanics of functional and pathological amyloid materials. *Nature Nanotechnology* **2011,** *6* (8), 469-479.

7. Pham, Q. P.; Sharma, U.; Mikos, A. G., Electrospinning of polymeric nanofibers for tissue engineering applications: a review. *Tissue engineering* **2006,** *12* (5), 1197-1211.

8. Chapman, R.; Danial, M.; Koh, M. L.; Jolliffe, K. A.; Perrier, S., Design and properties of functional nanotubes from the self-assembly of cyclic peptide templates. *Chemical Society Reviews* **2012,** *41* (18), 6023-6041.

9. Bryan, G.; Gibbs, P., Zinc - a major inorganic component of nereid jaws. *J. Mar. Biol. Assoc. of the UK* **1979,** (59), 969-973.

10. Bryan, G.; Gibbs, P., Metals in nereid polychaetes: the contribution of metals in the jaws to the total body burden. . *J. Mar. Biol. Assoc. of the UK* **1980,** *60*, 641-654.

11. Broomell, C. C., Critical role of zinc in hardening of Nereis jaws. *Journal of Experimental Biology* **2006,** *209* (16), 3219-3225.

12. Broomell, C. C.; Zok, F. W.; Waite, J. H., Role of transition metals in sclerotization of biological tissue. *Acta Biomaterialia* **2008,** *4* (6), 2045-2051.

13. Hartgerink, J. D., PhD Thesis. *Scripps Research Institute, La Jolla, CA* **1999**.

14. Hartgerink, J. D.; Beniash, E.; Stupp, S. I., Self-Assembly and Mineralization of Peptide-Amphiphile Nanofibers. *Science* **2001,** *294* (5547), 1684-1688.

15. Cremlyn, R. J., *An Introduction to Organosulfur Chemistry*. John Wiley and Sons: Chichester, 1996.

16. Stupp, S. I., Self-Assembly and Biomaterials. *Nano Letters* **2010,** *10* (12), 4783-4786.

17. Couet, J.; Samuel, J. D. J. S.; Kopyshev, A.; Santer, S.; Biesalski, M., Peptide-Polymer Hybrid Nanotubes. *Angewandte Chemie International Edition* **2005,** *44* (21), 3297-3301.

18. Couet, J.; Biesalski, M., Conjugating self-assembling rigid rings to flexible polymer coils for the design of organic nanotubes. *Soft Matter* **2006,** *2* (12), 1005.

19. Couet, J.; Biesalski, M., Polymer‐Wrapped Peptide Nanotubes: Peptide‐Grafted Polymer Mass Impacts Length and Diameter. *Small* **2008,** *4* (7), 1008-1016.

20. Mizrahi, M.; Zakrassov, A.; Lerner-Yardeni, J.; Ashkenasy, N., Charge transport in vertically aligned, self-assembled peptide nanotube junctions. *Nanoscale* **2012,** *4* (2), 518.

21. Hartgerink, J. D.; Granja, J. R.; Milligan, R. A.; Ghadiri, M. R., Self-assembling peptide nanotubes. *Journal of the American Chemical Society* **1996,** *118* (1), 43-50.

22. Greef, T. F. A. D.; Smulders, M. M. J.; Wolffs, M.; J.Schenning, A. P. H.; Sijbesma, R. P.; Meijer, E. W., Supramolecular Polymerization. *Chem. Rev.* **2009,** *109*, 5697-5754.

23. Karas, J. A.; Scanlon, D. B.; Forbes, B. E.; Vetter, I.; Lewis, R. J.; Gardiner, J.; Separovic, F.; Wade, J. D.; Hossain, M. A., 2-Nitroveratryl as a Photocleavable Thiol-Protecting Group for Directed Disulfide Bond Formation in the Chemical Synthesis of Insulin. *Chemistry – A European Journal* **2014,** *20* (31), 9549-9552.

24. Xu, T.; Zhao, N.; Ren, F.; Hourani, R.; Lee, M. T.; Shu, J. Y.; Mao, S.; Helms, B. A., Subnanometer Porous Thin Films by the Co-assembly of Nanotube Subunits and Block Copolymers. *ACS Nano* **2011,** *5* (2), 1376-1384.

25. Steinem, C.; Janshoff, A.; Vollmer, M. S.; Ghadiri, M. R., Reversible Photoisomerization of Self-Organized Cylindrical Peptide Assemblies at Air−Water and Solid Interfaces. *Langmuir* **1999,** *15* (11), 3956-3964.

26. Sumner, D. R., Long-term implant fixation and stress-shielding in total hip replacement. *Journal of Biomechanics* (0).

27. Middleton, J. C.; Tipton, A. J., Synthetic biodegradable polymers as orthopedic devices. *Biomaterials* **2000,** *21*, 2335-2346.

28. Engels, T. A. P.; Söntjens, S. H. M.; Smit, T. H.; Govaert, L. E., Time-dependent failure of amorphous polylactides in static loading conditions. *Journal of Materials Science: Materials in Medicine* **2009,** *21* (1), 89-97.

29. Govaert, L. E., *Time-Dependent Failure in Load-Bearing Polymers. A Potential Hazard in Structural Applications of Polylactides*. Nova Science Publishers: 2008.

30. Young, R. J.; Lovell, P. A., *Introduciton to Polymers*. Third Edition ed.; CRC Press: Boca Raton, FL, 2011.

31. Fernandez-Lopez, S.; Kim, H. S.; Choi, E. C.; Delgado, M.; Granja, J. R.; Khasanov, A.; Kraehenbuehl, K.; Long, G.; Weinberger, D. A.; Wilcoxen, K. M.; Ghadiri, M. R., Antibacterial agents based on the cyclic D,L-alpha-peptide architecture. *Nature* **2001,** *412* (6845), 452-455.

32. Vaccaro, E.; Waite, J. H., Yield and Post-Yield Behavior of Mussel Byssal Thread: A Self-Healing Biomolecular Material. *Biomacromolecules* **2001,** *2* (3), 906-911.

Appendices

The results presented in appendices A-D describe preliminary work. They are provided to serve as a foundation for new research within each area.

APPENDIX A: SYNTHESIS AND CHARACTERIZATION OF SALT-BRIDGED DLCP ASSEMBLIES

Introduction

In prior studies, salt-bridged DLCPs, cyclo-[(L-Glu-D-Leu)$_4$] and cyclo-[(L-Lys-D-Leu)$_4$], were used as a co-assembly pair.[1] Here the synthesis and assembly of the peptide cyclo-[L-Glu-D-Leu-L-Lys-D-Leu)$_4$], referred to as ELKL2, is presented. Rather than requiring a mixture of two peptides, ELKL2 is able to form self-self salt bridges to stabilize growing assemblies. Salt-bridged peptides provide advantages over QL4 because they are water soluble and have the potential for pH- and solute-controlled triggerable assembly. Furthermore, the electrostatic bond energies are higher than van der Waals forces and hydrogen bonds and consequently may provide more stable structures.

Results and Discussion

ELKL2 was synthesized using common peptide synthesis methods.[2] Upon cleavage from the resin, peptides were precipitated in cold ether and resuspended in multiple aqueous buffers and solvents. ELKL2 is highly soluble in aqueous buffers across the pH range of 3-12 and is insoluble in non-polar solvents. Assembly was

attempted at both high and low pH, but was only achieved by dissolving ELKL2 in TFA and incubating the TFA solution in the presence of water vapor (see methods for assembly of QL4). The resultant structures are presented in Figure A1.

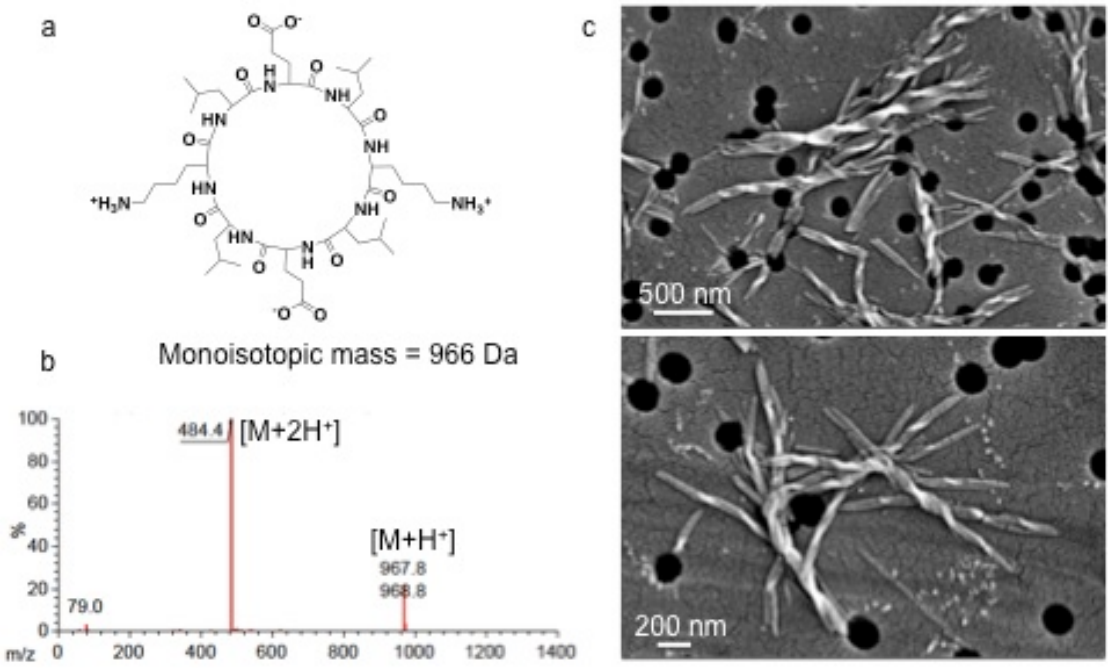

Figure A1. Synthesis and structural analysis of cyclo-[(ELKL)$_2$]. (a) Chemical structure and mass of ELKL2. (b) Confirmation by ESI-TOF mass spectroscopy. The singly charged ion is apparent at 967.8 m/z and the doubly charged ion is apparent at 484.4 m/z.

ELKL2 assembles into small, twisted structures that wind together. It is worth noting that these structures are roughly an order of magnitude smaller in both length and width as compared to QL4 fibers. The average length and width of ELKL2 structures are approximately 3 μm and 50 nm, respectively. The helical morphology of ELKL2 is unlike any DLCP structures mentioned to date in the literature.[3]

Conclusions

The discrepancy between QL4 fibers and ELKL2 assemblies is striking. Indeed, ELKL2 appears significantly more closely related to a traditional twisting amyloid fiber[4] than a rigid, DLCP assembly. This analysis suggests that there is significant freedom to control assembly morphology, even within the geometrically constrained DLCP system. Future results should seek to confirm the orientation of individual monomers within the twisting fibers. Modern electron microscopy based analysis methods would lend themselves to structural characterization of a material of this size.[5]

Materials and Methods

Self-Assembly Self-assembly was achieved by dissolving 2.5 mgs/ml of ELKL2 in neat TFA. The TFA-peptide solution was incubated in a large beaker containing water, and the system was covered. The assembly occurred as water vapor diluted the TFA solution. Structures were isolated after 48-72 hours and were viewed on SEM. SEM methods are described in Chapters 2 and 3.

Acknowledgements

In this study, structures were analyzed on SEM by P.K. Richie Tay.

APPENDIX B: CONTROL OF ASSEMBLY AND SIZE THROUGH SEEDING

Introduction

A challenge that persists in many self-assembling systems is the control of assembly size. Chapters 2 and 3 provide examples of QL4 structures that are permitted to grow to their maximum length and width. However, for many applications, including mechanical fillers, control over the size and aspect ratio is necessary.

Within amyloid systems, seeds have been used to initiate amyloid assembly.[6] Herein sonicated QL4 fibers are used as seeds to examine whether it is possible to adjust the length distribution of assembled QL4 fibers by adjusting the concentration of seeds.

Results and Discussion

QL4 was dissolved at a concentration of 2.5 mgs/ml within neat TFA. Water was added until a 60:40 ratio of TFA:water was achieved. Immediately afterwards, various serial dilutions of sonicated QL4 bundled fibers were added to the assembly solutions. The capped vials were left untouched for 24 hours. An analysis of brightfield microscopy images was used to measure the lengths of QL4 assemblies. The data from this analysis is presented in Figure B1.

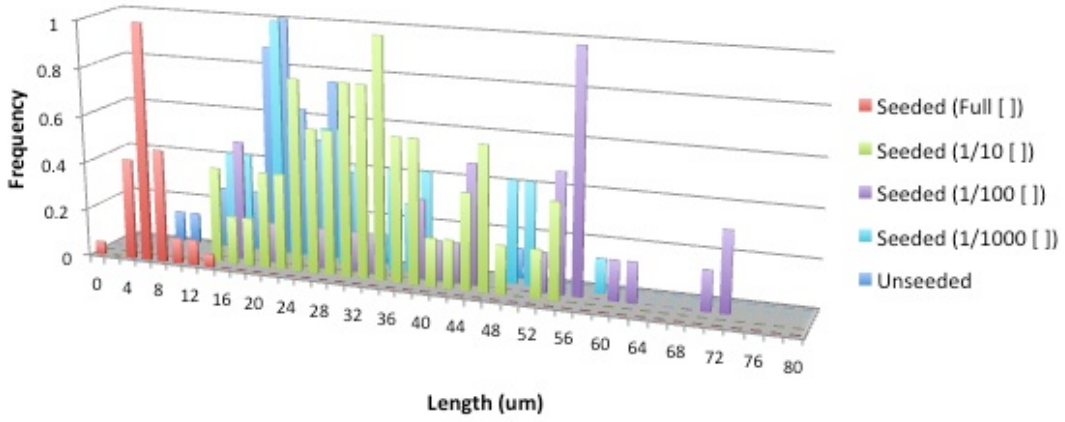

Figure B1. Length distribution of seeded QL4 fibers assemblies. A 10x serial dilution of sonicated QL4 seeds was added to QL4 assemblies. At full concentration, the seeds shifted the average length of QL4 structures to approximately 6 μm. As the concentration of seeds decreased there was a corresponding increase n the length of QL4 structures. Unseeded samples and dilutions of 1/1000 showed similar results.

There is a large shift in the size of QL4 structures that appears to be dependent on the amount of seed added. One would expect that at high seed concentration, nucleation begins in many areas, leading to a large number of smaller structures. Alternatively, at low seeding concentration, assembly is nucleated in many fewer areas, leading to fewer, larger structures. Eventually the concentration of seeds will drop low enough that there is no observable effect.

At the 'full' seed concentration, DLCP assemblies exhibit an average length of just 6 μm, significantly below the unseeded average of ~25 μm. Alternatively when seeds are diluted 1:10 or 1:100, the average length of the assembly extends beyond what is observed for unseeded. At full dilution (1:1000), the seeds appear to have no impact and the distribution closely parallels that of unseeded assemblies.

Conclusions

While these results are preliminary, they indicate the potential to control assembly length through seeding. An added benefit of seeding the assembly is that the assembly time is decreased from multiple days to just 24 hours (some cloudiness was observed in a few hours). Seeding of DLCP assemblies will not afford high fidelity control over size as one could expect from other assembling systems such as DNA, however it may allow enough control and homogeneity in the structures to increase their utility. An analysis seed identity as well as seed concentration and structure size through seeding will likely lead to interesting results.

Materials and Methods

Preparation of seeds Seeds were prepared by probe sonication of a solution of bundled QL4 fibers in water. Prior to experimentation, seeds were diluted to adjust their concentration, then concentrated to ensure that the ratio of TFA:Water within the assembly vessel was not disturbed.

Self-Assembly Self-assembly was achieved by dissolving 2.5 mgs/ml of ELKL2 in neat TFA. Water was added to the solution until a ratio of 60:40 TFA:water was achieved. Seeds at varying concentrations were then added to the solution, mixed, capped, and let stand for 24 hours.

APPENDIX C: FABRICATION AND CHARACTERIZATION OF QL4-LOADED POLYMER THIN FILMS

Introduction

The use of QL4 structures as reinforcing elements within polymer composites continues to be an area of interest. Due to QL4 fibers' large size, it is evident that the reinforcing of nanofibers is likely not the best materials system with which to analyze their performance. As a stepping-stone toward understanding the behavior of QL4-PDLLA solid composites under static compression, films were cast to analyze properties under tension in hydrated conditions.

Results and Discussion

QL4 structures were assembled and mixed with dissolved PDLLA as is described in Chapter 3. The solution was placed in a PDMS mold and left to dry overnight. After preliminary drying, films were placed in a drying oven at 38C for 2-4 hours. Figure C1 provides a schematic of the fabrication method.

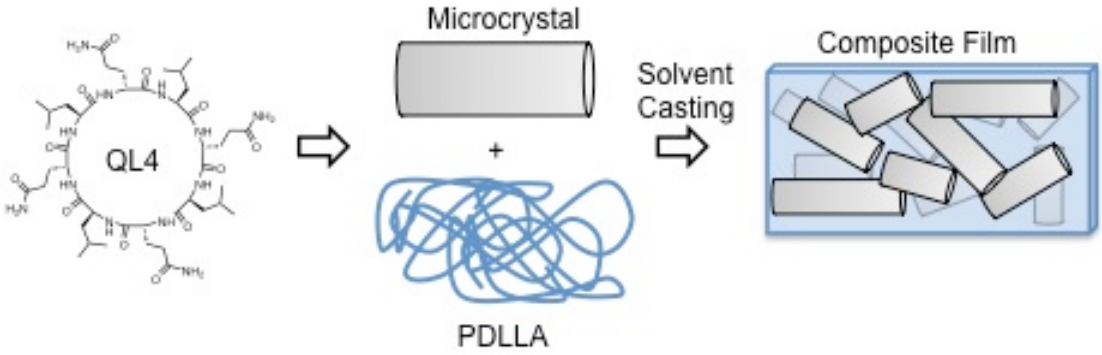

Figure C1. Schematic of QL4-PDLLA composite films. QL4 Fibers/microcrystals were blended with PDLLA in acetone/DCM and cast in PDMS molds.

The resultant films were removed from their molds and characterized by FT-IR and SEM. The Amide I and Amide II signals generated by DLCPs act in orthogonal planes to one another.[7] This enables the analysis of orientation while a film is being strained. Within composite PDLLA films with 5% peptide loading by weight, both the Amide I and Amide II are visible. SEM analysis of the thin film surface shows that in the absence of QL4, the PDLLA film is smooth, while in QL4 containing samples, structures can be seen along the surface and are aligned isotropically.

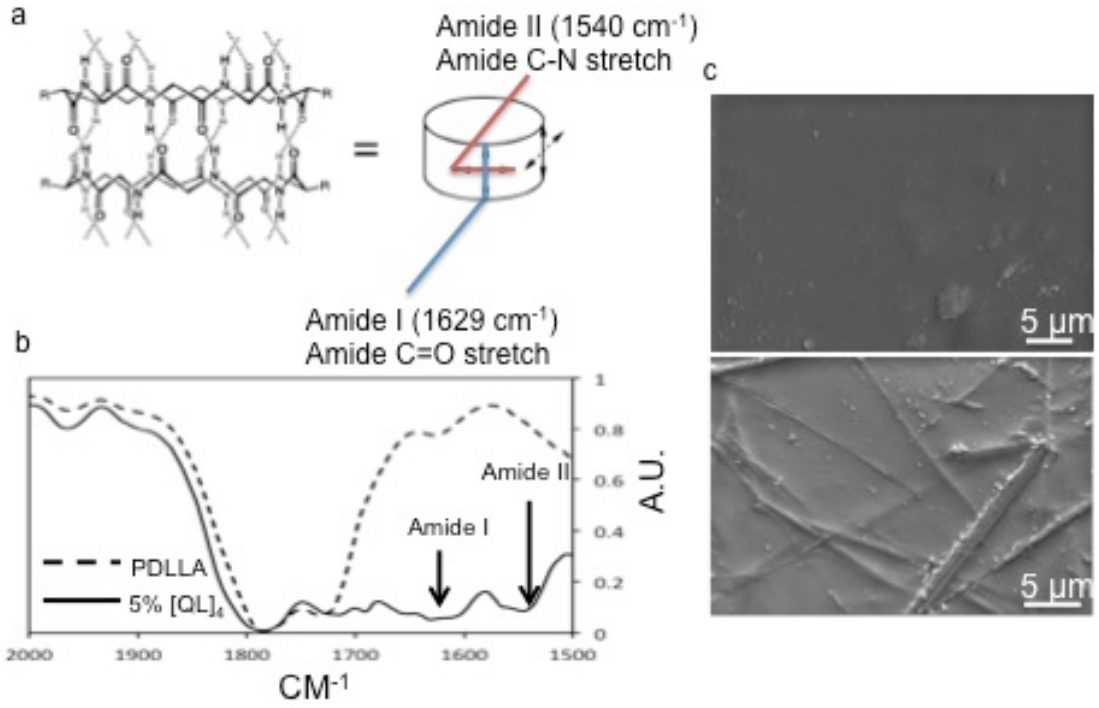

Figure C2. Structure of composite films. (a) Amide I and Amide II provide unique signals in FT-IT. This allows one to identify the orientation of a tube or fiber on a surface or within a material. (b) When QL4 is embedded in a PDLLA film, both Amide I and Amide II signals are visible. (c) A pure PDLLA film has a smooth surface [top] while a QL4-loaded film has a rough surface in which QL4 fibers are easily visualized [bottom].

Films were pulled at a fixed strain rate on an Instron materials testing machine. Both composite and non-composite films exhibited similar moduli, on the order of 500 MPa. Both samples display the expected deformation pattern; an initial stiff region followed by strain softening and plastic deformation. Composite films show a lower yield stress, but higher flow stress, perhaps indicating that plastic deformation is retarded by the presence of the QL4 structures. As there are no

chemical crosslinks acting to bind QL4 fibers to the polymer matrix, it is not surprising that similar moduli and stress values would be achieved when tested in tension.

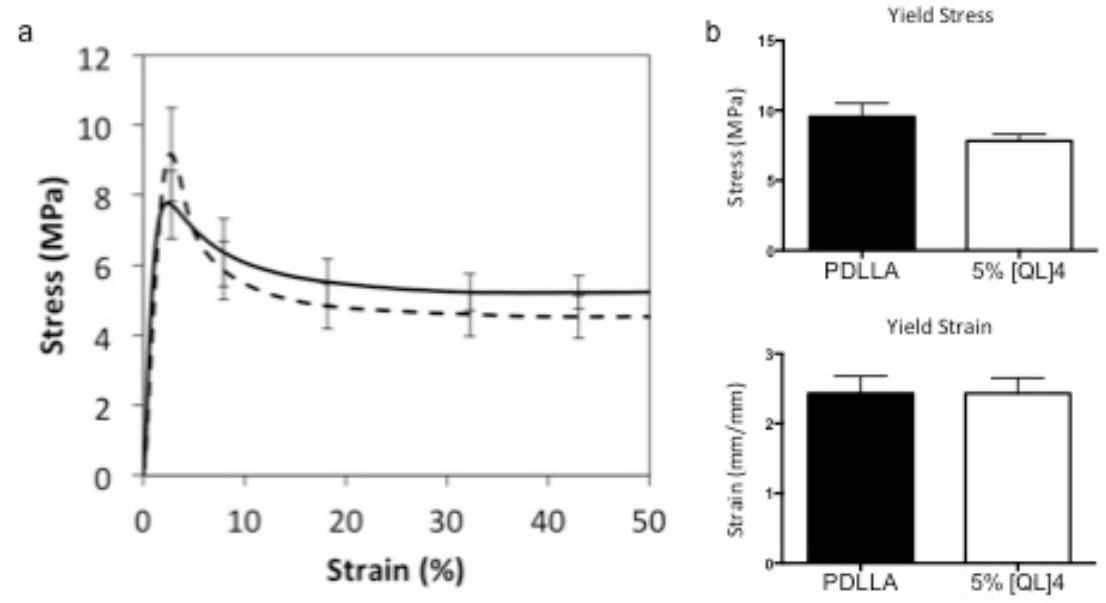

Figure C3. Stress/strain relationship in composite and non-composite films. (a) Stress versus strain curves show the similarity in properties between QL4-doped and pure PDLLA films. One interesting difference is that the strain softening effect is much less pronounced in the composite film versus pure PDLLA. (b) Yield stress and yield strain of PDLLA and composite films.

After deformation, composite films were analyzed by FT-IR and electron microscopy. The first notable observation can be made by eye. Composite films change opacity when strained while pure PDLLA films maintain their transparency. This effect is due to microcracking the occurs between the filler and the matrix material as seen in Figure C4c. FT-IR analysis of the Amide II signal suggests that QL4 fibers are reorienting within the matrix as would be expected during deformation if the fibers are unable to form a stable, interpenetrating network. SEM

analysis shows significant separation of QL4 fibers from the polymer matrix as well as broken fibers.

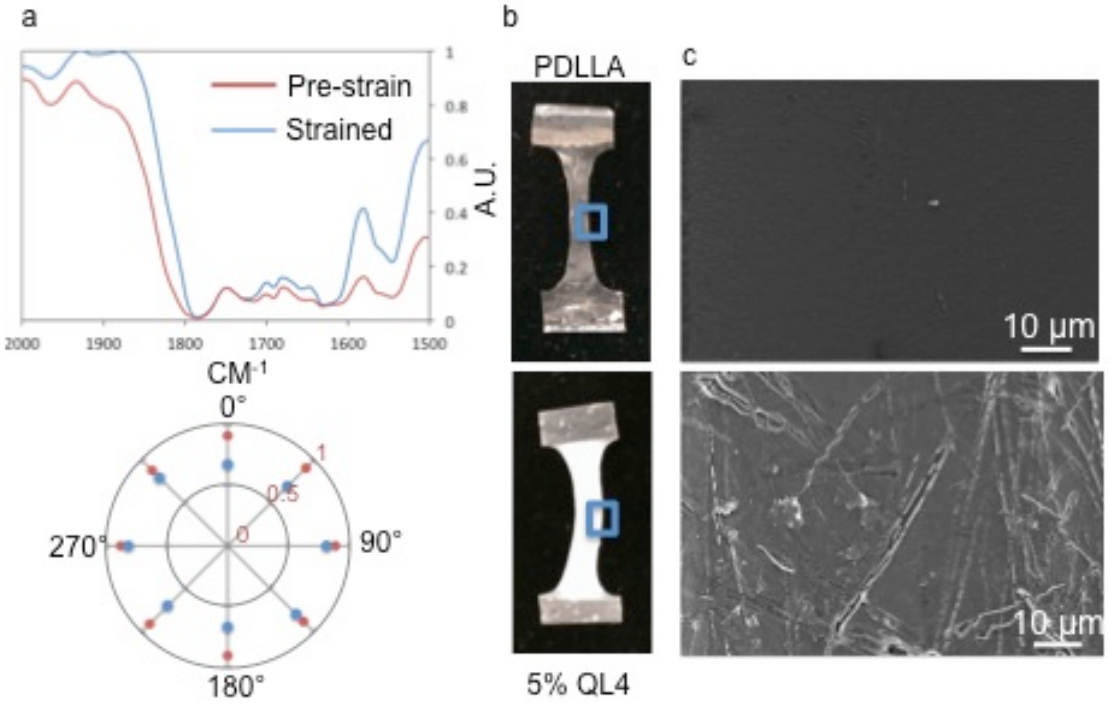

Figure C4. Post-strain structural changes in composite and non-composite films. (a) [Top] FT-IR analysis of pre-strain and strained PDLLA composites shows a decreased Amide II signal, indicating that fibers are reoriented within the matrix. [Bottom] The reorientation can be visualized in the form of a polar plot. The signal is strongest orthogonal to the strain-axis of the film. (b) Photographs of films. Composite films become opaque as they stretch. (c) [Top] pure PDLLA film. [Bottom] Composite PDLLA film displaying cracks and delamination.

Conclusions

The preceding analysis provides a stepping-stone toward analysis of solid composites under static load. Fiber reorientation, delamination, and decreased strain softening indicate that the load is being exerted on the QL4 fibers as well as the polymer matrix. In tension, the impact may appear minimal due to cracking and

delamination that decreases any potential reinforcement. However, when tested in compression, crack propagation is no longer a concern and it is expected that QL4 fibers will have a more significant impact.

Materials and Methods

Fabrication of films QL4 peptides were synthesized in accordance with the methods described throughout. QL4 fibers and PDLLA were combined in 3:1 acetone:DCM mixed thoroughly, and degassed to remove any bubbles. The degassed solution was carefully poured into a shallow PDMS mold and spread to remove any air bubbles. Samples were left to dry overnight and then incubated for 2-4 hours in a drying oven at 38C. Once dry, films were carefully removed from the mold and dogbones were punched from the films for use in mechanical testing.

Mechanical testing Films were tested on an Instron materials testing apparatus. Films were hydrated at 38C in PBS to mimic *in vivo* conditions. The stress versus strain measurements were taken at fixed strain rate.

APPENDIX D: ELASTIN-LIKE PEPTIDE FILMS WITH ENHANCED TOUGHNESS

Introduction

Materials toughness is defined as the total amount of energy that can be absorbed by a material before failure. Biomaterials, particularly silks, have remarkable toughness that surpasses their synthetic analogues. [8,9] Often this toughness is achieved by synthesizing a composite in which one component is held together through 'sacrificial' bonds that are able to break, and possibly reform, upon stress. This allows the material to be both strong and extensible. Here we examine the use of ELKL2 assemblies (as described in Appendix A) as a crosslinking molecule within an elastin-mimetic peptide (EMP) matrix.

Results and Discussion

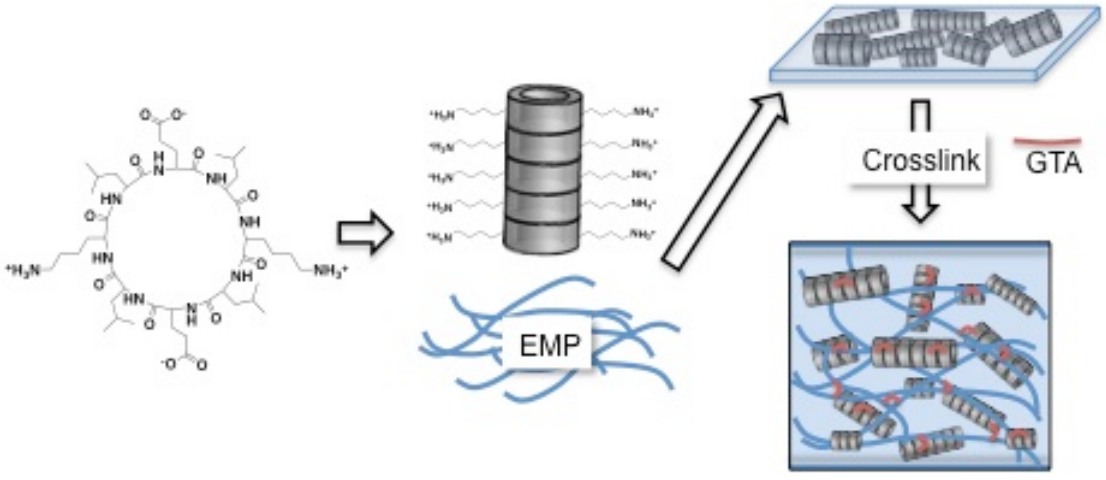

Figure D1. Schematic of ELKL/EMP tough composites. ELKL2 peptides are combined with elastin mimetic peptides, then cast into films via a controlled solvent evaporation method. The resultant film is crosslinked with glutaraldehyde vapor. This results in the formation of crosslinks between ELKL2 structures, ELKL2 structures and EMPs, and between EMPs.

ELKL2 Peptides were synthesized and assembled as described in Appendix A. ELKL2 was chosen because it contains lysine residues that can be easily crosslinked through glutaraldehyde via vapor or solution methods. The elastin mimetic protein LysB10 was used as the matrix material.[10] EMPs are particularly interesting protein materials because they exhibit a reverse phase transition. At high temperatures, EMPs crosslink to form solids, while at low temperatures they remain as liquids. This allows for easy synthesis of films, fibers, and particles. In order to toughen the material, there must be an extensible matrix that is able to exert forces on the reinforcing element. The lysines present in LysB10 are also able to crosslink with glutaraldehyde. This results in a system with 3 forms of crosslinks: DLCP-DLCP, EMP-EMP, and EMP-DLCP, all of which should act to stabilize the system.

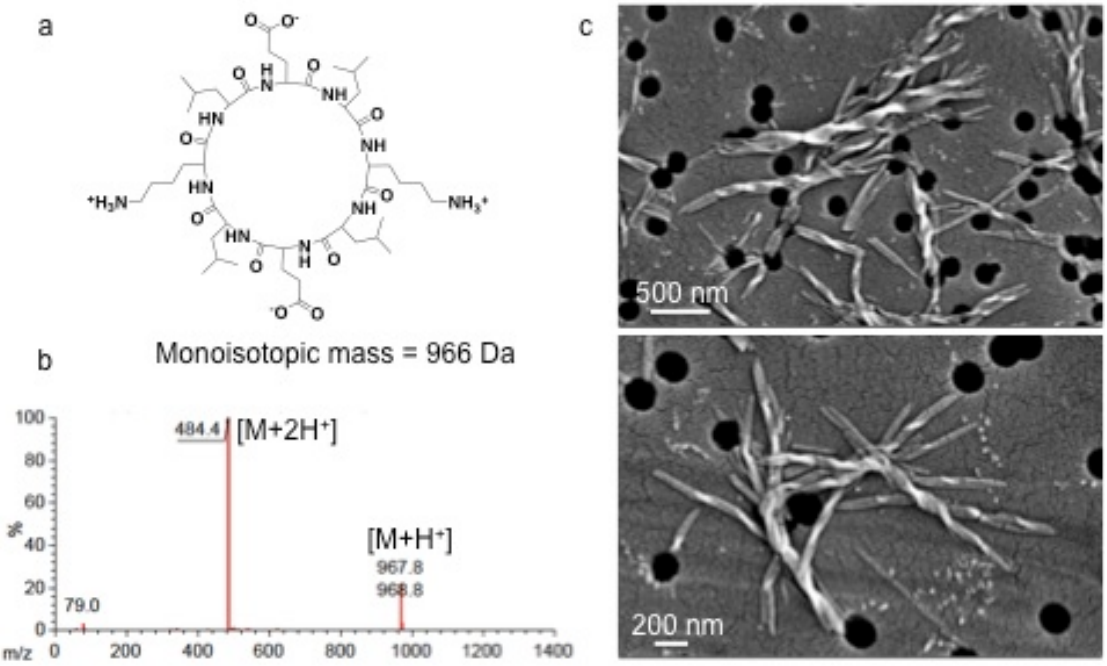

Figure D2. Synthesis and structural analysis of cyclo-[(ELKL)$_2$]. (a) Chemical structure and mass of ELKL2. (b) Confirmation by ESI-TOF mass spectroscopy. The singly charged ion is apparent at 967.8 m/z and the doubly charged ion is apparent at 484.4 m/z.

Fabricated films were stable to touch and could be strained by hand (Figure D3). The structure of the fabricated films was visualized by eletron microscopy. The surface appeared relatively smooth (Figure D3) while the cross-section showed a tangled, fibrous matrix which is expected for EMP films.[11] Due to the small size of ELKL2 and the fibrous nature of the EMP film, it is not possible to detect embedded ELKL2 structures within the film.

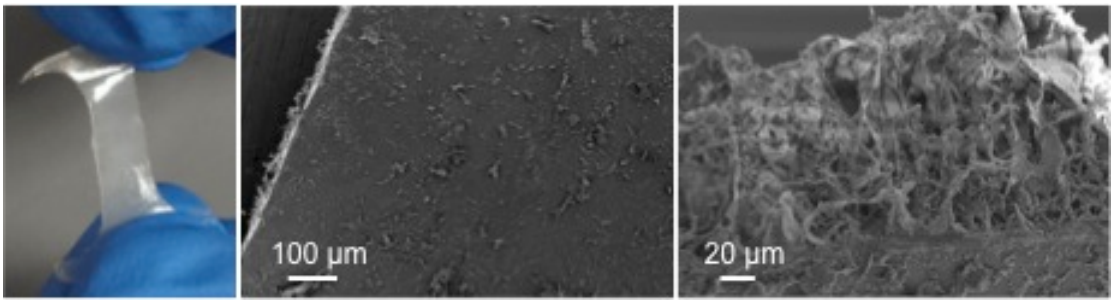

Figure D3. Morphology of composite film. [Left to right] Composite films can be stretched by hand. SEM micrographs of the surface indicate that the films are relatively smooth. The cross section shows a dense tangle of protein fibers.

Pure EMP films, crosslinked EMP films, and crosslinked composite films were tested on an Instron materials testing apparatus. Tests were done in PBS at 38C to mimic *in vivo* conditions. Because of the elastomeric nature of the matrix material, cyclic strain tests were done. Films were strained by 30% and allowed to recover to their initial length. Each sample was subjected to two strain cycles so that sample conditioning could be observed.

All samples exhibit a similar stress-strain curve in which there is an initial stiff region, followed by a softening and continued extension. When the material is allowed to relax, it exerts very little force. In total, this demonstrates that the EMP and EMP composite films have high hysteresis (energy dissipation). Upon

crosslinking, the stiffness of the film is increased dramatically from ~7MPa to ~30MPa, a roughly 4-fold increase. The crosslinked composite exhibits a further increase up to ~60 MPa. In total there is a roughly 8-fold increase in modulus upon addition of ELKL2 and crosslinking.

The yield stress shows a similar but more pronounced pattern. The uncrosslinked film has a yield stress of 0.34 MPa, while the composite crosslinked film has a yield stress of 3.8 MPa. This represents an 11-fold increase in yield stress. The dramatically improved yield stress and the preserved extensibility (up to 30% which was as far as was tested) demonstrate that the inclusion of ELKL2 as a crosslinking agent dramatically improves the materials toughness of EMP films.

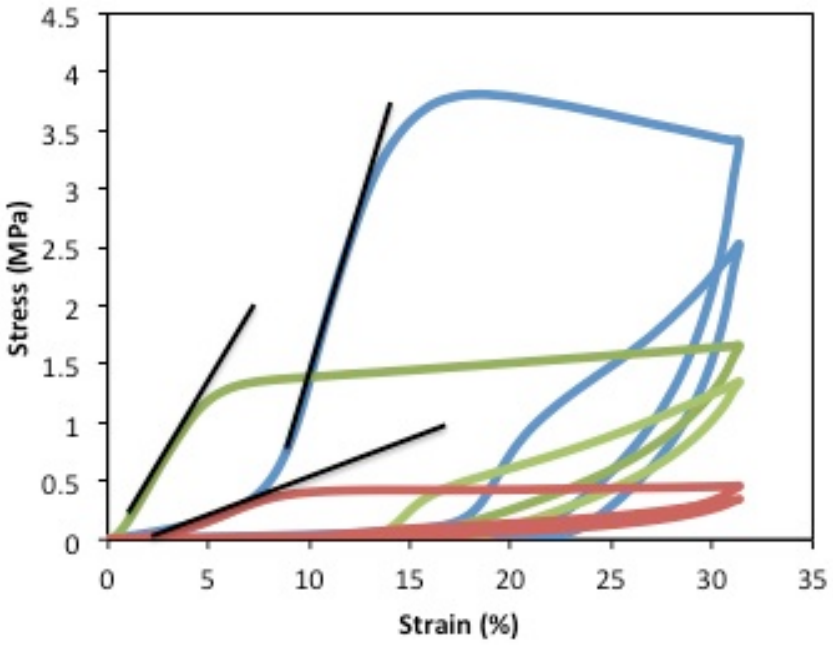

Sample	Modulus	Yield Stress
No X-links	7 MPa	0.34 MPa
X-linked	29.63 MPa	1.28 MPa
X-linked + ELKL	58.51 MPa	3.8 MPa

Figure D4. Mechanics of composite and non-composite EMP films. [Top] Cyclic stress-strain curves for films. The 'toe' region at the base of the composite curve is due to slack that was introduced upon submerging the sample into liquid. [Bottom] Table of modulus and Yield stress values.

Conclusions

Material toughness is important for structures that must absorb significant amounts of energy without fracture. Nature achieves toughness through clever hierarchical structure and the use of sacrificial bonds.[12,13] Herein, we provide similar reinforcement by the addition of a hierarchically assembled filler material that is crosslinked into an elastomeric matrix. These preliminary results suggest

that there may be interesting applications of DLCP structures as toughening agents within composites. Furthermore, DLCP structures may be able to reform their intramolecular bonds, creating a material that not only improves toughness but self-heals as well.

Materials and Methods

Casting films Films were cast from 100mg/ml solutions of LysB10. The solution was kept on ice to maintain solubility during the casting process. 50 µl of solution was added to a Teflon mold. The mold was incubated in the presence of an open beaker of water to control the rate of film dehydration. After 48 hours, the mold was filled with water and the film was lifted from the surface. The film was then punched in dogbones for mechanical testing.

Mechanical testing Films were tested on an Instron materials testing apparatus. Films were hydrated at 38C in PBS to mimic *in vivo* conditions. The stress versus strain measurements were taken at fixed strain rate. Each sample was strained to 30%, allowed to relax, and then strained again for a total of 2 complete cycles.

Acknowledgements

This work was completed in collaboration with Dr. Wookhyun Kim and Dr. Elliot Chaikof. Dr. Kim provided elastin-mimetic peptides and performed supporting work during film fabrication and mechanical analyses.

REFERENCES

1. Hartgerink, J. D., PhD Thesis. *Scripps Research Institute, La Jolla, CA* **1999**.

2. McMurray, J. S., Solid phase synthesis of a cyclic peptide using Fmoc chemistry. *Tetrahedron Letters* **1991,** *32* (52), 7679-7682.

3. Chapman, R.; Danial, M.; Koh, M. L.; Jolliffe, K. A.; Perrier, S., Design and properties of functional nanotubes from the self-assembly of cyclic peptide templates. *Chemical Society Reviews* **2012,** *41* (18), 6023-6041.

4. Ridgley, D. M.; Barone, J. R., Evolution of the Amyloid Fiber over Multiple Length Scales. *ACS Nano* **2013,** *7* (2), 1006-1015.

5. Nannenga, B. L.; Shi, D.; Leslie, A. G.; Gonen, T., High-resolution structure determination by continuous-rotation data collection in MicroED. *Nature methods* **2014,** *11* (9), 927-930.

6. Xue, W.-F.; Homans, S. W.; Radford, S. E., Systematic analysis of nucleation-dependent polymerization reveals new insights into the mechanism of amyloid self-assembly. *Proceedings of the National Academy of Sciences* **2008,** *105* (26), 8926-8931.

7. Kim, H. S.; Hartgerink, J. D.; Ghadiri, M. R., Oriented self-assembly of cyclic peptide nanotubes in lipid membranes. *J. Am. Chem. Soc* **1998,** *120* (18), 4417-4424.

8. Keten, S.; Xu, Z.; Ihle, B.; Buehler, M. J., Nanoconfinement controls stiffness, strength and mechanical toughness of beta-sheet crystals in silk. *Nature Materials* **2010,** *9* (4), 359-367.

9. Vaccaro, E.; Waite, J. H., Yield and Post-Yield Behavior of Mussel Byssal Thread: A Self-Healing Biomolecular Material. *Biomacromolecules* **2001,** *2* (3), 906-911.

10. Sallach, R. E.; Cui, W.; Wen, J.; Martinez, A.; Conticello, V. P.; Chaikof, E. L., Elastin-mimetic protein polymers capable of physical and chemical crosslinking. *Biomaterials* **2009,** *30* (3), 409-422.

11. Caves, J. M.; Cui, W.; Wen, J.; Kumar, V. A.; Haller, C. A.; Chaikof, E. L., Elastin-like protein matrix reinforced with collagen microfibers for soft tissue repair. *Biomaterials* **2011,** *32* (23), 5371-5379.

12. Harrington, M. J.; Gupta, H. S.; Fratzl, P.; Waite, J. H., Collagen insulated from tensile damage by domains that unfold reversibly: In situ X-ray investigation of

mechanical yield and damage repair in the mussel byssus. *JOURNAL OF STRUCTURAL BIOLOGY* **2009,** *167* (1), 47-54.

13. Rubin, D. J.; Miserez, A.; Waite, J. H., Diverse strategies of protein sclerotization in marine invertebrates: structure–property relationships in natural biomaterials. *Advances in Insect Physiology* **2010,** *38*, 75-133.